

# X-ray Reflection Modeling in the Era of High-Resolution Spectroscopy

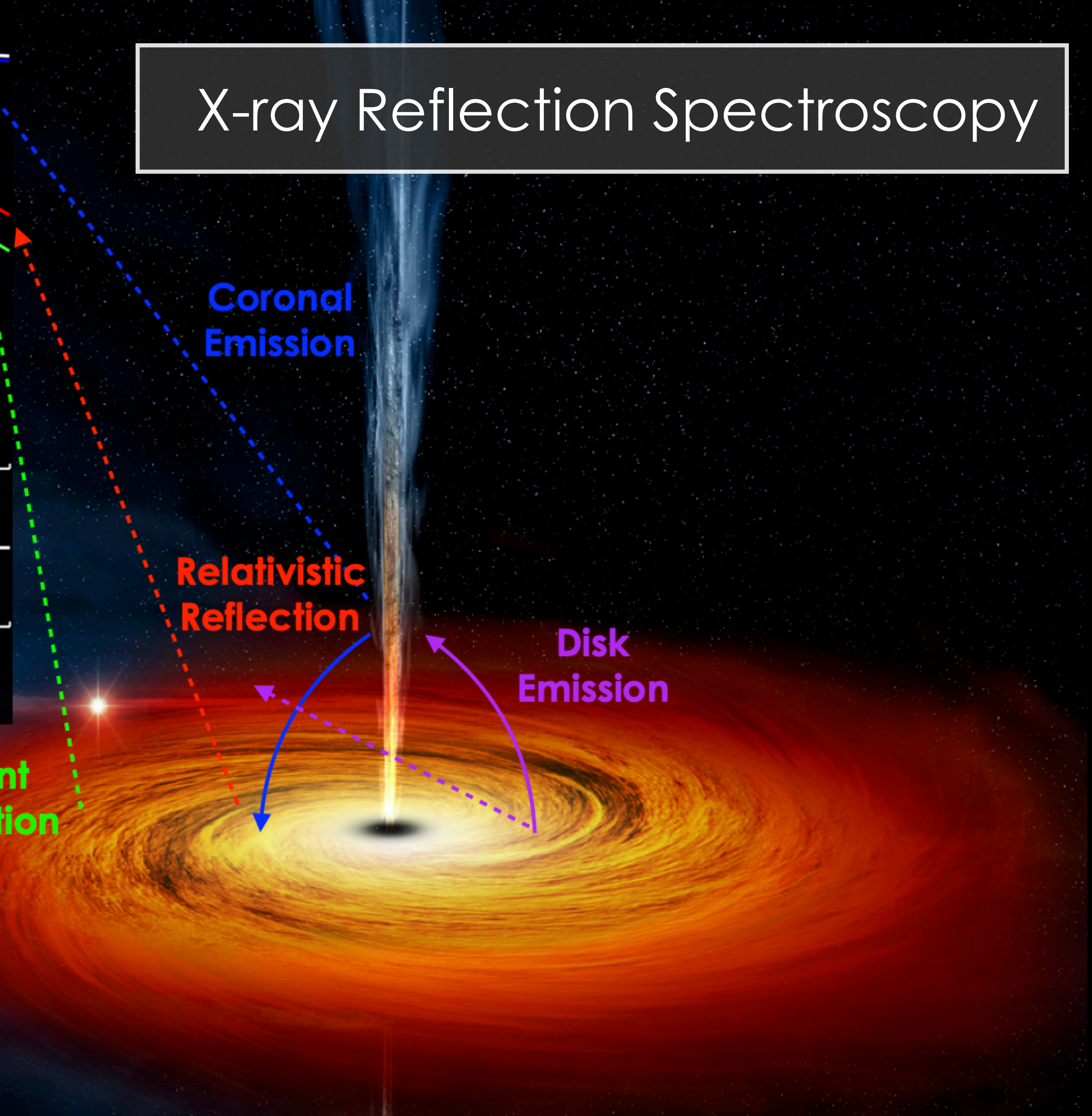
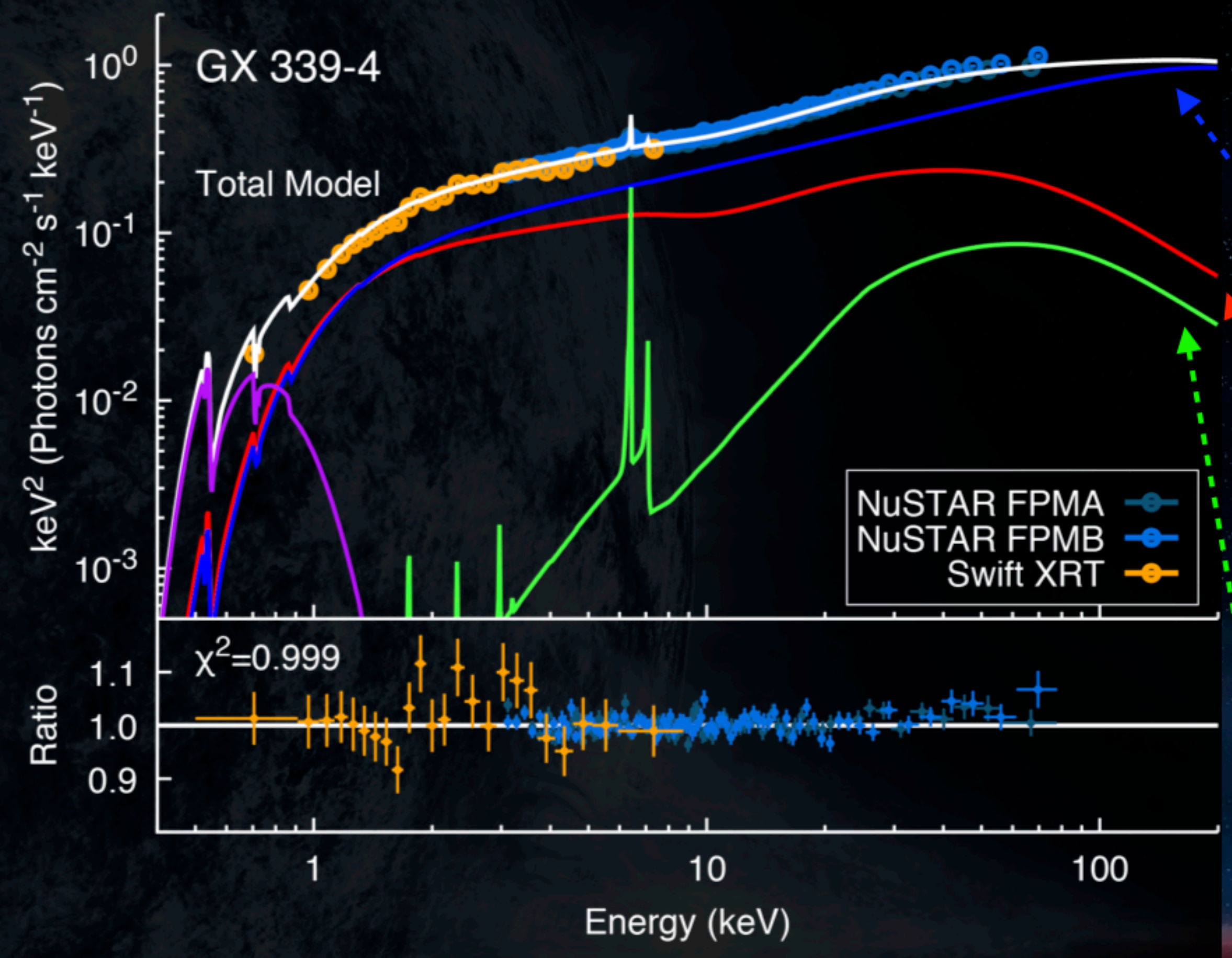
Javier A. García  
NASA Goddard Space Flight Center



Chandra Workshop—High-Resolution X-ray Spectroscopy  
MIT, Cambridge, MA—Aug 1, 2023

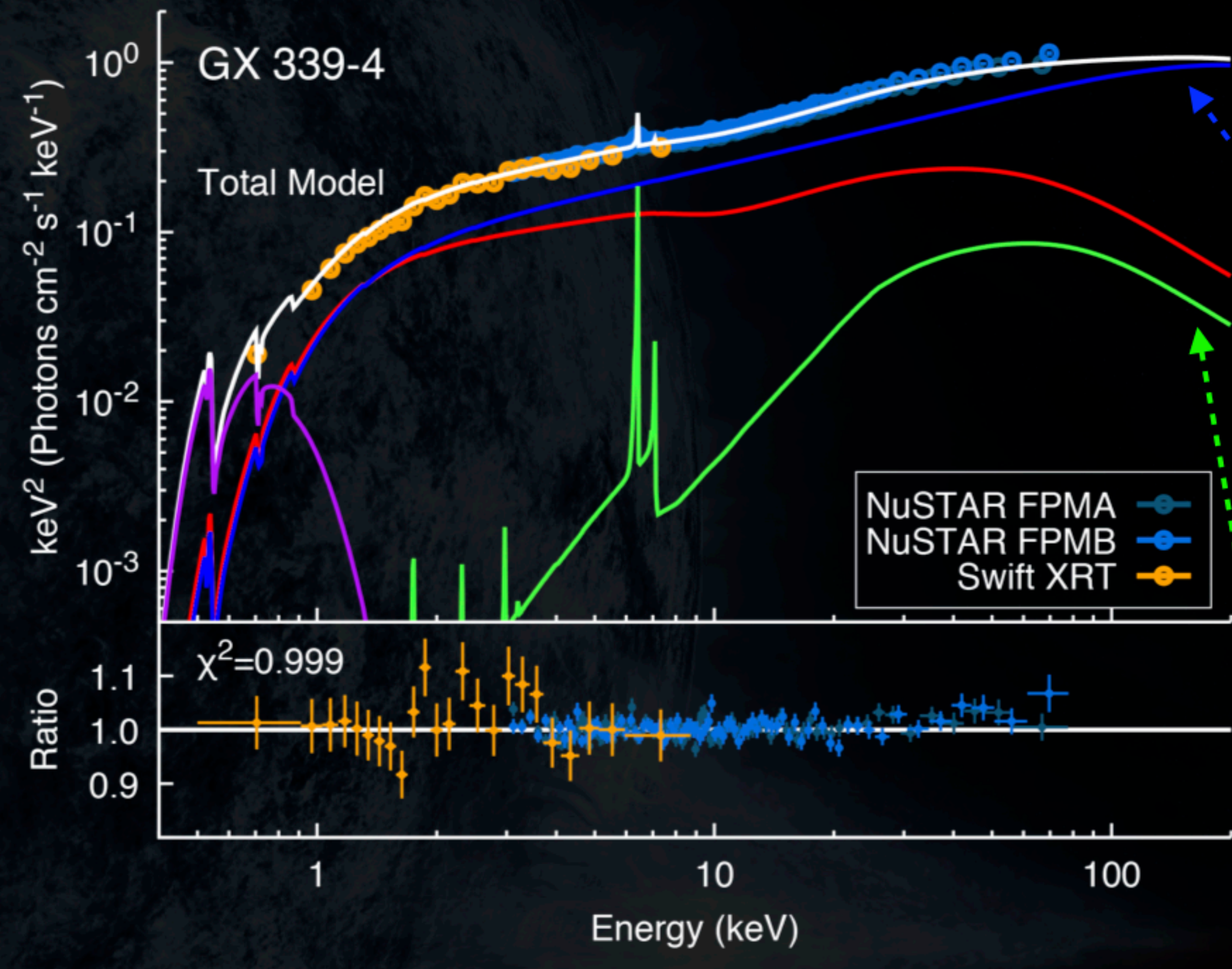


# X-ray Reflection Spectroscopy





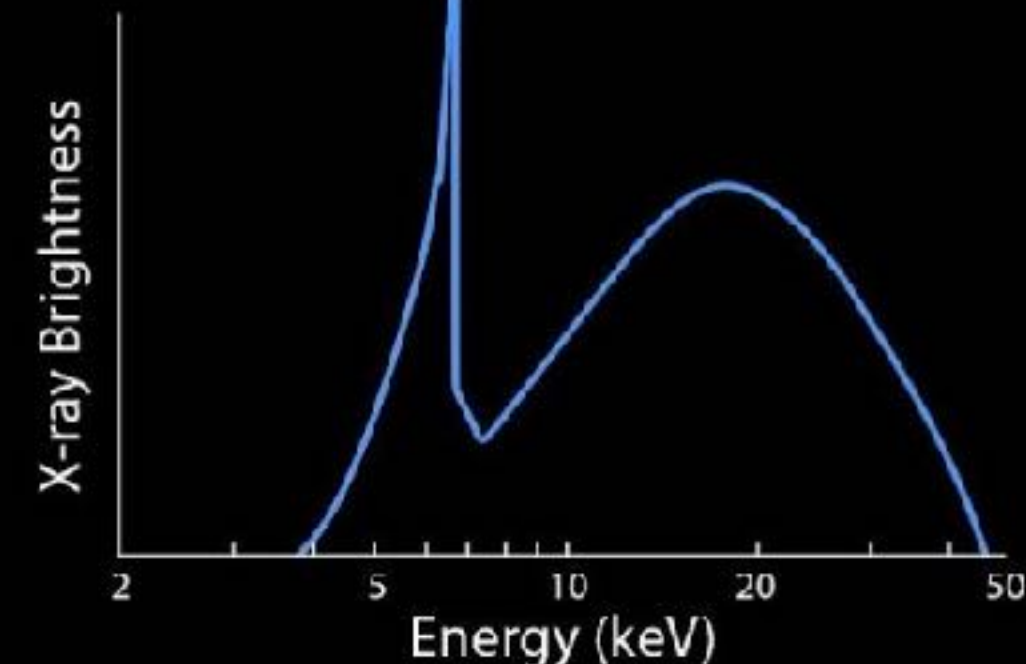
# X-ray Reflection Spectroscopy



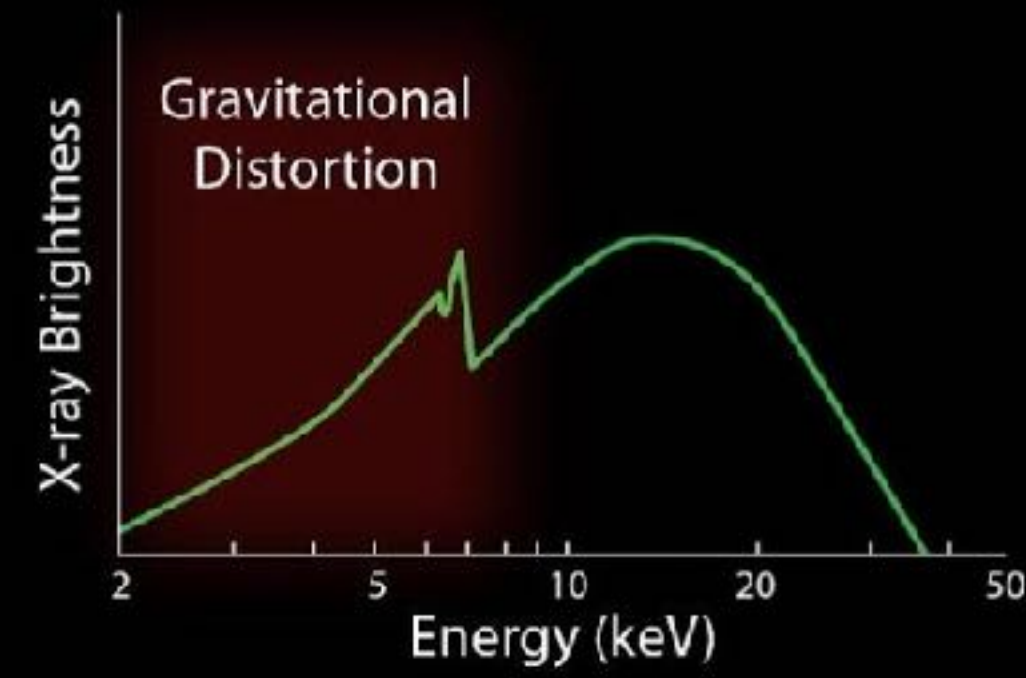
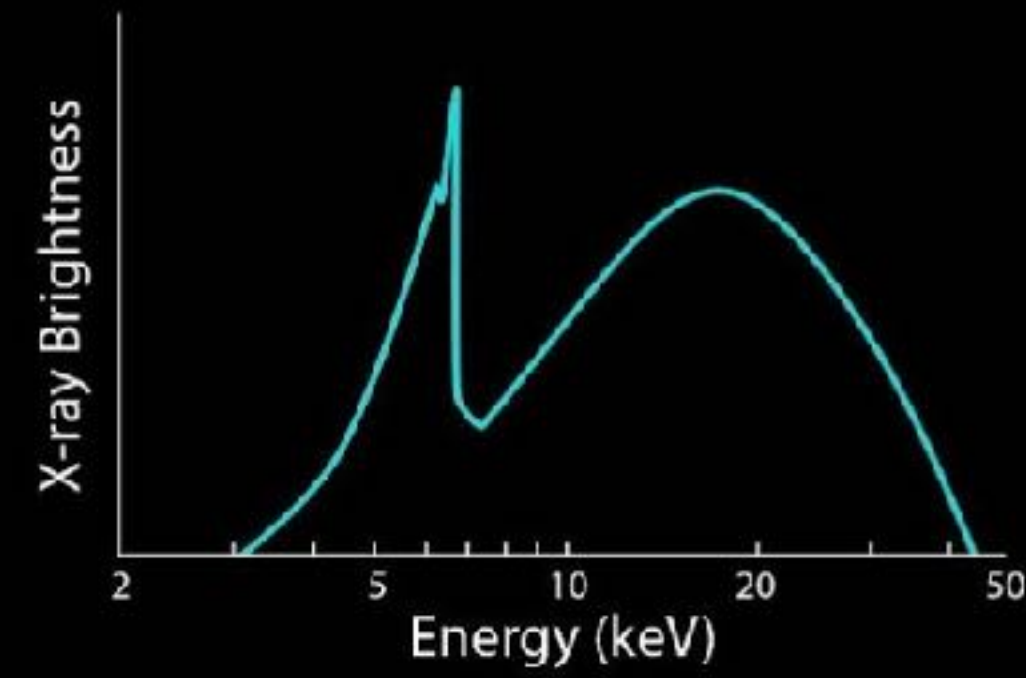
**Corona Emission**

**Relativistic Reflection**

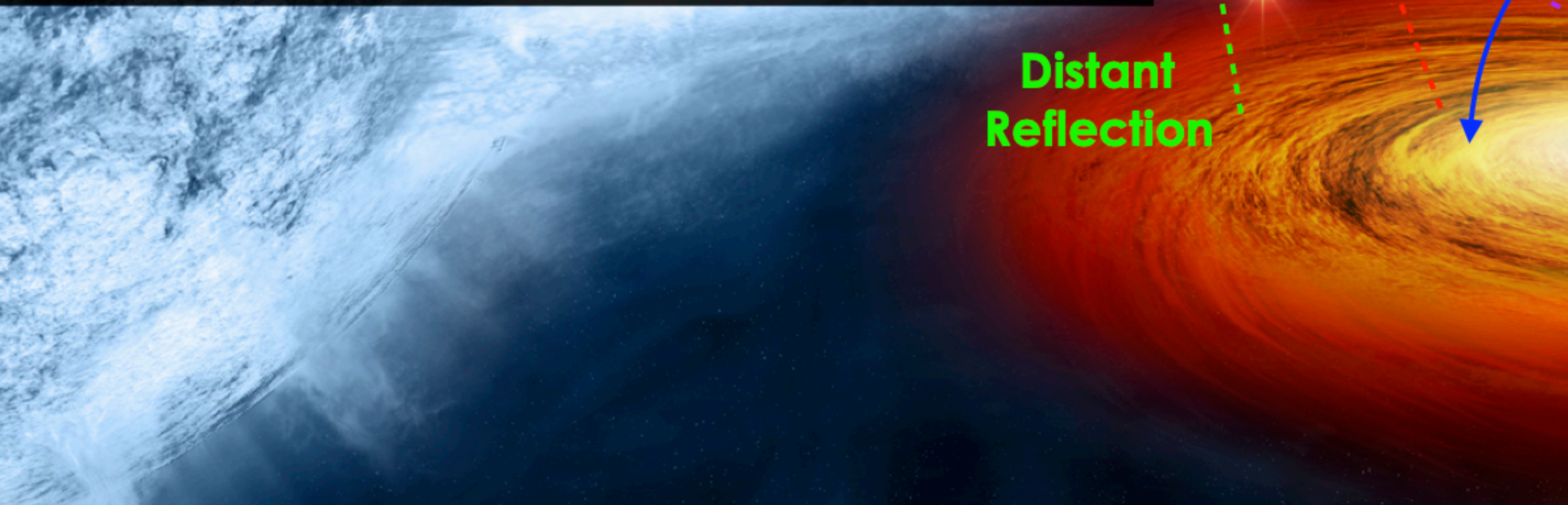
**Distant Reflection**



**Faster BH rotation**

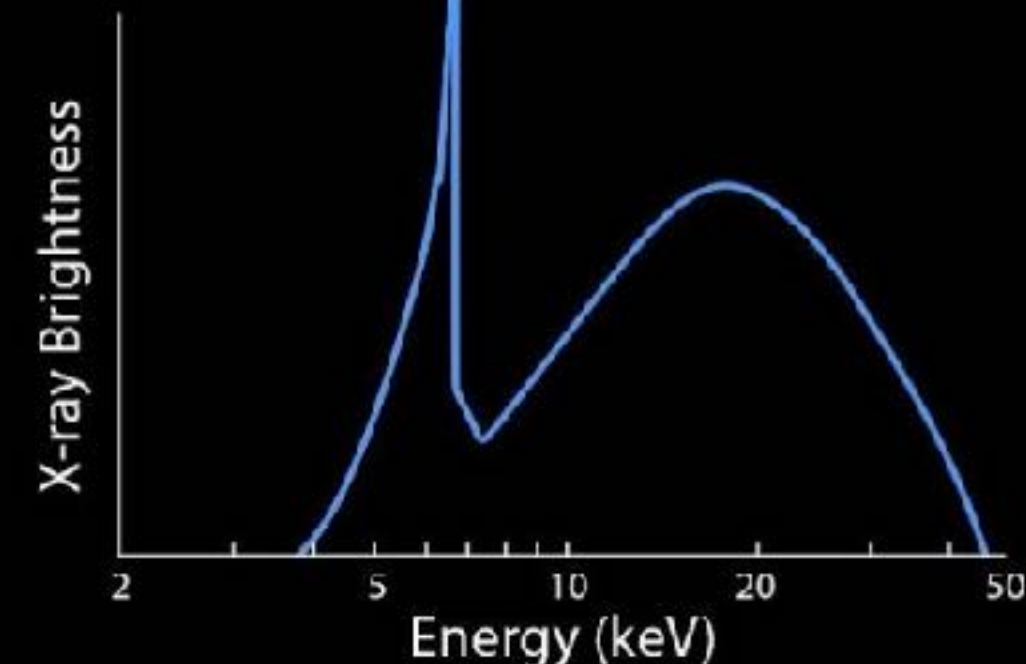
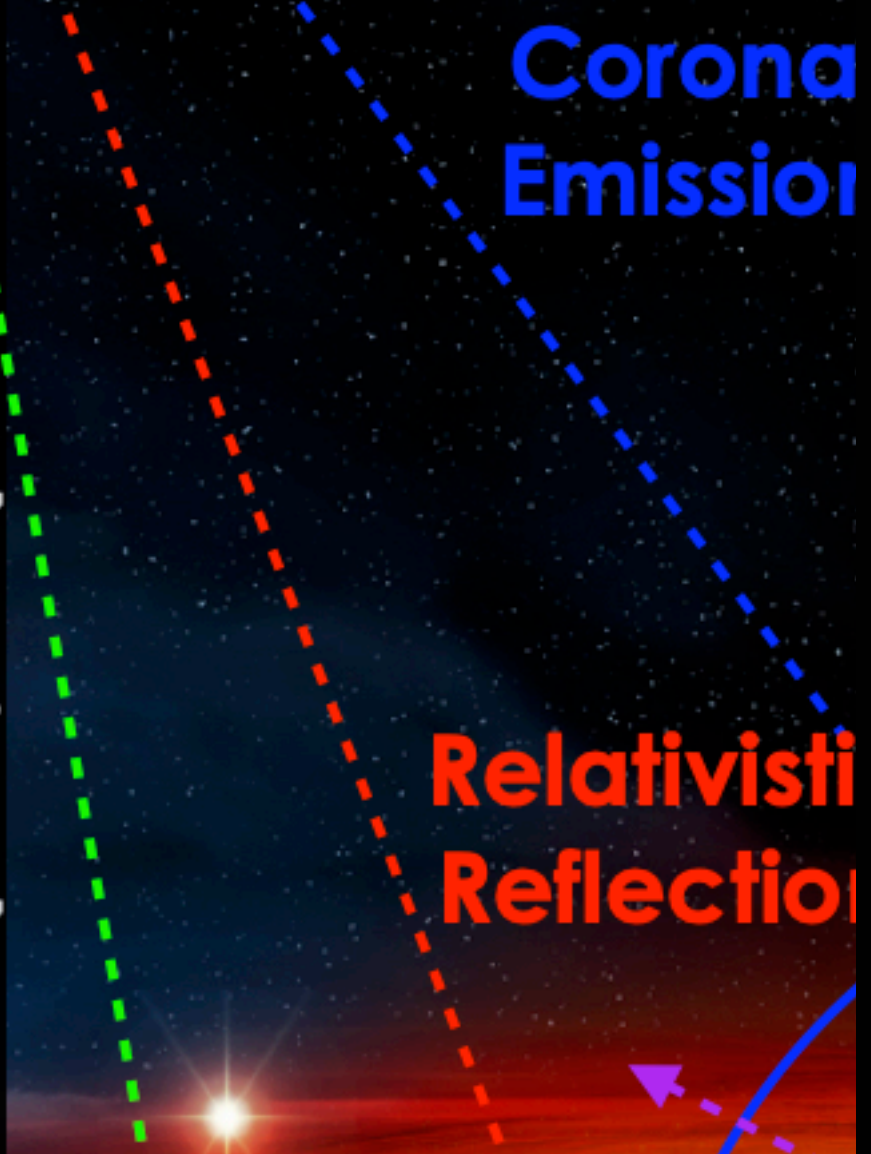
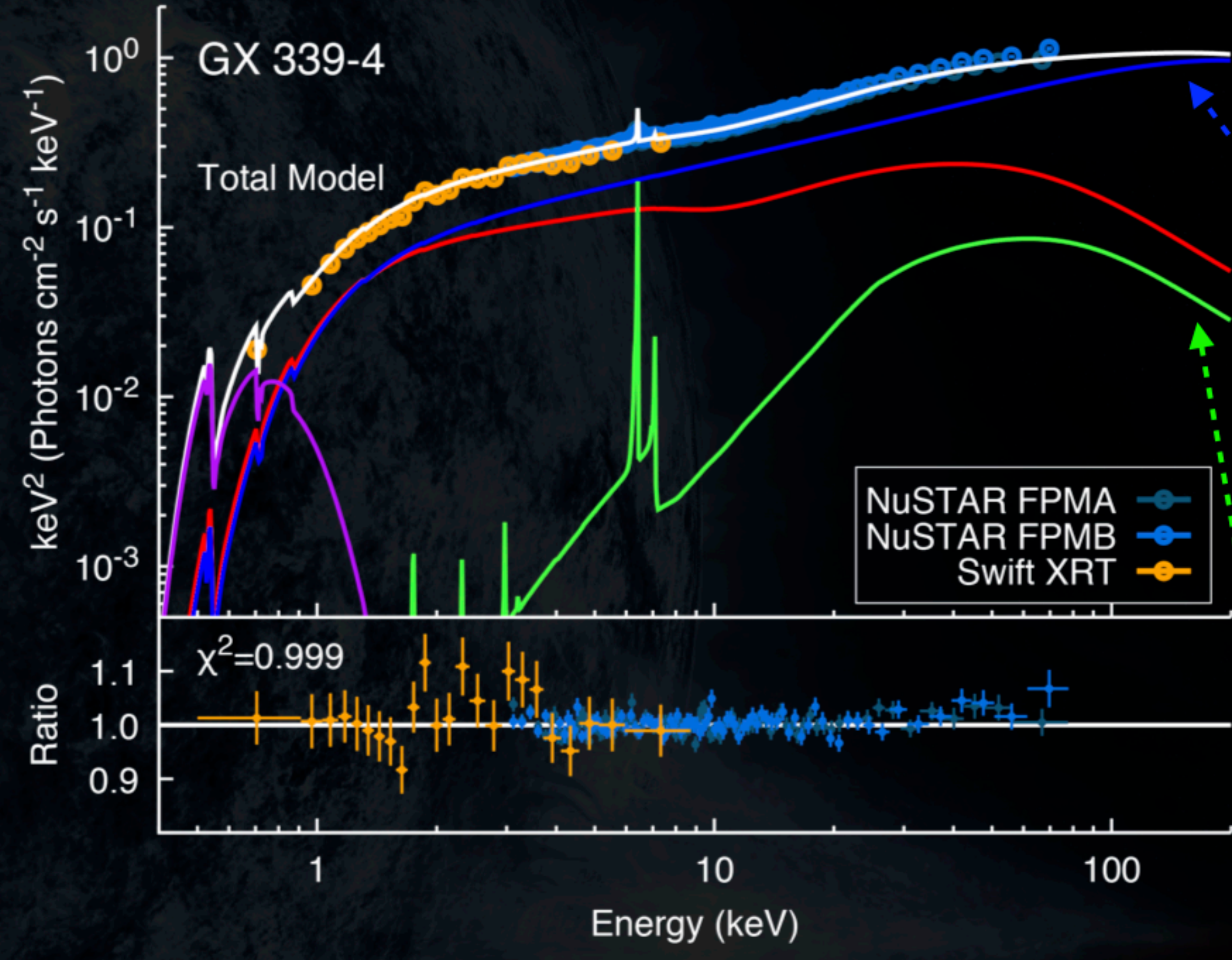


**Stronger Relativistic Distortion**

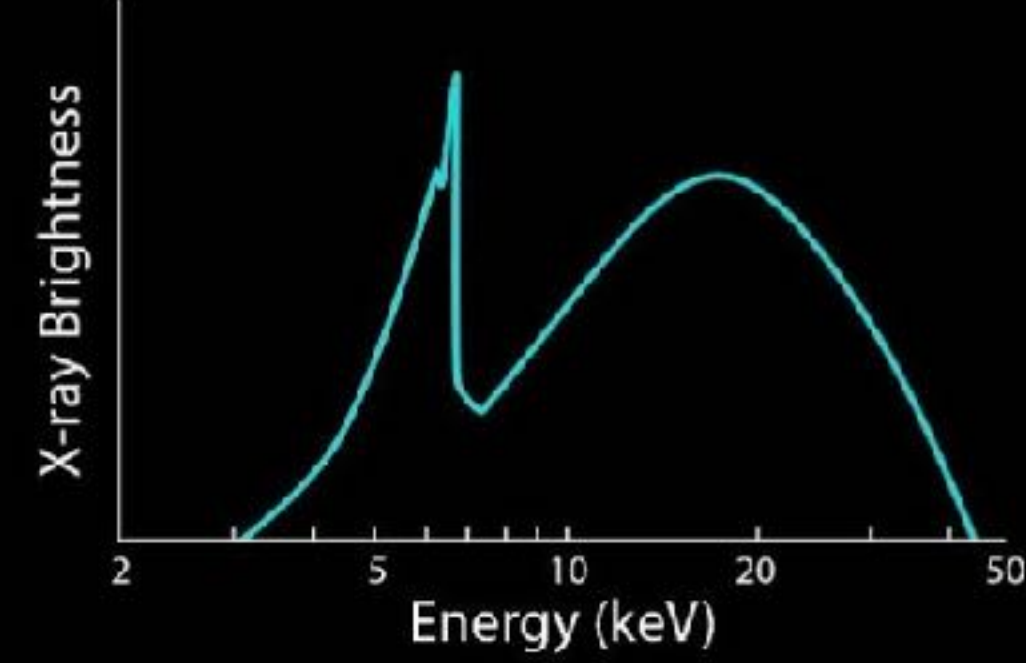




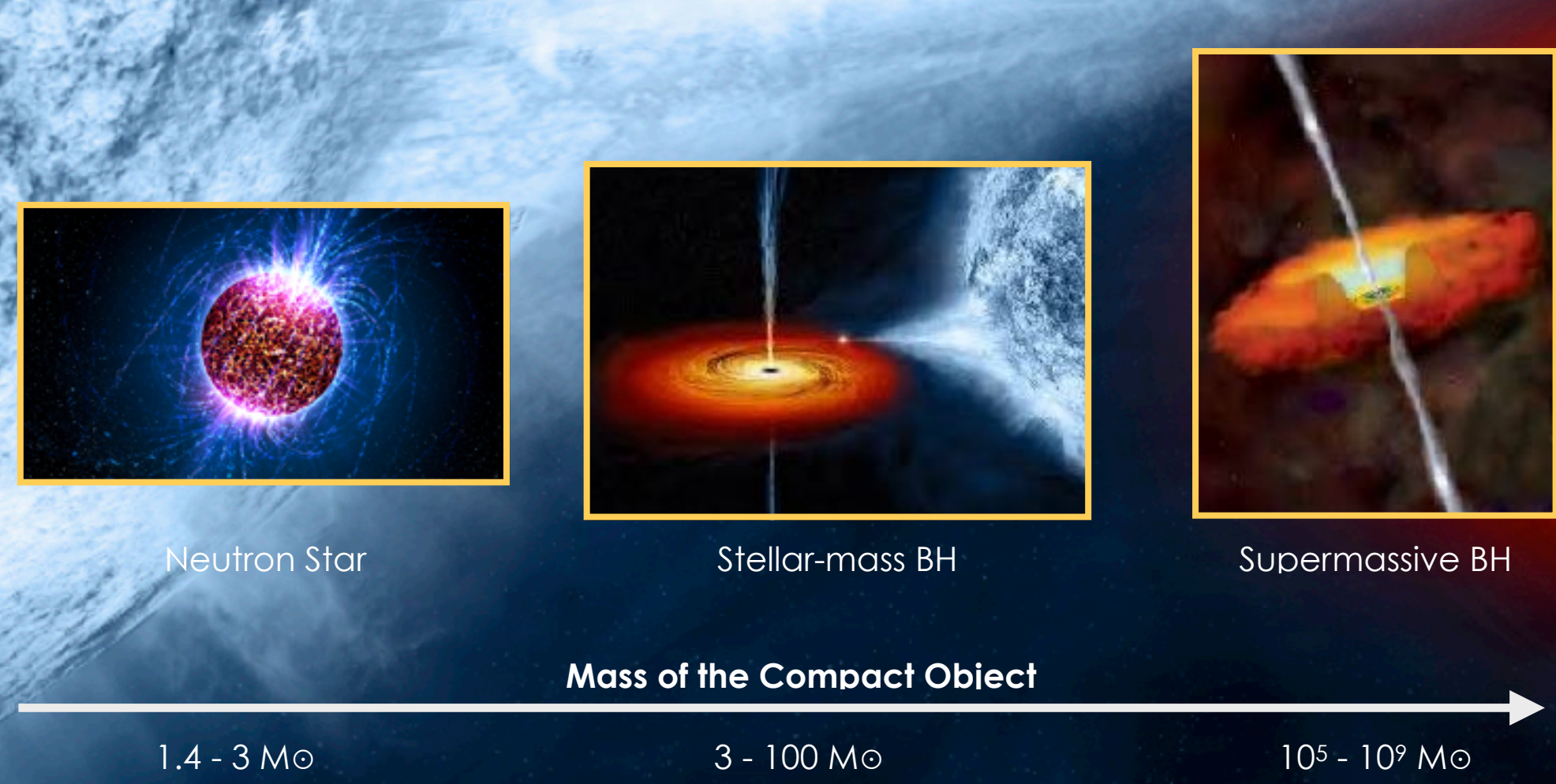
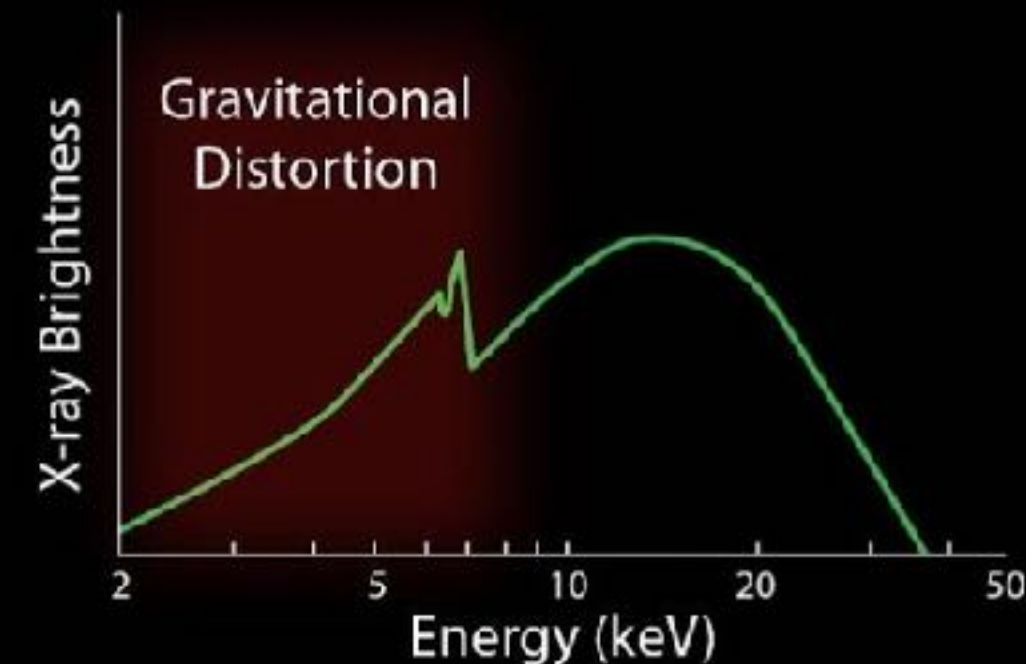
# X-ray Reflection Spectroscopy



**Faster BH rotation**

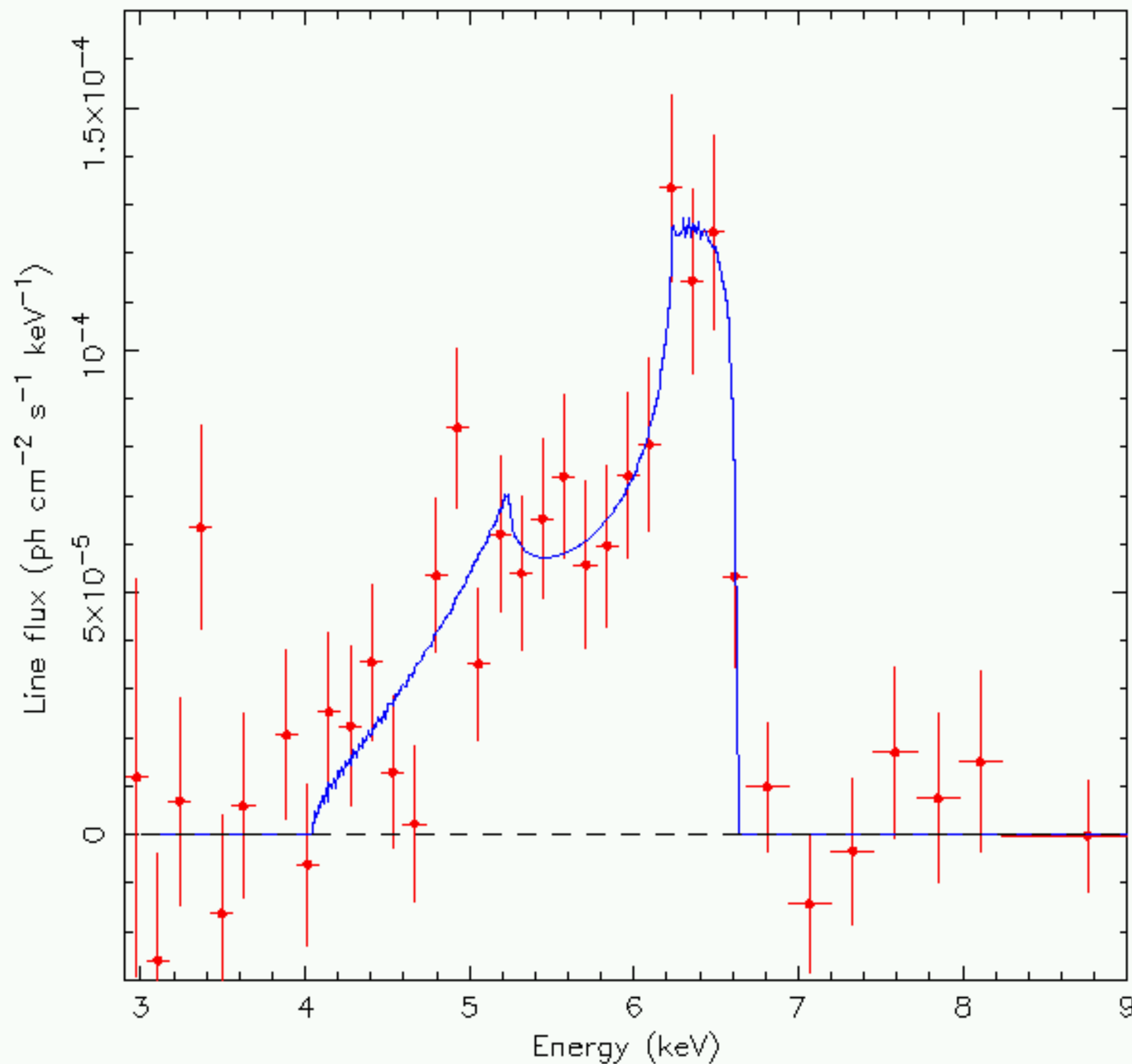


**Stronger Relativistic Distortion**





# First Detections of X-ray Reflection



**1990's:** ROSAT, ASCA. First CCDs flying on X-ray observatories. First detections of a distorted Fe K line, which was interpreted as emission affected by relativistic effects near the BH (Tanaka et al. 1995; Nandra et al. 1997; Fabian et al. 2000).

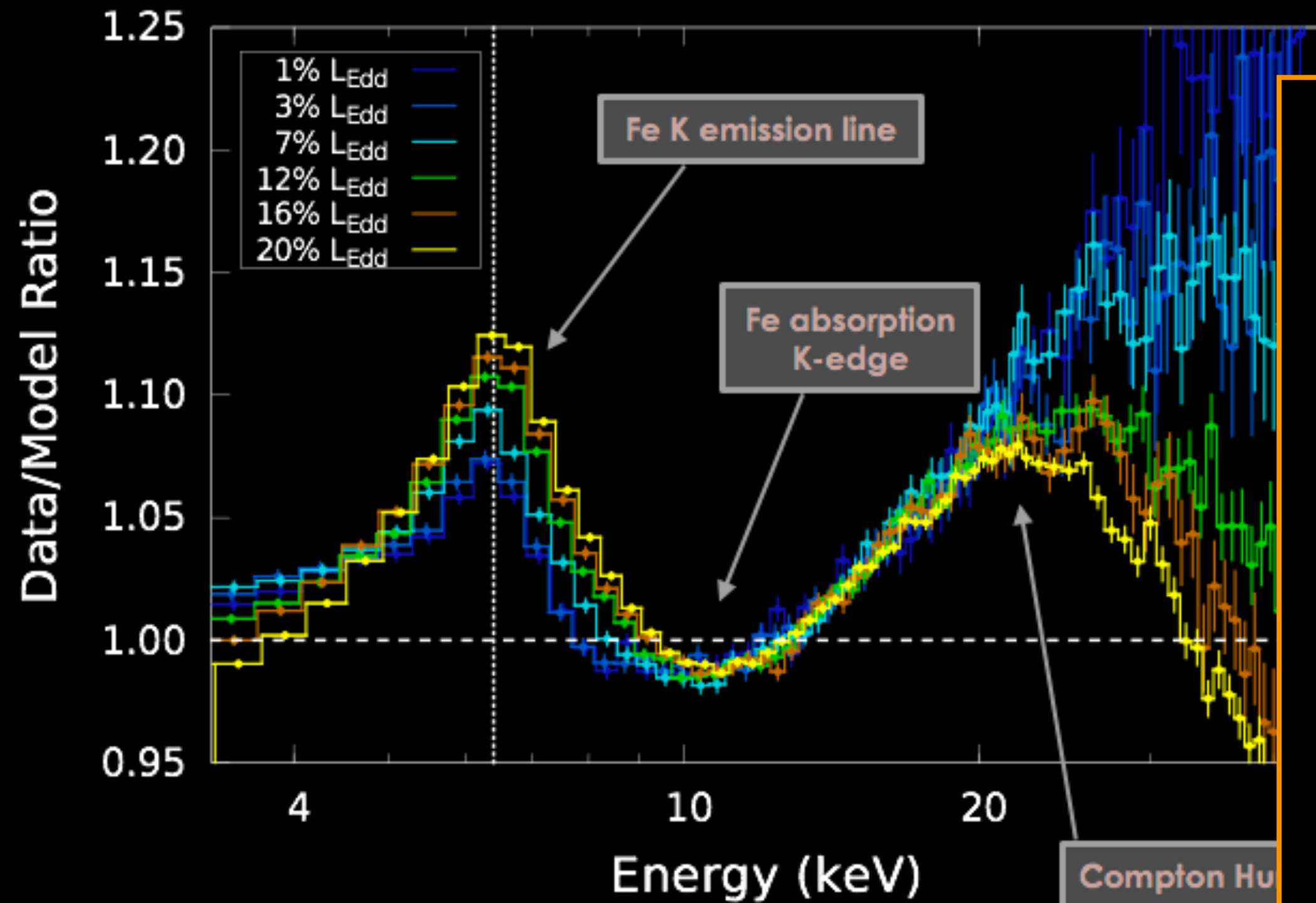
The line profile of iron K-alpha from MCG-6-30-15 observed by the ASCA satellite (Tanaka et al. 1995)

Resolution **0.12 keV** @ 6 keV



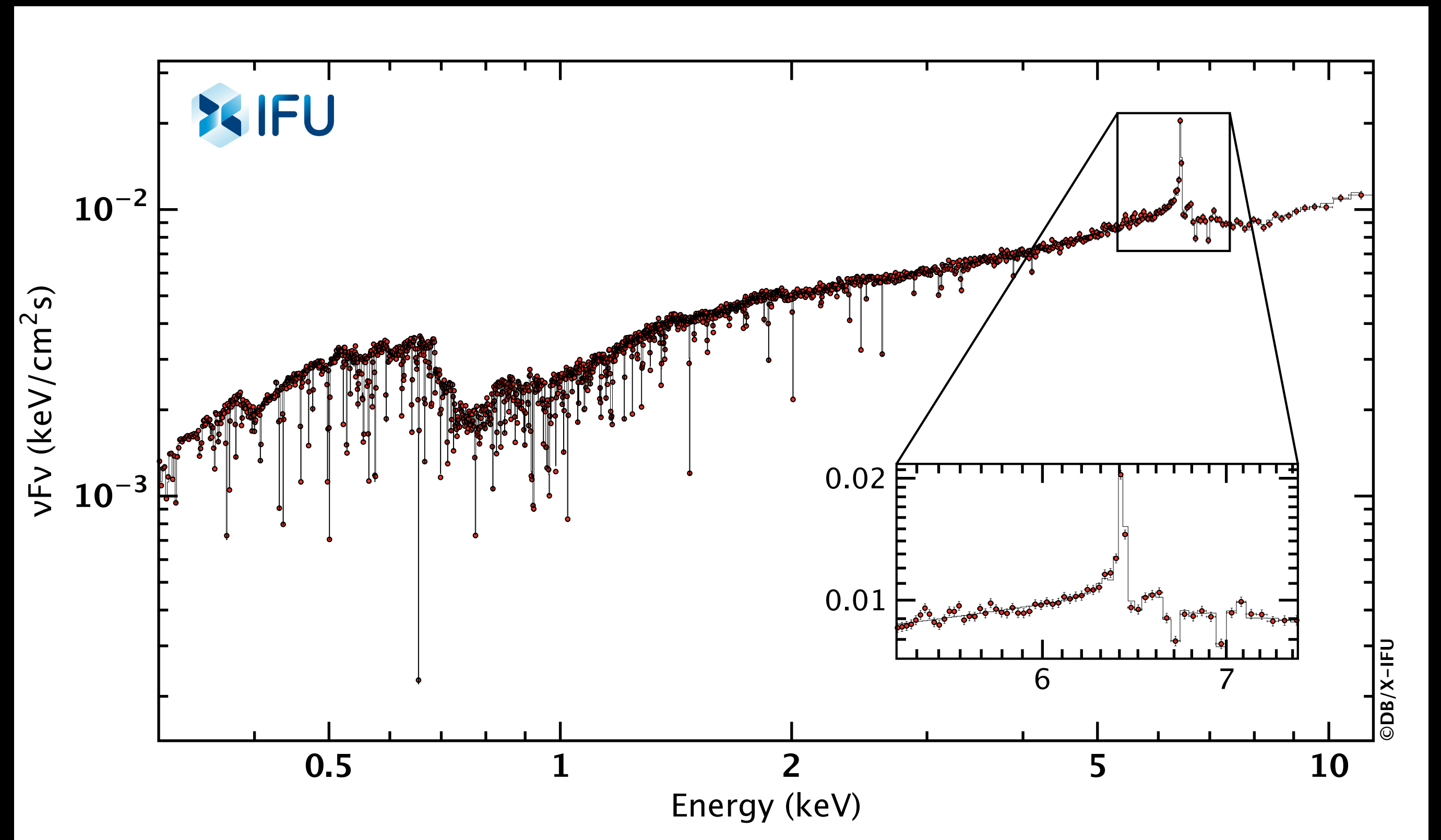
# Past, Present, and Future X-ray Detectors

*RXTE*—Decommissioned in 2012  
Resolution 1 keV @ 6 keV



JG+15

*Athena*—Expected 2030s  
Resolution  $\sim 2.5$  eV @ 6 keV

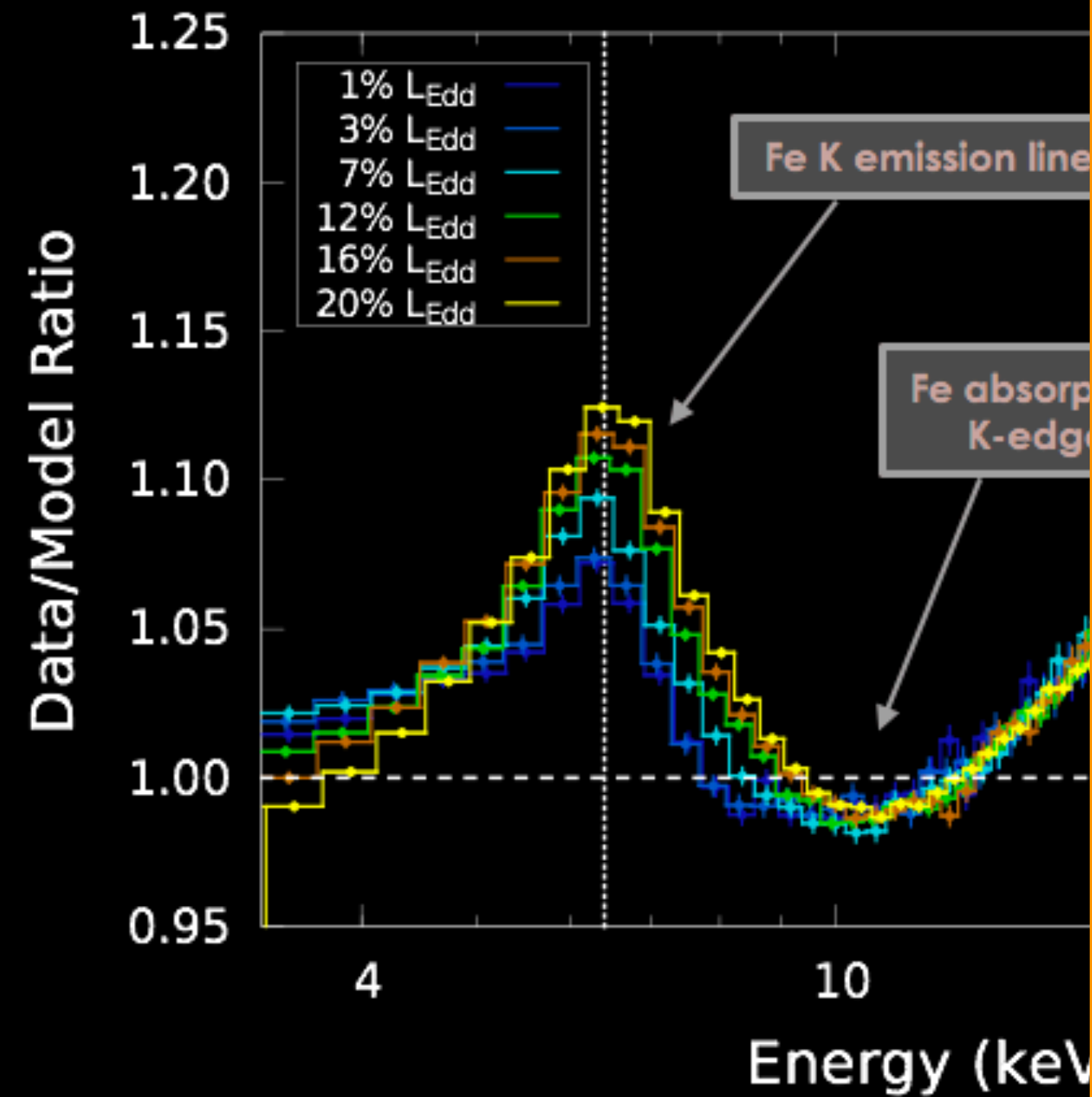


Barret & Cappi (2019)



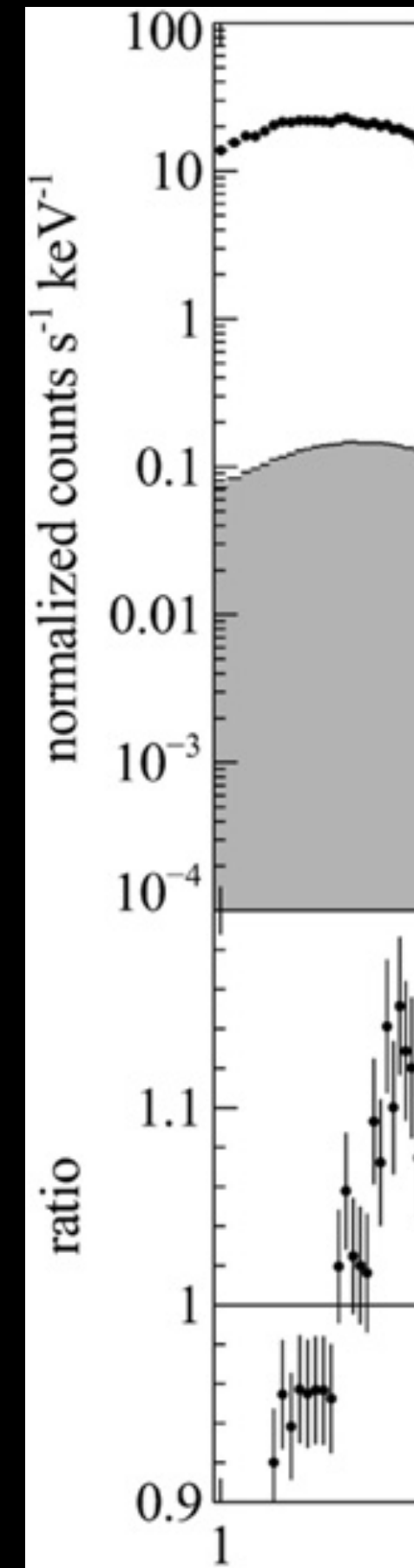
# Past, Present, and Future X-ray Detectors

*RXTE*—Decommissioned  
Resolution 1 keV



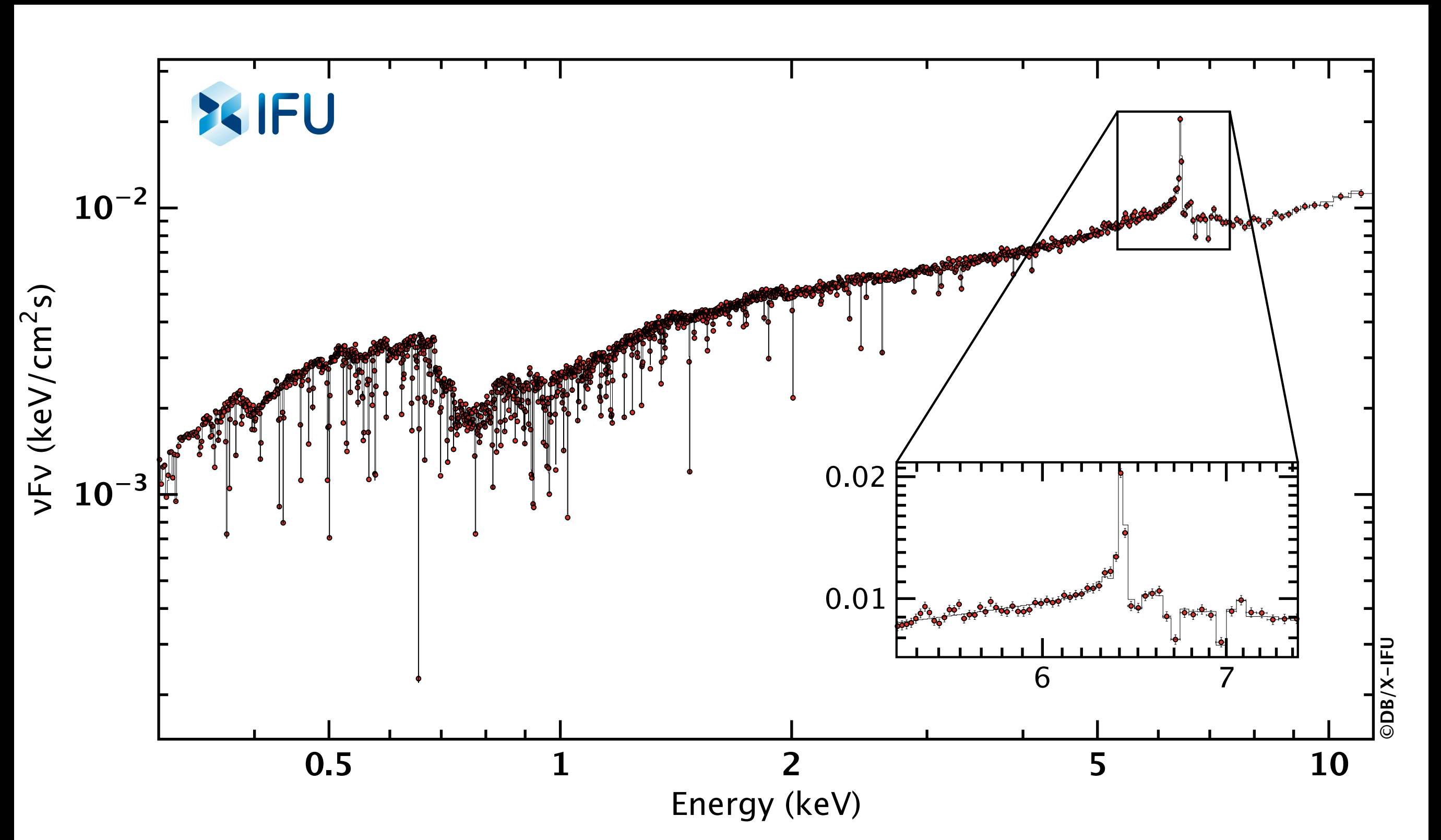
JG+15

*NuSTAR*—Launched 2012  
Resolution 0.4 keV @ 6 keV



Parker et al.

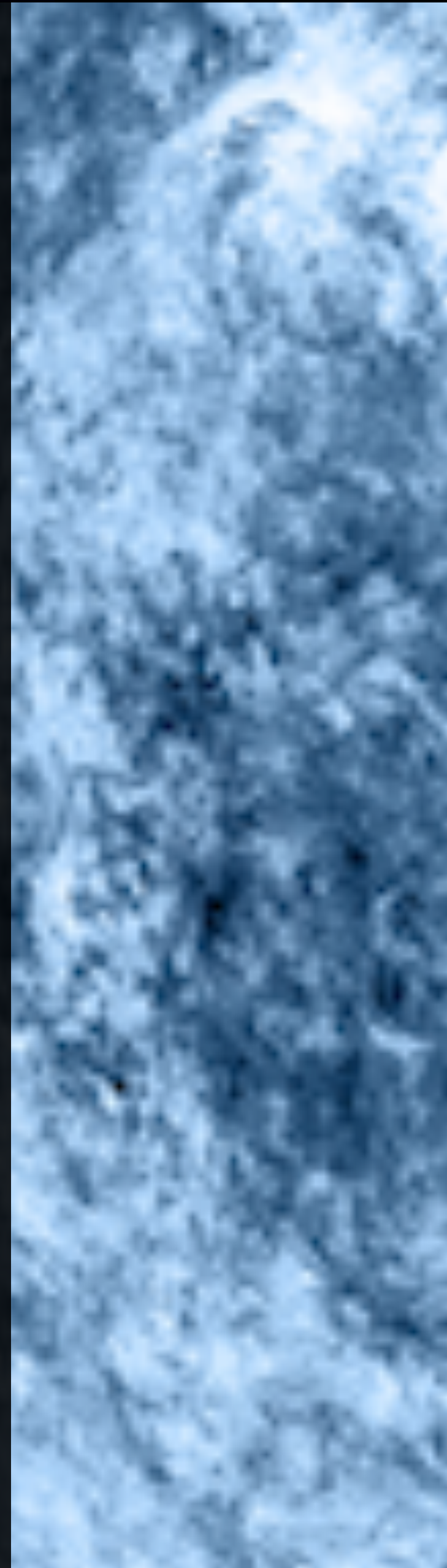
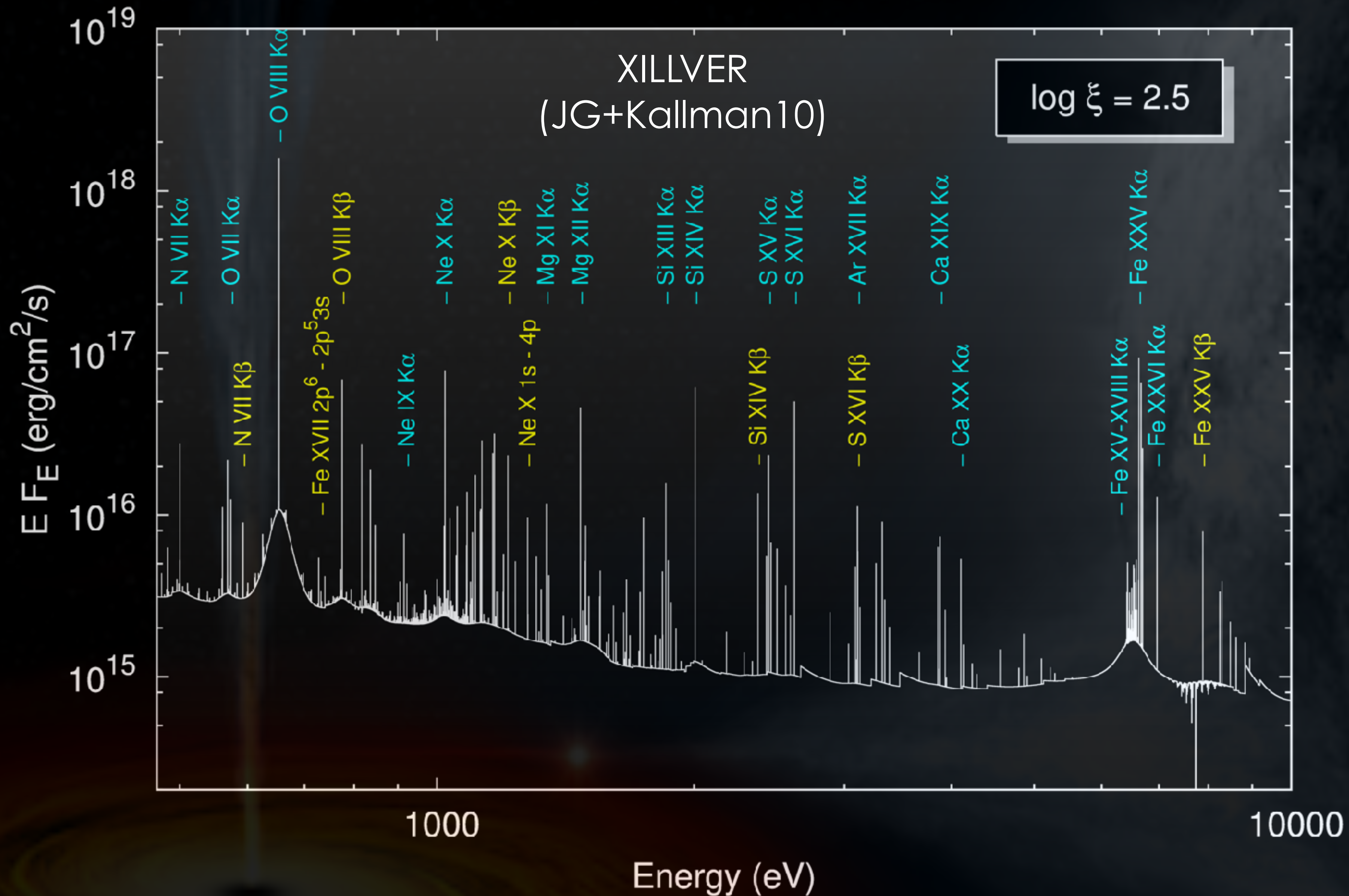
*Athena*—Expected 2030s  
Resolution ~2.5 eV @ 6 keV



Barret & Cappi (2019)

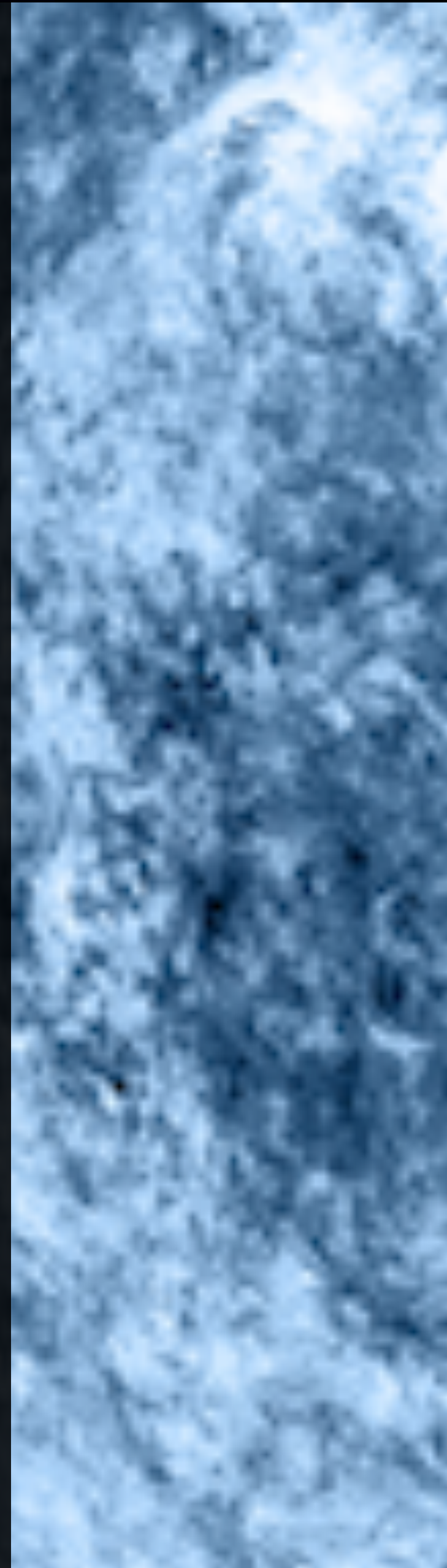
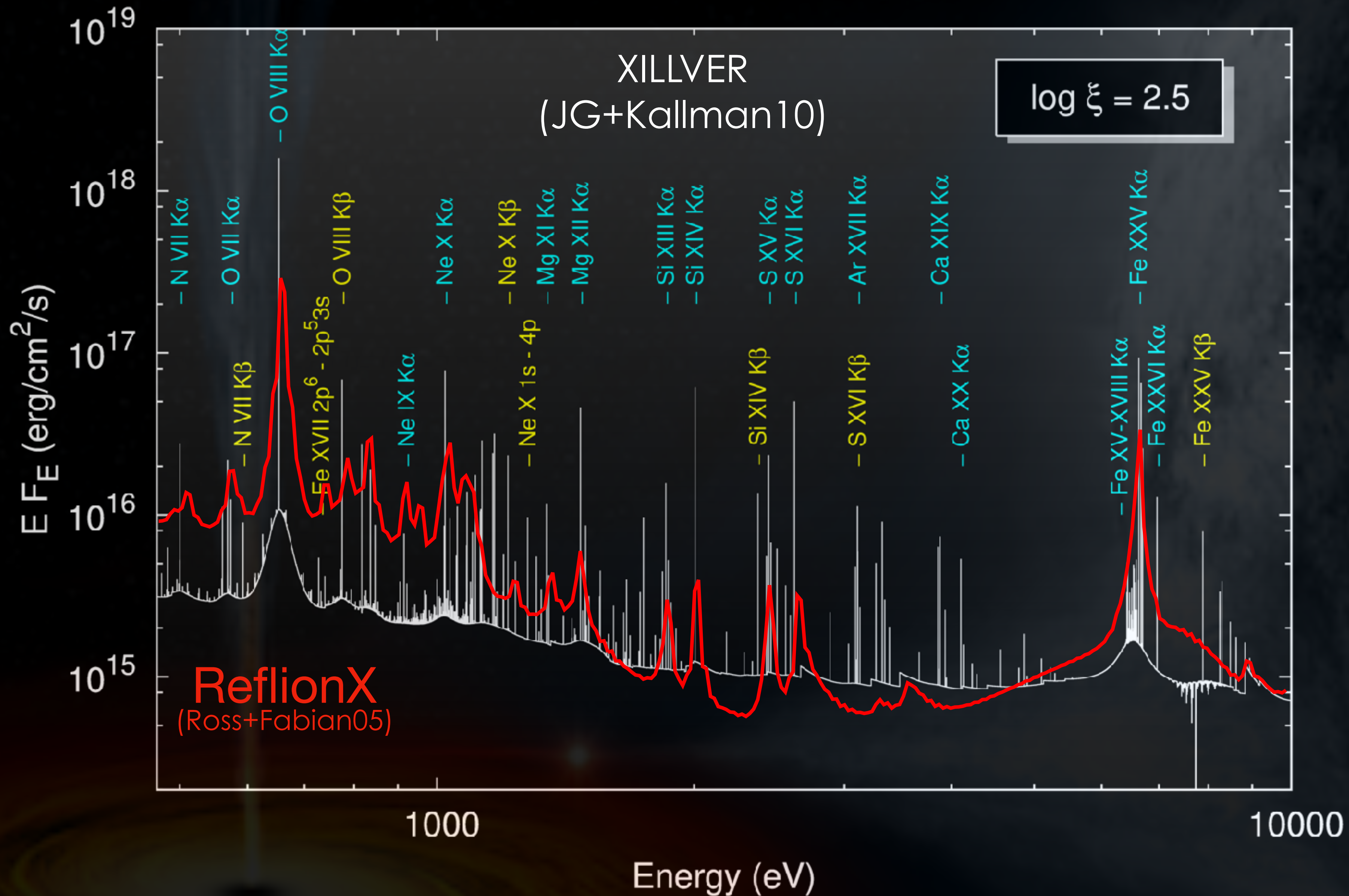


# X-ray Reflection at High-Resolution ( $\sim\mu\text{-cal}$ )



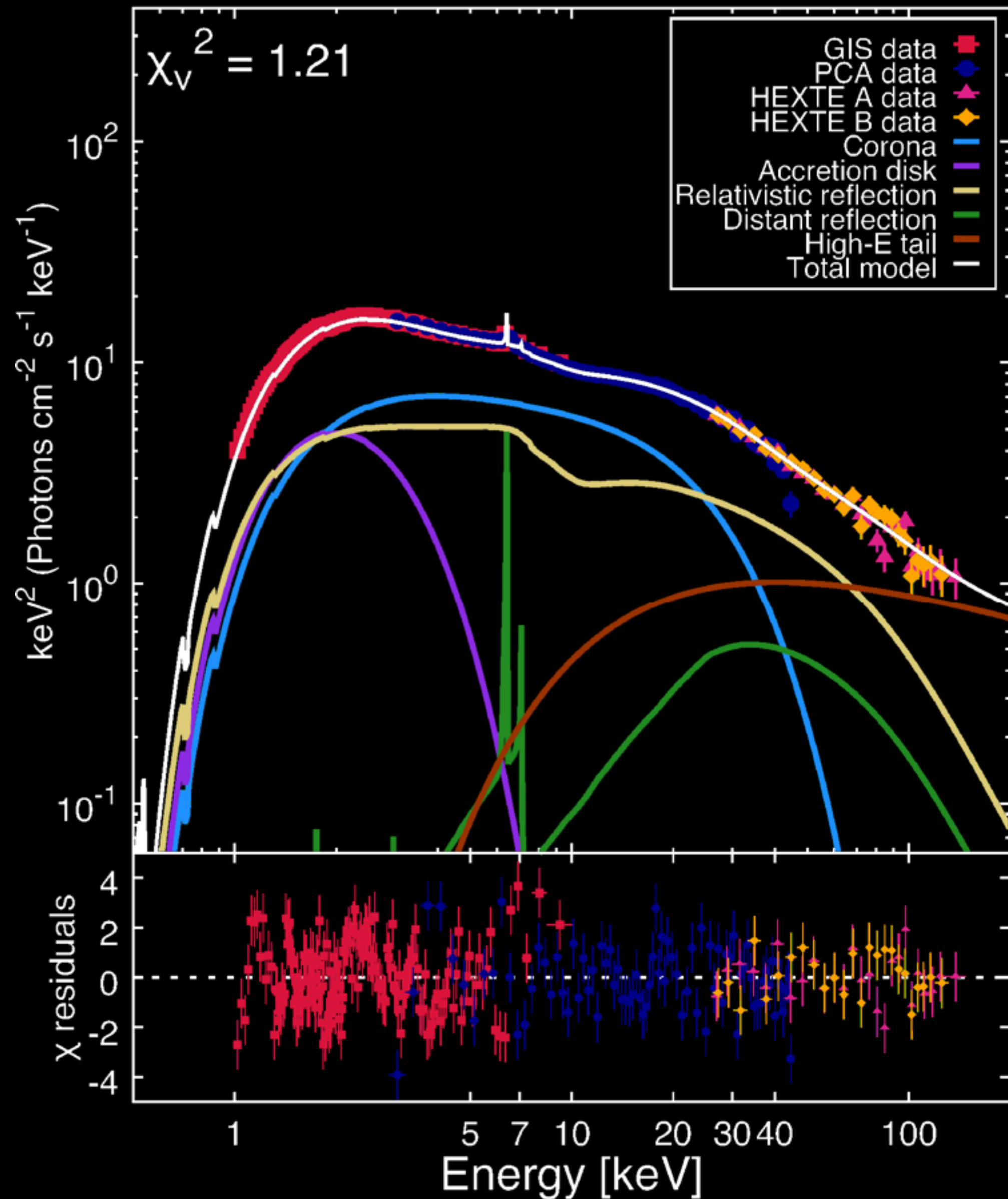


# X-ray Reflection at High-Resolution ( $\sim\mu$ -cal)

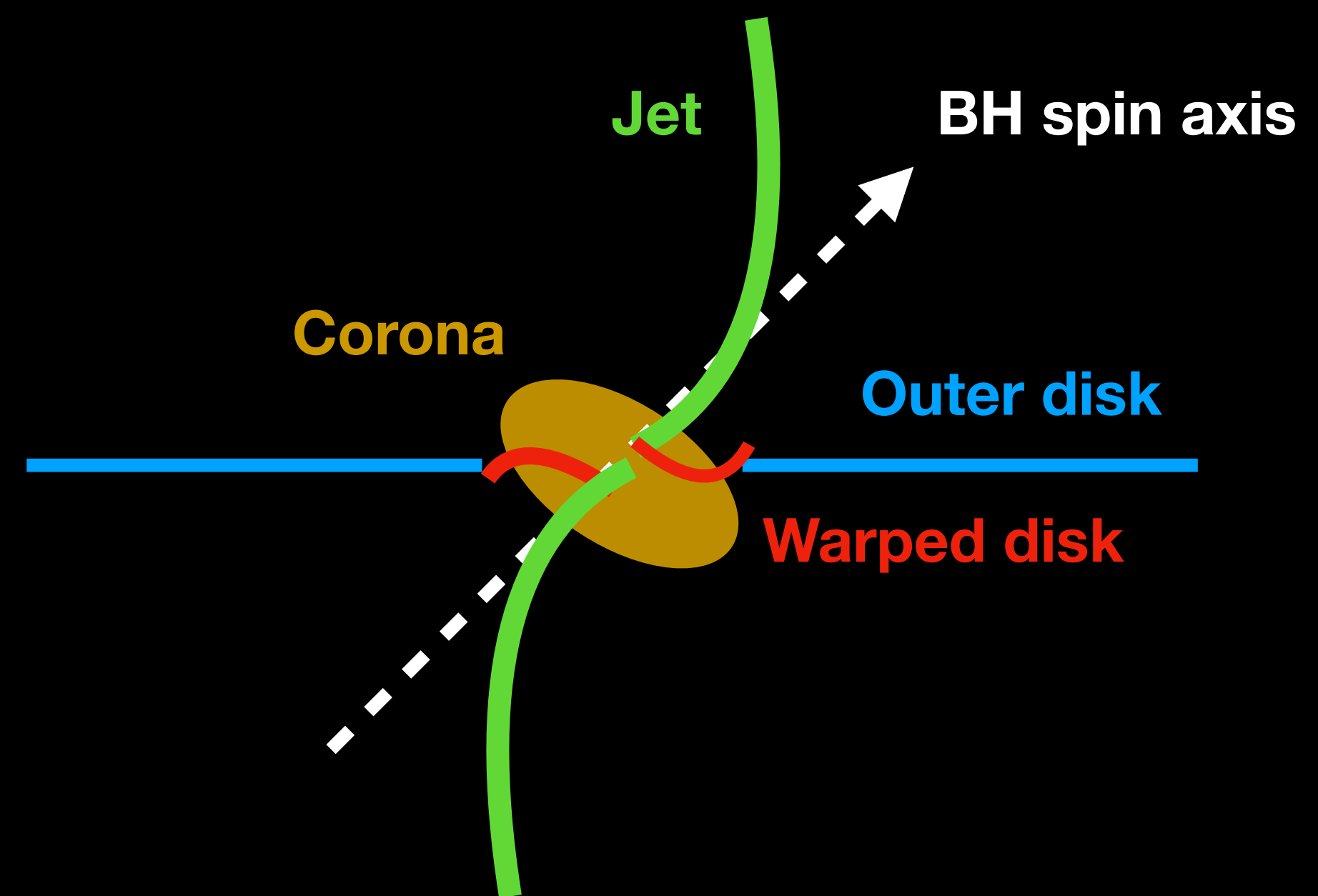




# XTE J1550—564: LOW INCLINATION DISK?



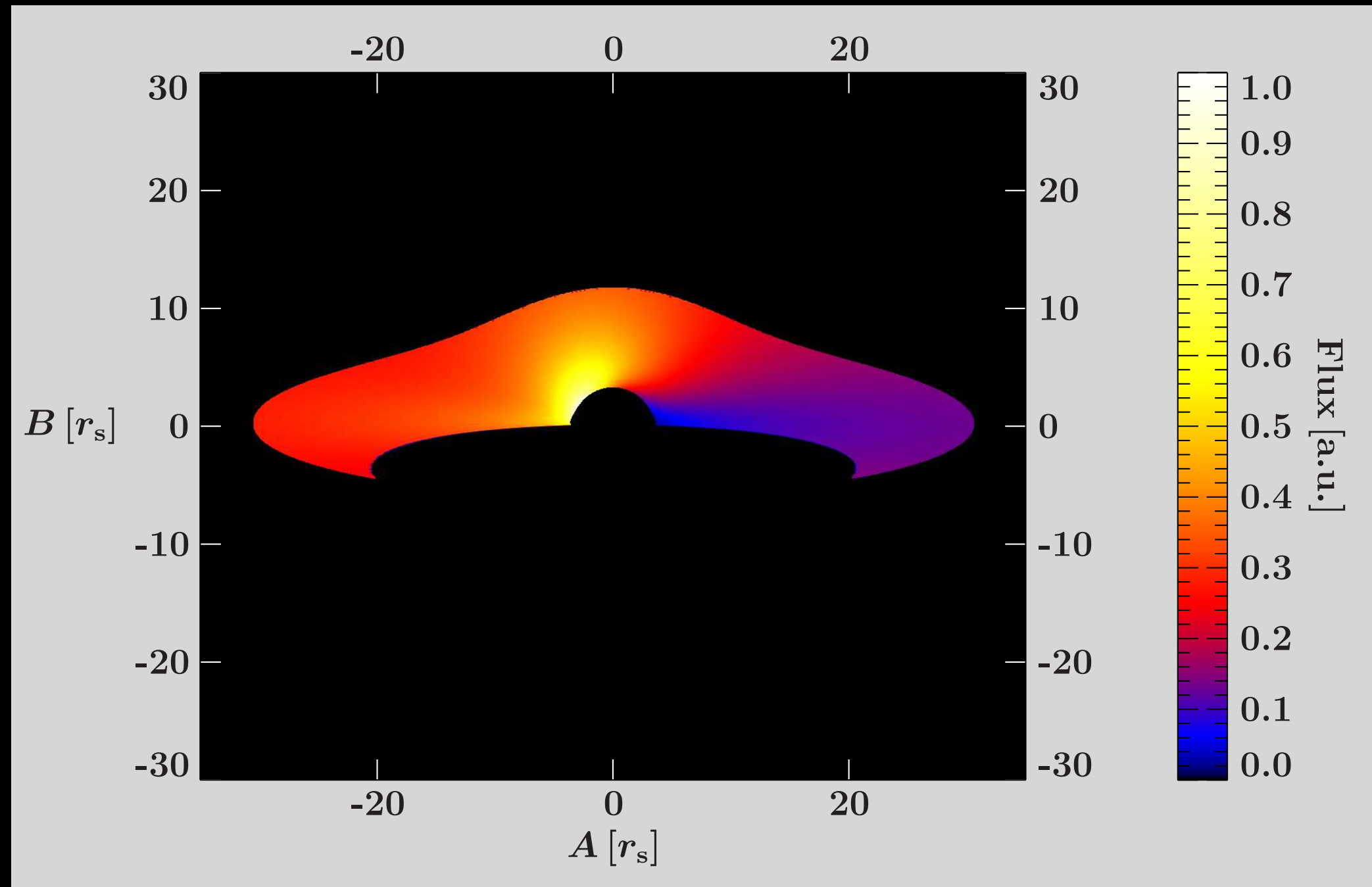
Inclination from reflection modeling inconsistent with radio jet and optical monitoring determinations of the orbital inclination,  $i \sim 40$  deg, as opposed to  $i \sim 75$  deg (Orosz et al. 2011, Steiner et al. 2012).



Possible misaligned inner accretion region?



# Irradiation of Flared Disks

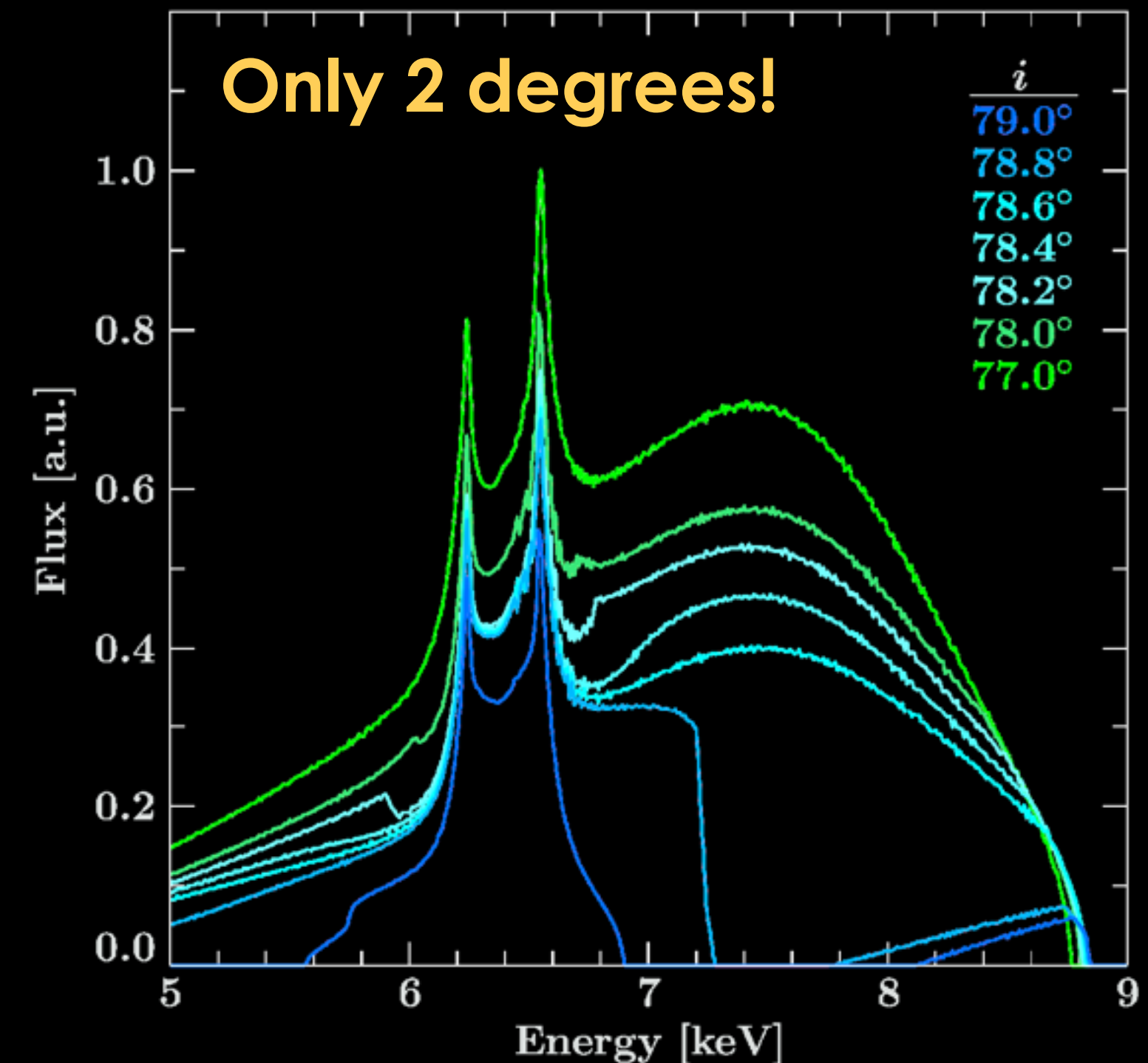


Brod et al. (2013)

Disk obscuration reduces the blue-wing of the Fe K emission  
—> **Resembles lower inclination!**

## Obscuration effects:

Under an inclination of **78.5°**, part of the disk is covered, affecting both the **line profiles** and the **time lags**



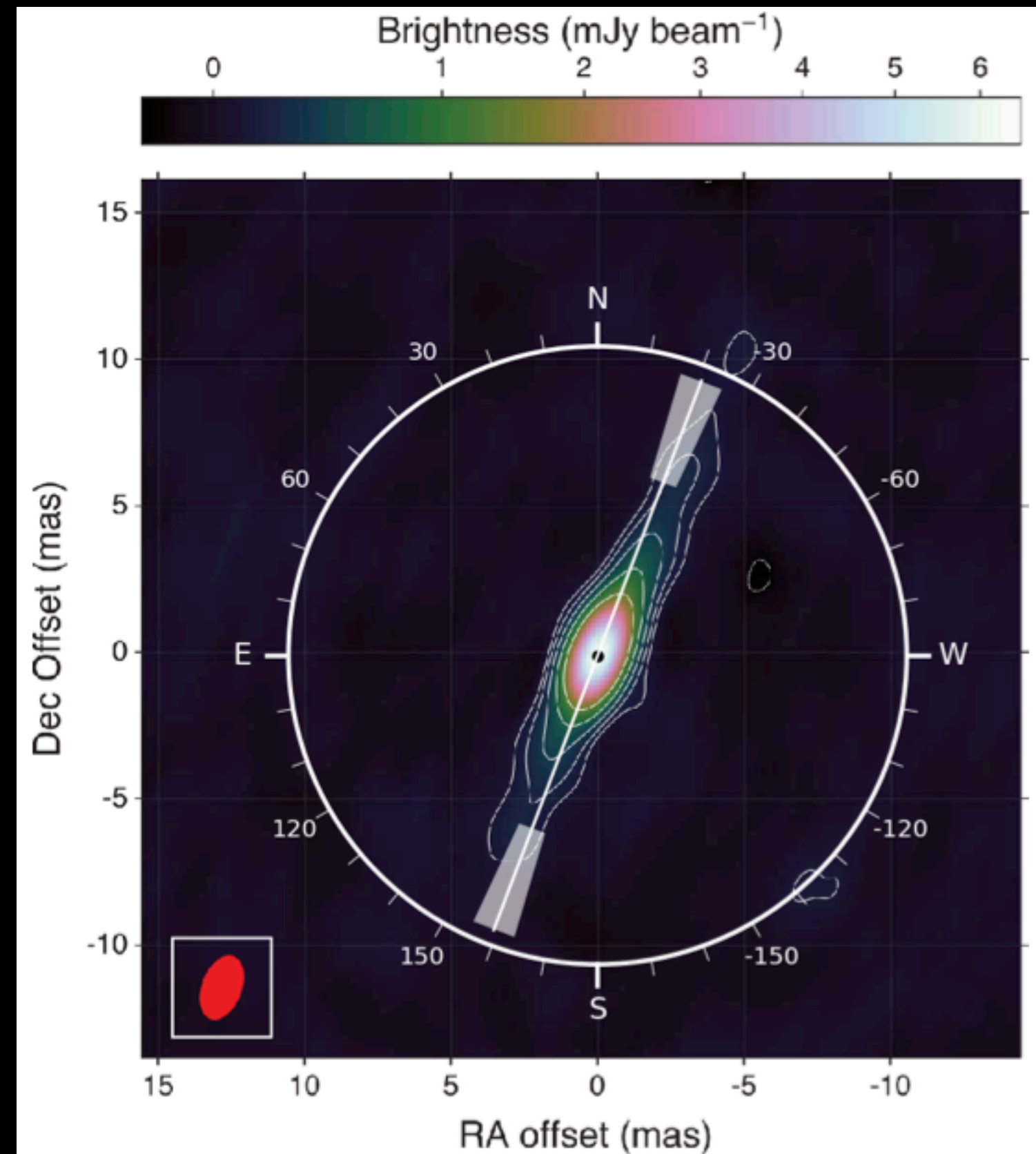


# X-ray Polarization Measurements: **Cyg X-1**



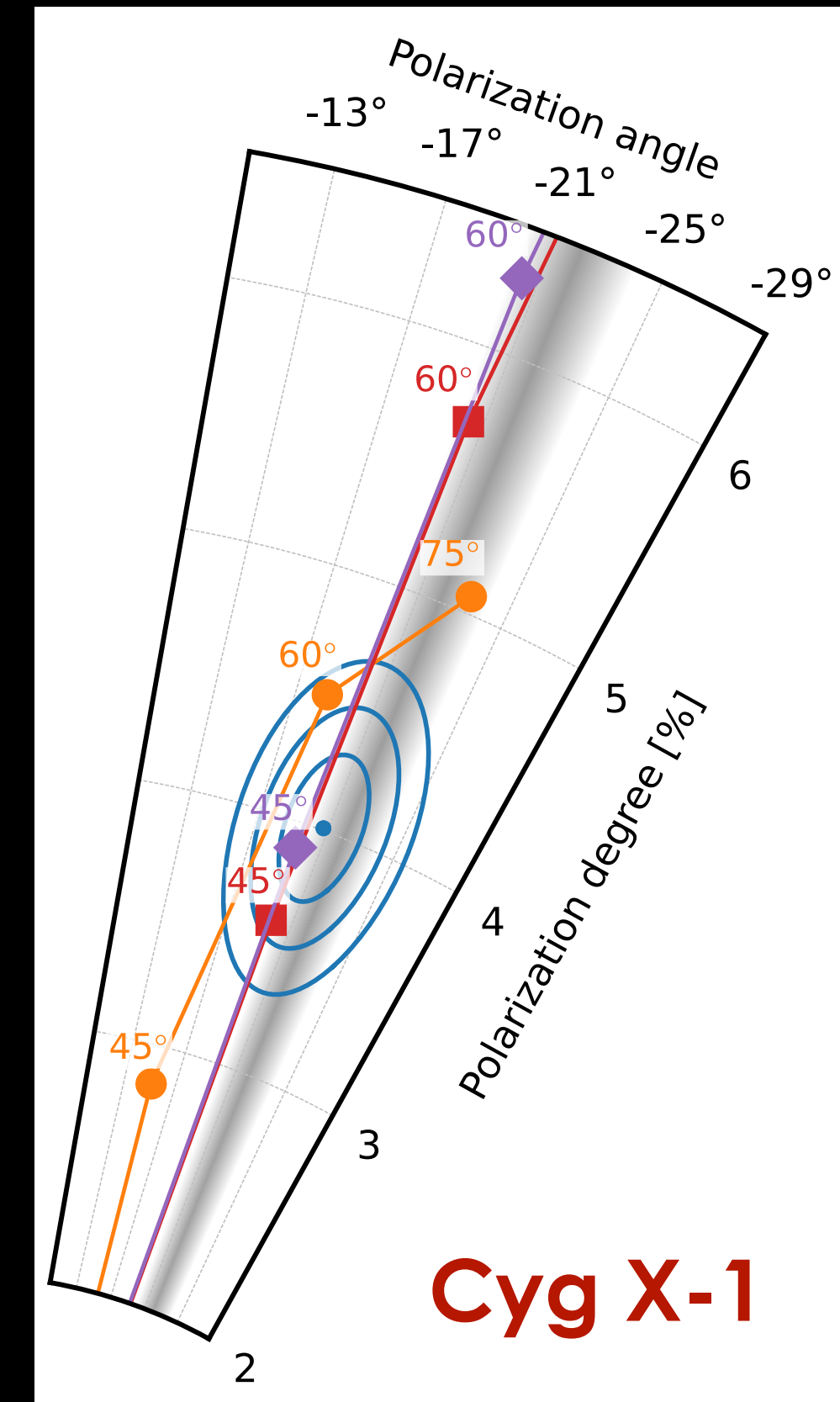
IXPE: The Imaging X-ray Polarimetry Explorer

Polarization angle parallel to the outflowing radio jet



Krawczynski, ..., JG+22

Detection of linear polarization degree of **4.0 +/- 0.2 %** in 2–8 keV (**>20 sigma**)



Larger than expected polarization requires a disk inclination larger than the orbit!



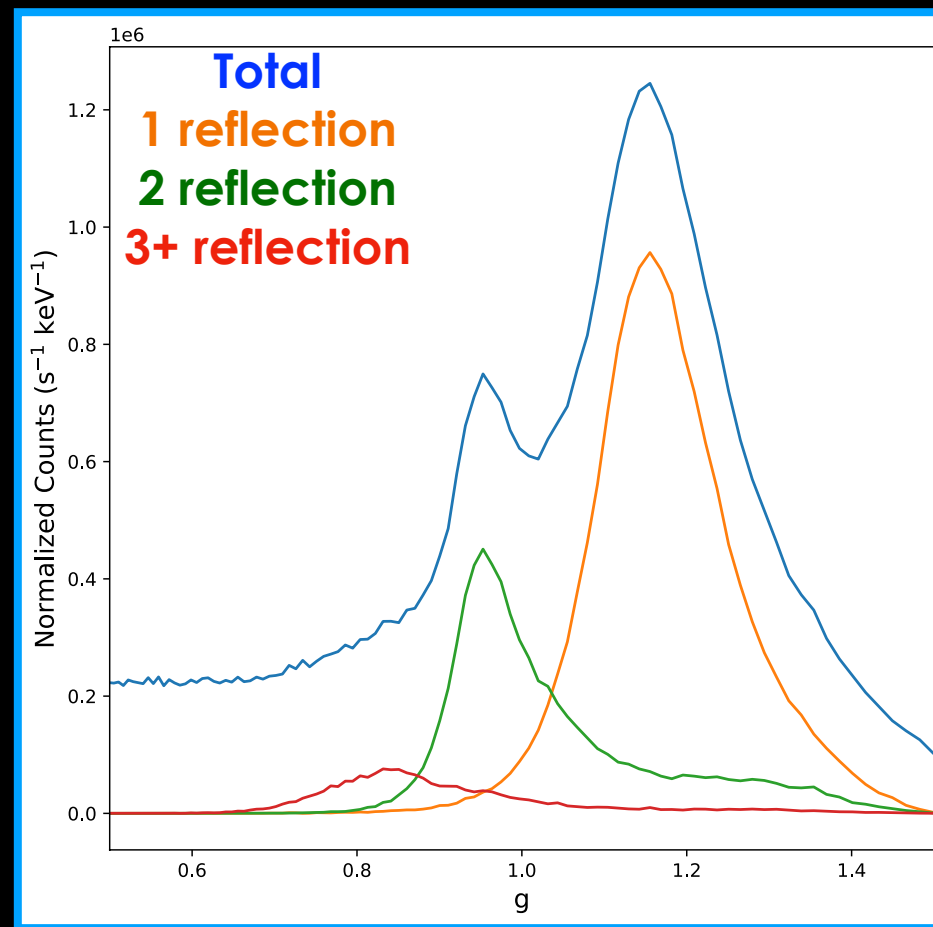
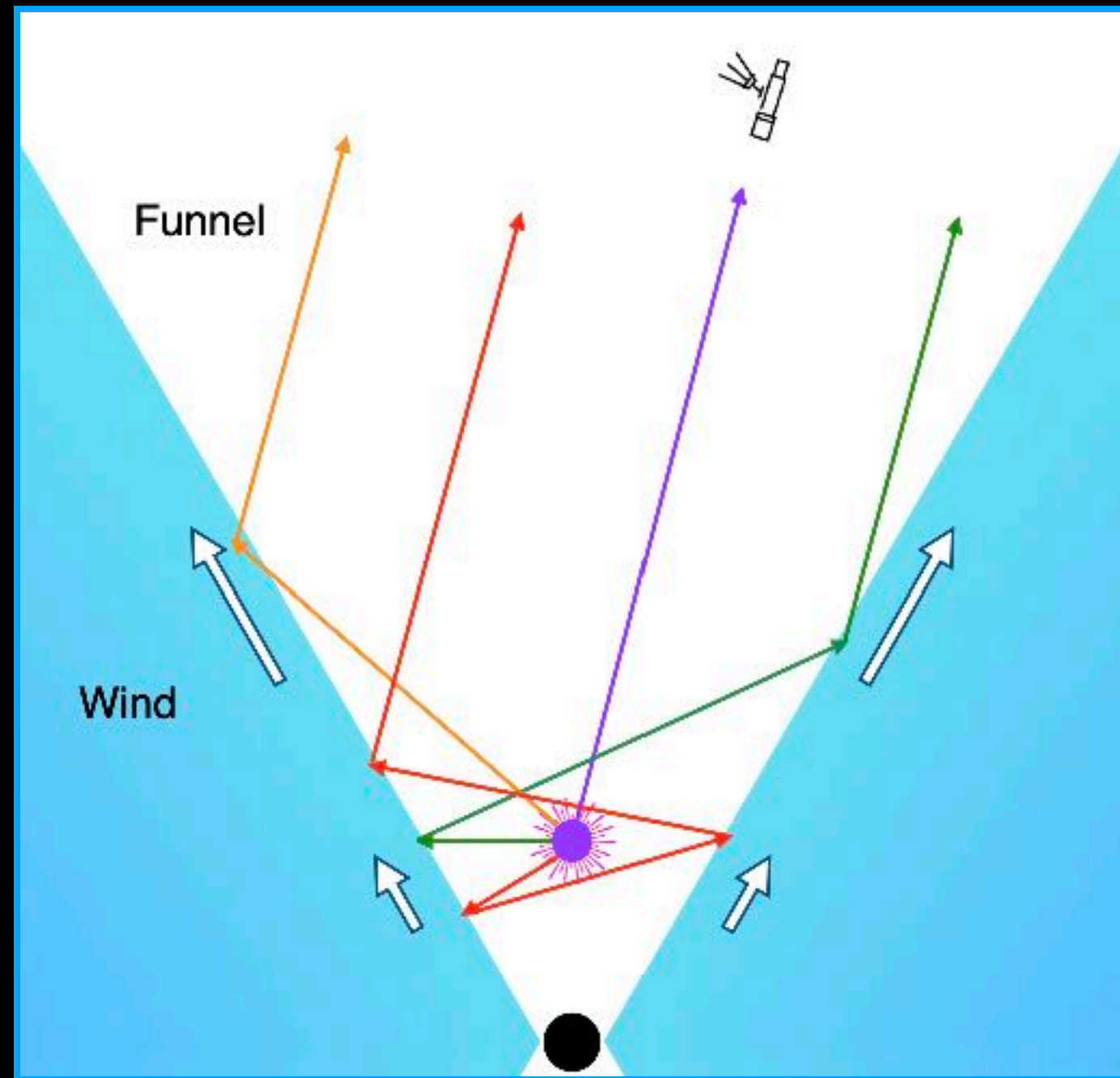
# Super-Eddington Accretion

Multiple reflections in a funnel  
(simulations by Zijan Zhang and Jane Dai)

Lamppost corona height:  $h_{\text{LP}}$

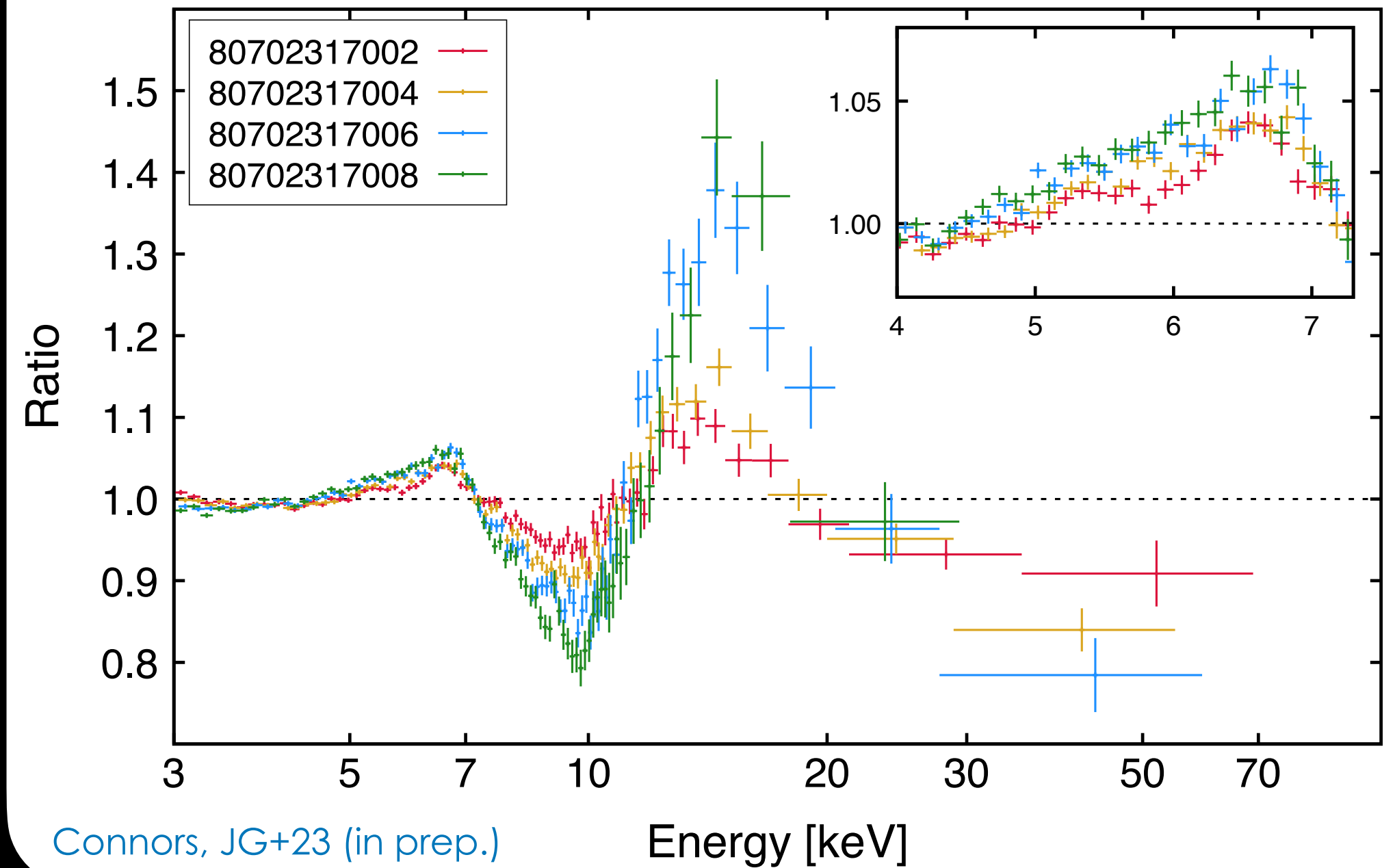
Funnel half open angle:  $\theta$

$$\text{Wind velocity: } v(r) = \left( \frac{r - 6R_g}{r + R_{\text{acc}}} \right) v_t$$



Monte Carlo  
Ray Tracing

4U 1543—47 observed by NuSTAR



$$h_{\text{LP}} = 30R_g, v_t = 0.5c, R_{\text{acc}} = 30R_g, \theta = 30^\circ$$



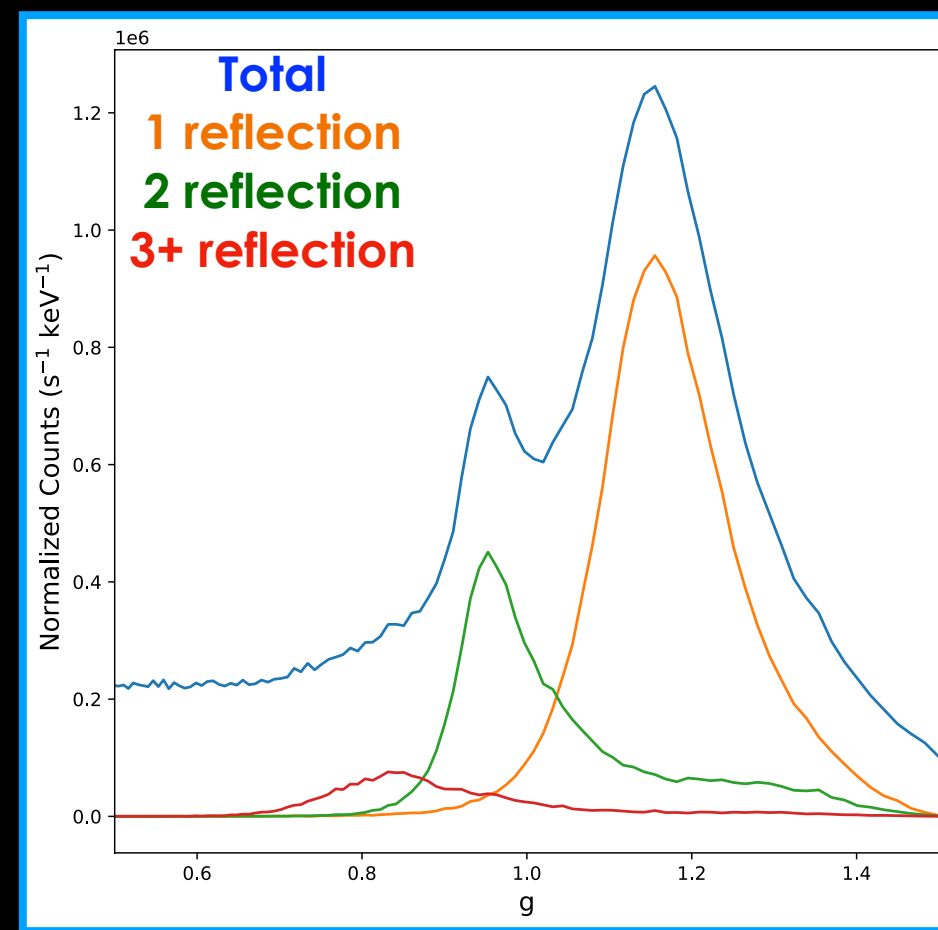
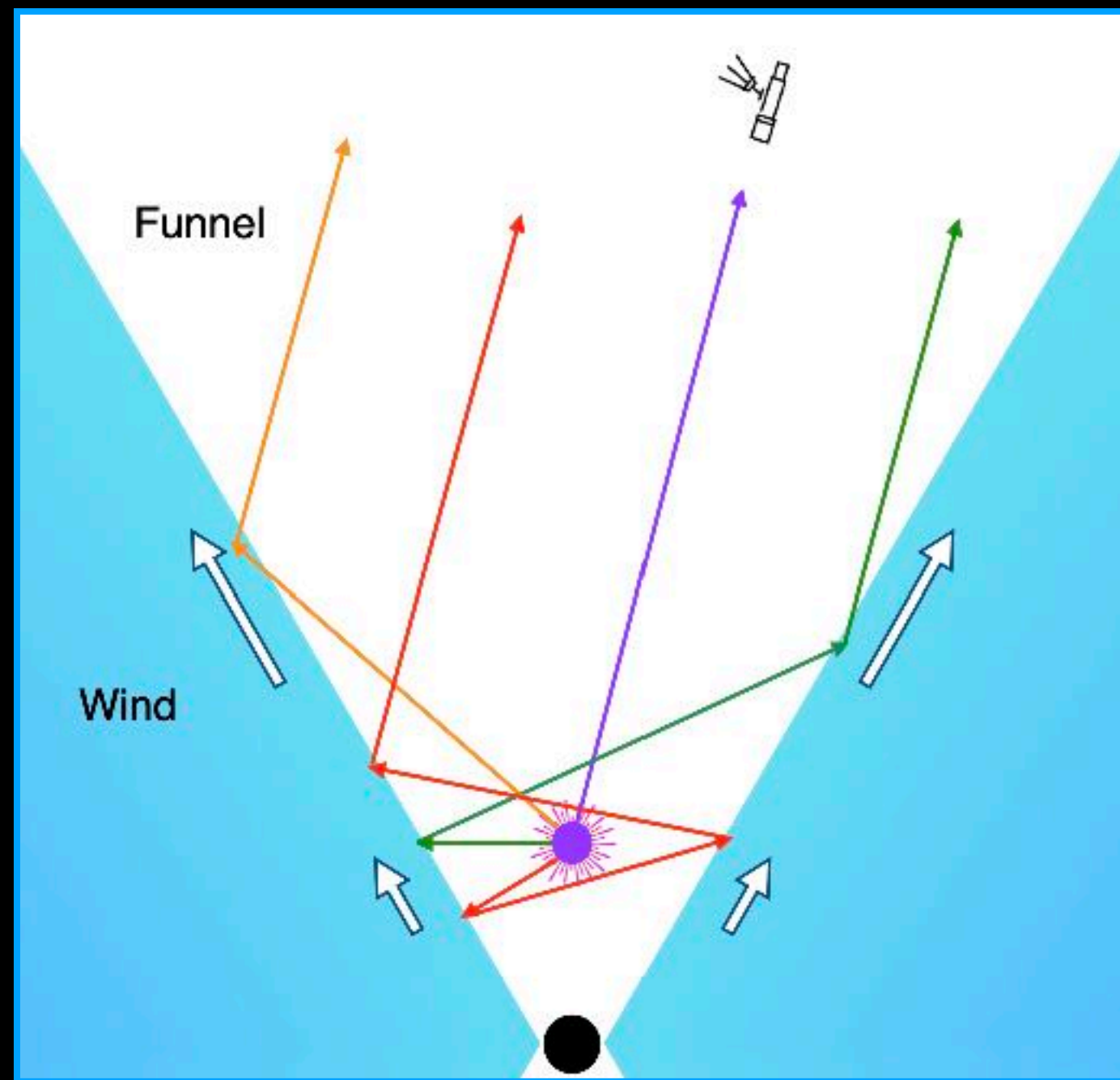
# Super-Eddington Accretion

Multiple reflections in a funnel  
(simulations by Zijan Zhang and Jane Dai)

Lamppost corona height:  $h_{LP}$

Funnel half open angle:  $\theta$

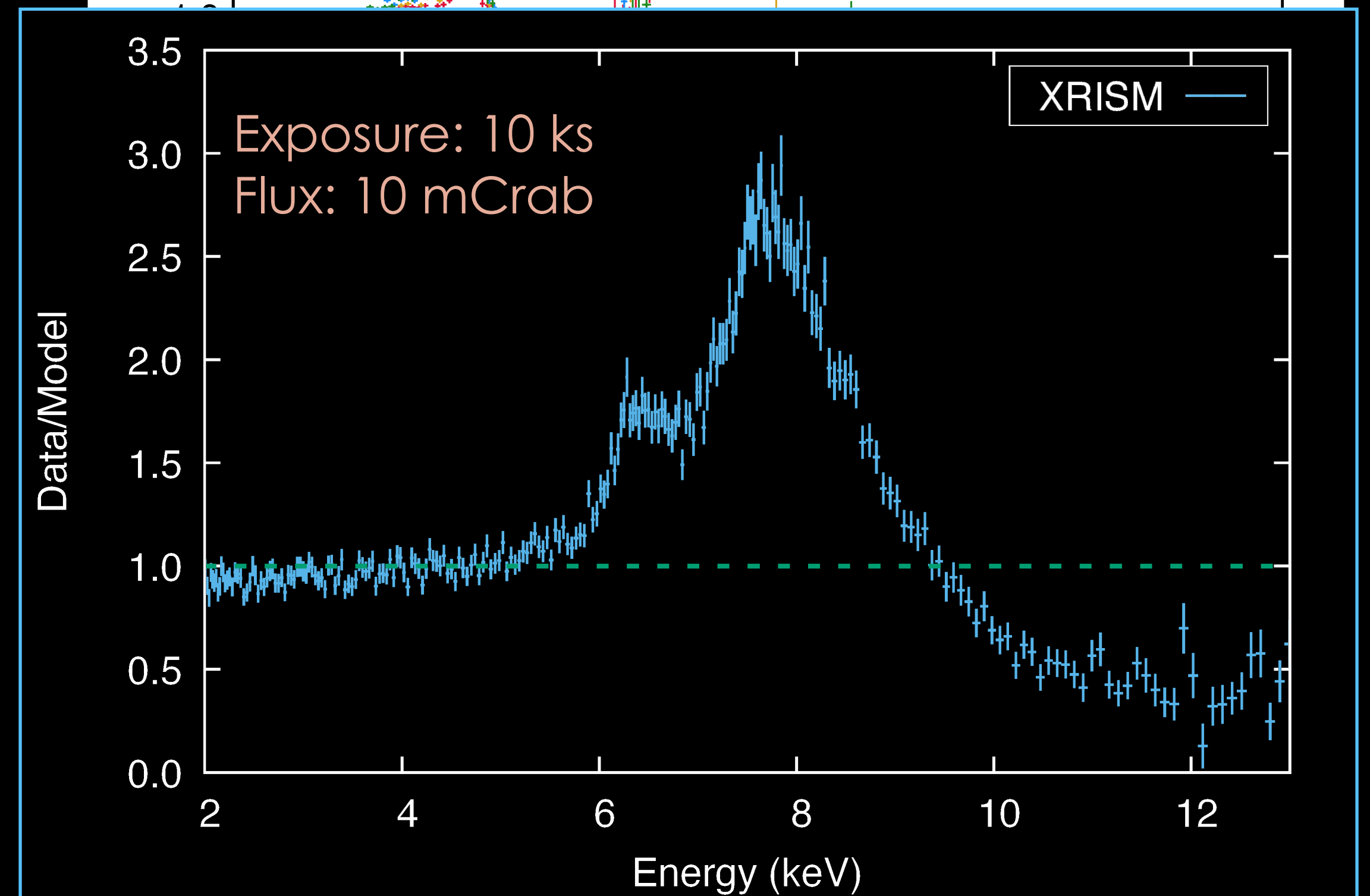
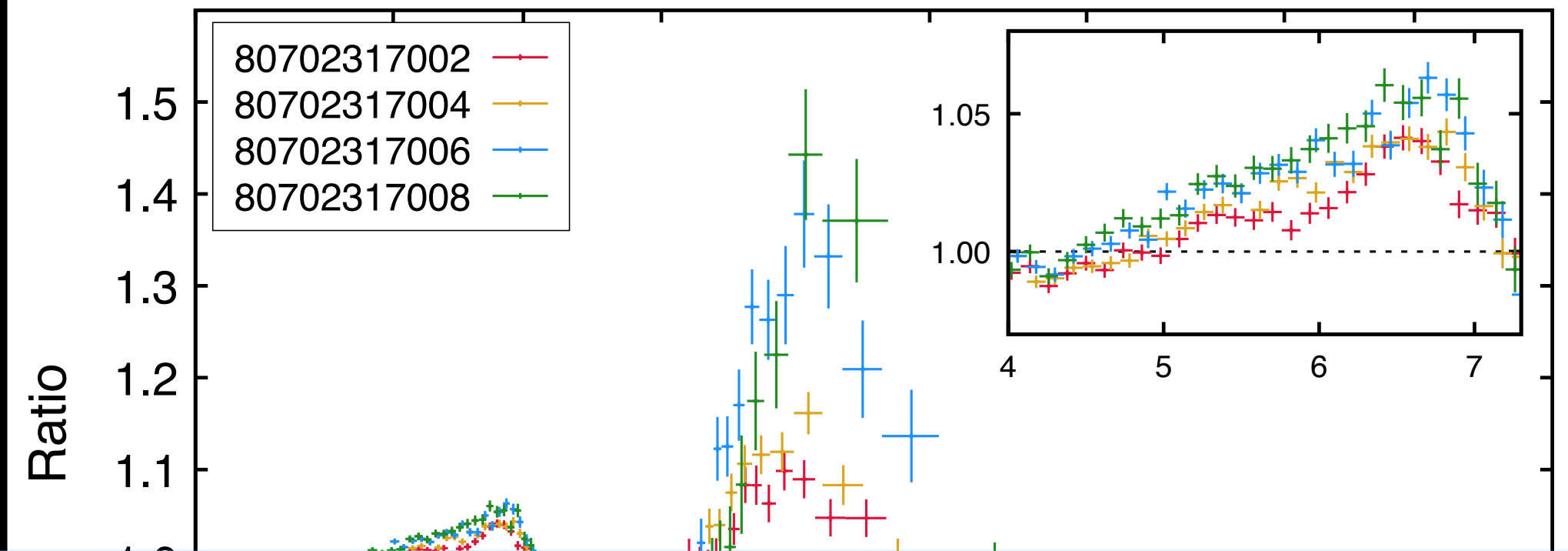
$$\text{Wind velocity: } v(r) = \left( \frac{r - 6R_g}{r + R_{acc}} \right) v_t$$



Monte Carlo  
Ray Tracing

$$h_{LP} = 30R_g, v_t = 0.5c, R_{acc} = 30R_g, \theta = 30^\circ$$

4U 1543—47 observed by NuSTAR





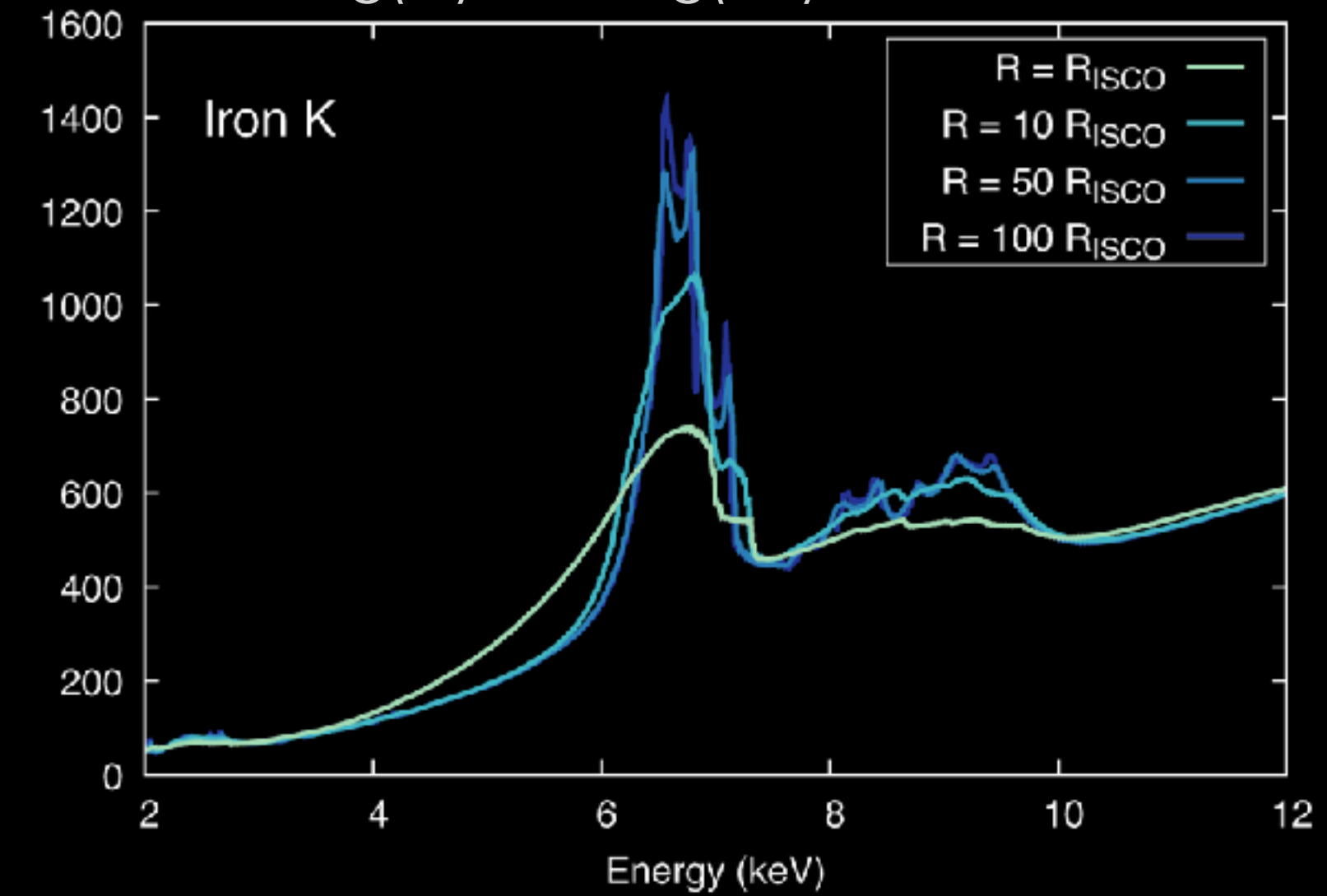
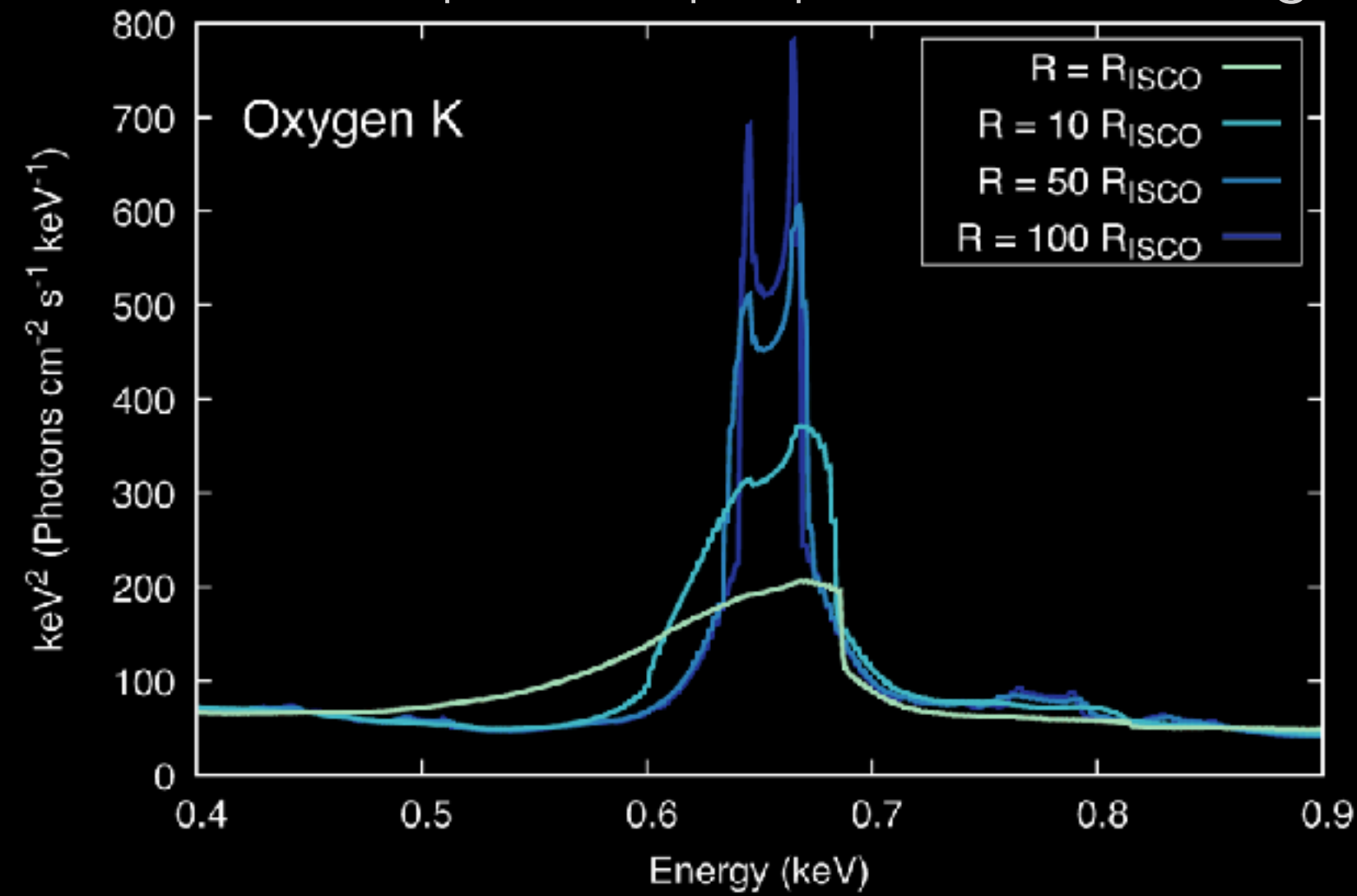
# Relativistic Reflection: **relxillNS**

**Table 2.** List of Parameters for the **relxillNS** Model

Parameter	Symbol (Units)	Range
Inner Emissivity Index	$q_1$	$[-10, 10]$
Outer Emissivity Index	$q_2$	$[-10, 10]$
Break Radius	$R_{\text{Br}} (R_g)$	$[1 - 1000]$
Spin Parameter	$a_*$ ( $cJ/GM^2$ )	$[-0.998, 0.998]$
Inclination	$i$ (degrees)	$[3, 87]$
Inner Disk Radius	$R_{\text{in}} (R_{\text{ISCO}})$	$[1, 1000]$
Outer Disk Radius	$R_{\text{out}} (R_g)$	$[1, 1000]$
Blackbody Temperature	$kT_{\text{bb}}$ (keV)	$[0.5, 10]$
Ionization Parameter	$\log(\xi/\text{erg cm s}^{-1})$	$[1, 4]$
Electron Number Density	$\log(n_e/\text{cm}^{-3})$	$[15, 19]$
Iron Abundance	$A_{\text{Fe}}$ (Solar)	$[0.5, 10]$
Reflection Fraction <sup>a</sup>	$R_{\text{frac}}$	$[0, 10]$

<sup>a</sup> If this parameter is set to negative values, the model only outputs the reflection component, without the continuum.

**relxillNS** spectra:  $q_1=q_2=0$ ,  $a=0$ ,  $i=30$  deg,  $kT_{\text{bb}}=4$  keV,  $\log(\xi)=3.1$ ,  $\log(n_e)=15$ ,  $A_{\text{Fe}}=5$ ,  $R_{\text{f}}=1$



JG, Dauser, Ludlam+22



# Relativistic Reflection: **relxillNS**

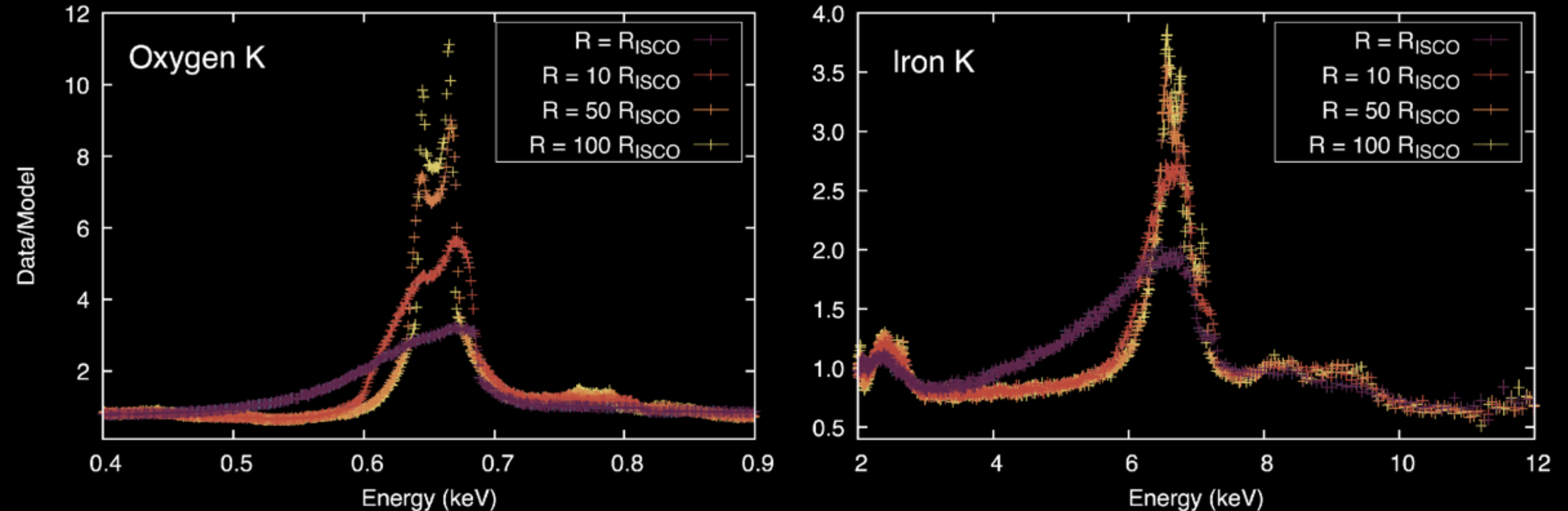
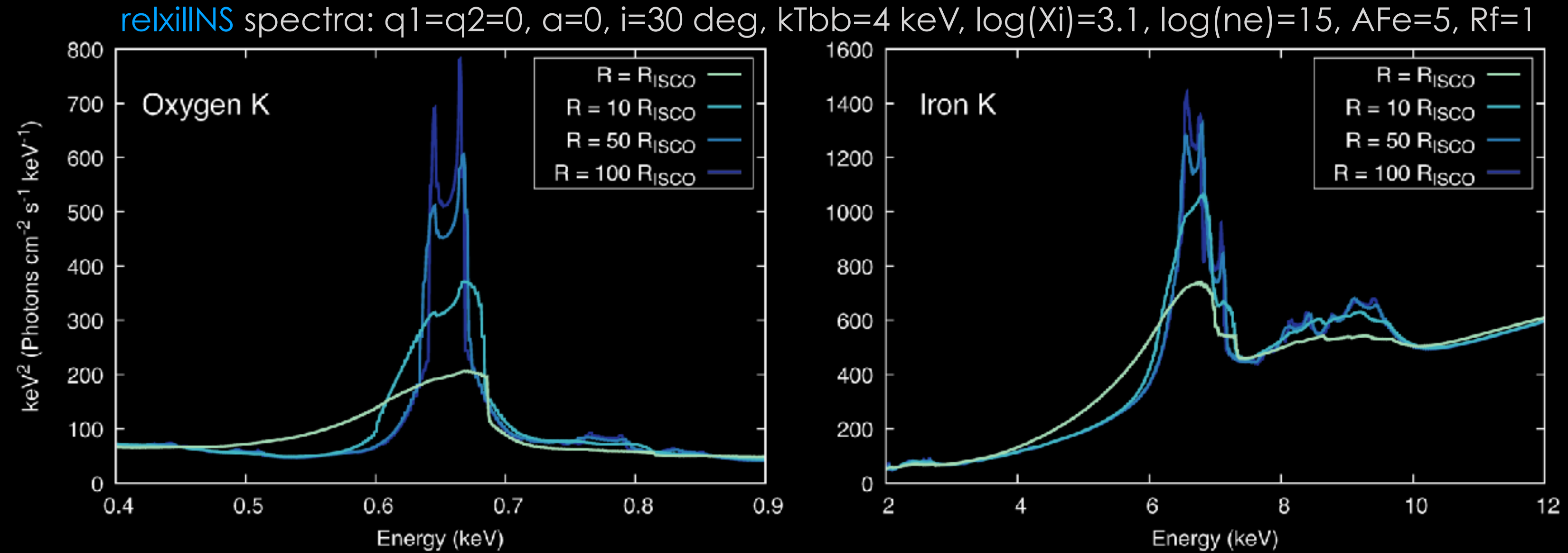
**Table 2.** List of Parameters for the **relxillNS** Model

Parameter	Symbol (Units)	Range
Inner Emissivity Index	$q_1$	$[-10, 10]$
Outer Emissivity Index	$q_2$	$[-10, 10]$
Break Radius	$R_{Br} (R_g)$	$[1 - 1000]$
Spin Parameter	$a_*$ ( $cJ/GM^2$ )	$[-0.998, 0.998]$
Inclination	$i$ (degrees)	$[3, 87]$
Inner Disk Radius	$R_{in} (R_{ISCO})$	$[1, 1000]$
Outer Disk Radius	$R_{out} (R_g)$	$[1, 1000]$
Blackbody Temperature	$kT_{bb}$ (keV)	$[0.5, 10]$
Ionization Parameter	$\log(\xi/\text{erg cm s}^{-1})$	$[1, 4]$
Electron Number Density	$\log(n_e/\text{cm}^{-3})$	$[15, 19]$
Iron Abundance	$A_{Fe}$ (Solar)	$[0.5, 10]$
Reflection Fraction <sup>a</sup>	$R_{frac}$	$[0, 10]$

<sup>a</sup> If this parameter is set to negative values, the model only outputs the reflection component, without the continuum.

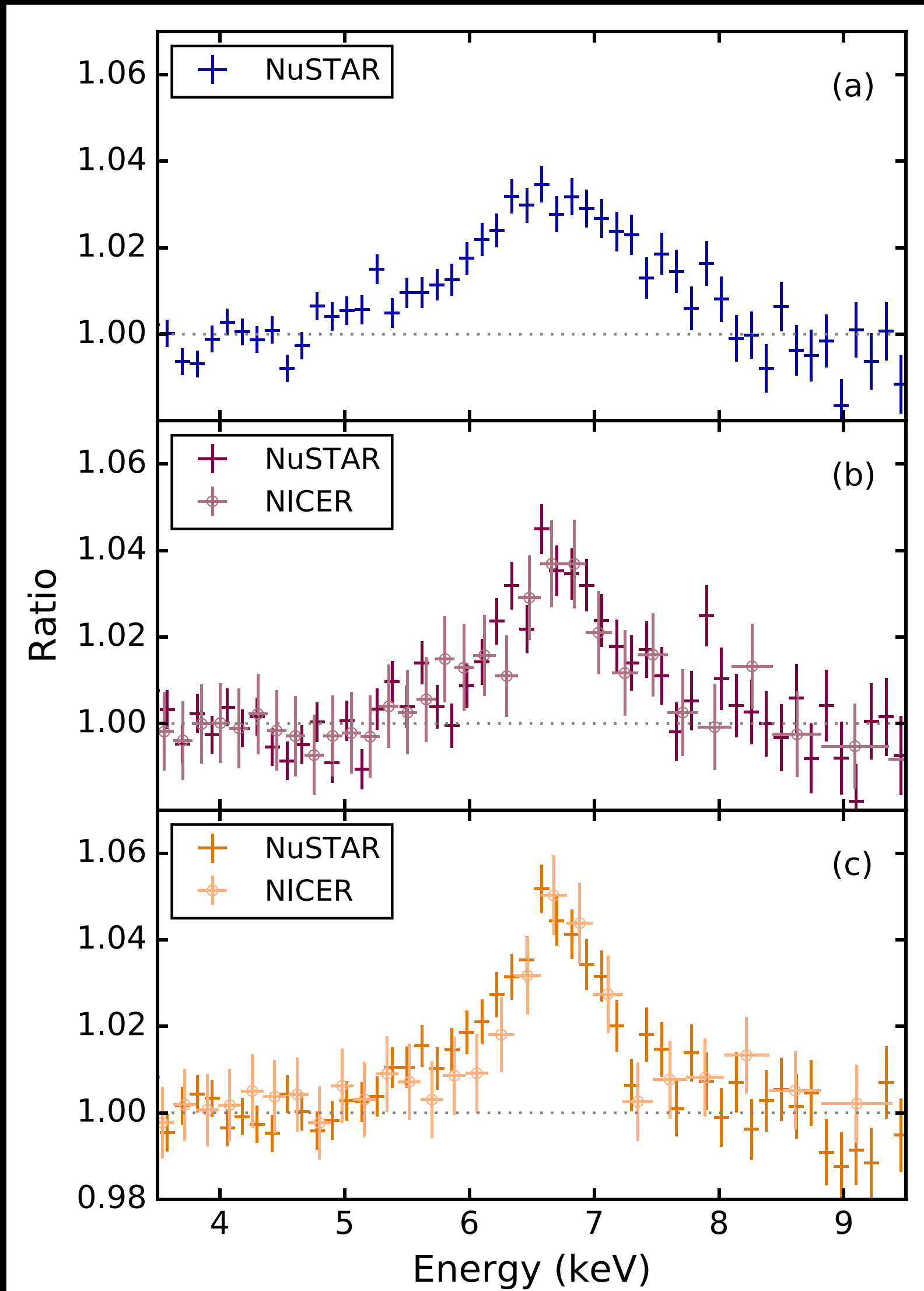
JG, Dauser, Ludlam+22

Simulated 10 ks **Athena X-IFU** observation of a 10 mCrab source

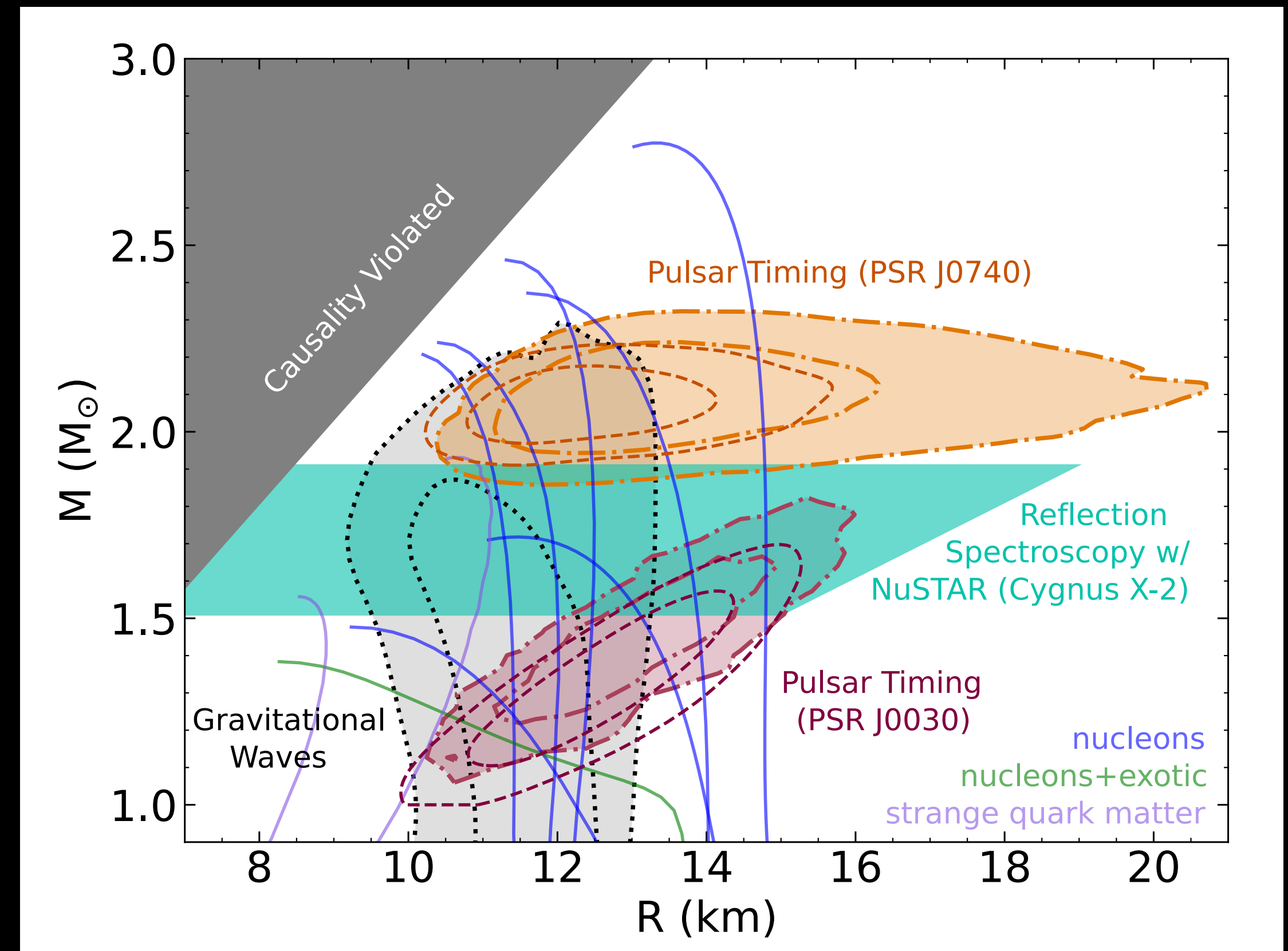




# Neutron Star Radii



NuSTAR observations of *Cygnus X-2* provide radius constraints complementary to other methods, helping to constrain models of the NS equation of state.



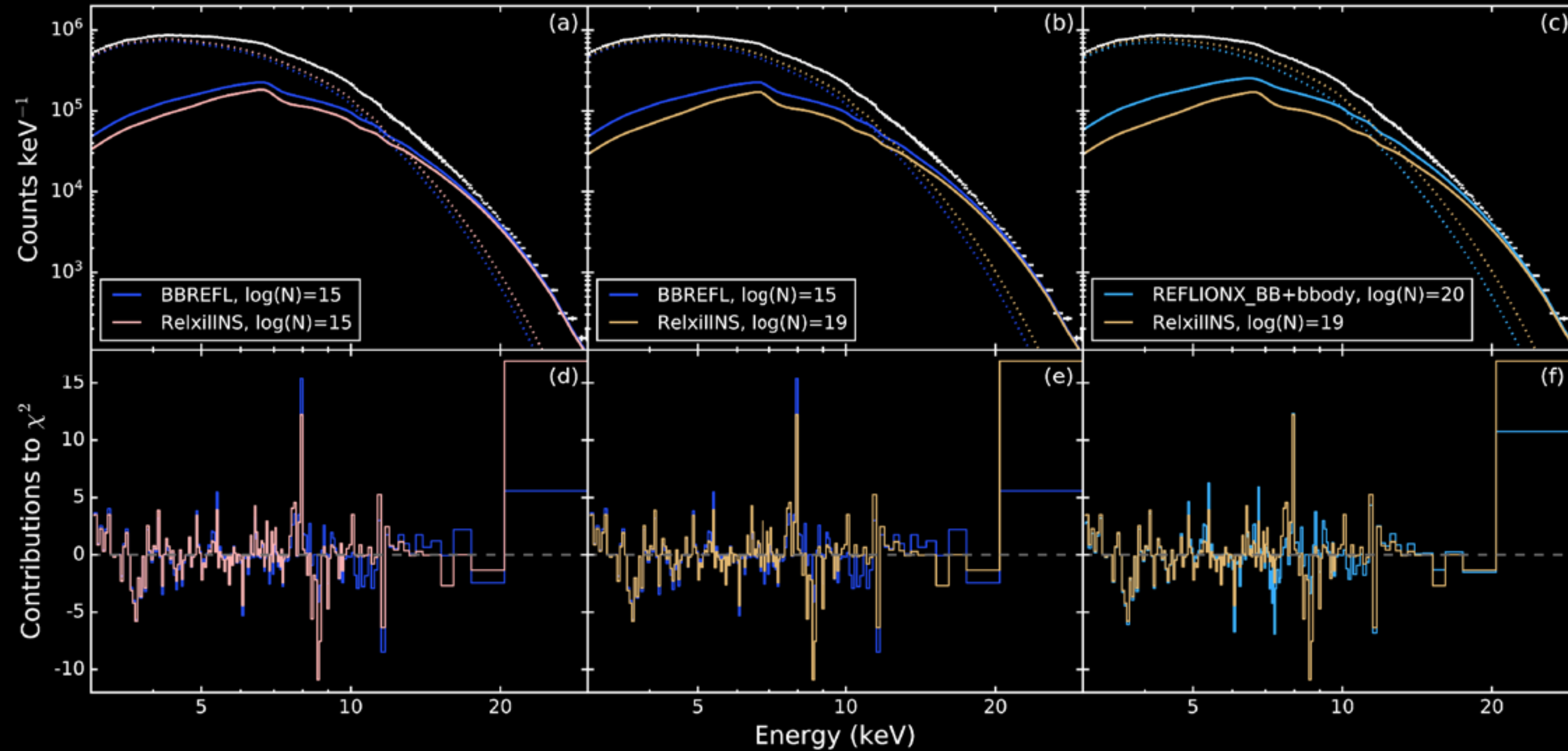


# Comparison with Previous Models

Test case **4U 1705—44**

Broadly consistent results between **relxillNS**, **BBRefl** and **ReflionX\_BB** when fitting NuSTAR data.

Larger discrepancies might be seen at softer energies



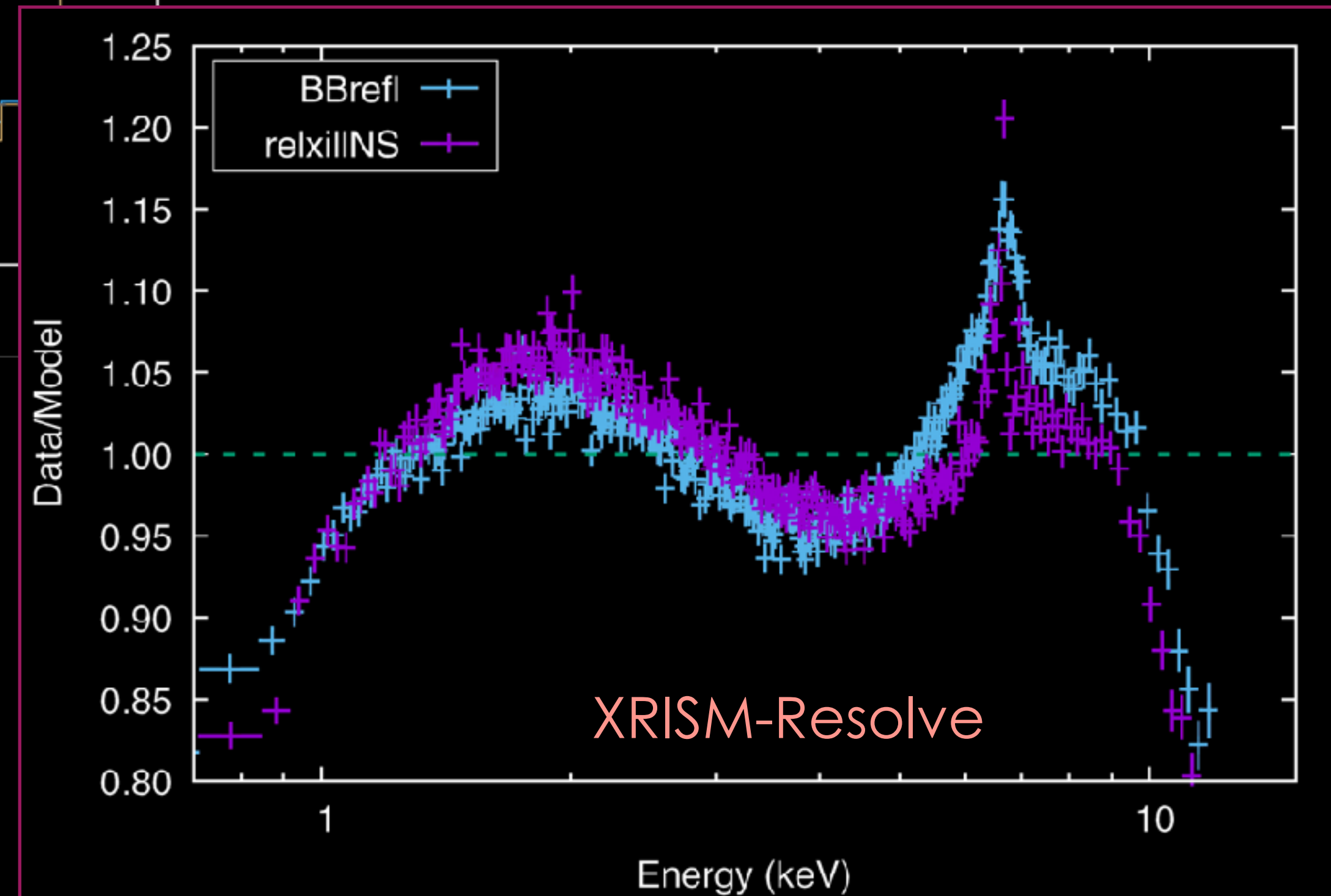
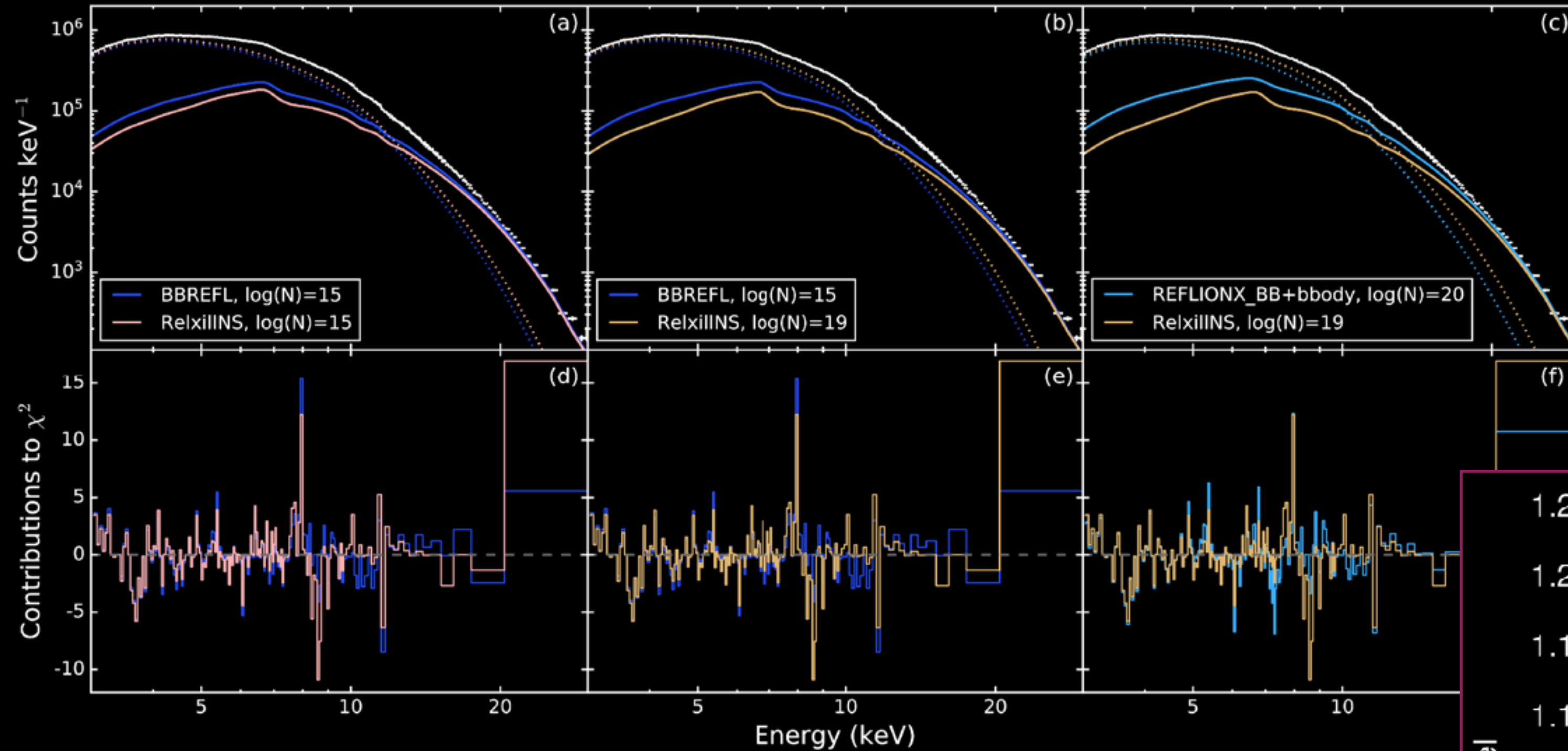


# Comparison with Previous Models

Test case **4U 1705—44**

Broadly consistent results between **relxillNS**, **BBrefl** and **ReflionX\_BB** when fitting NuSTAR data.

Larger discrepancies might be seen at softer energies



High-resolution spectra (microcal) could distinguish between models

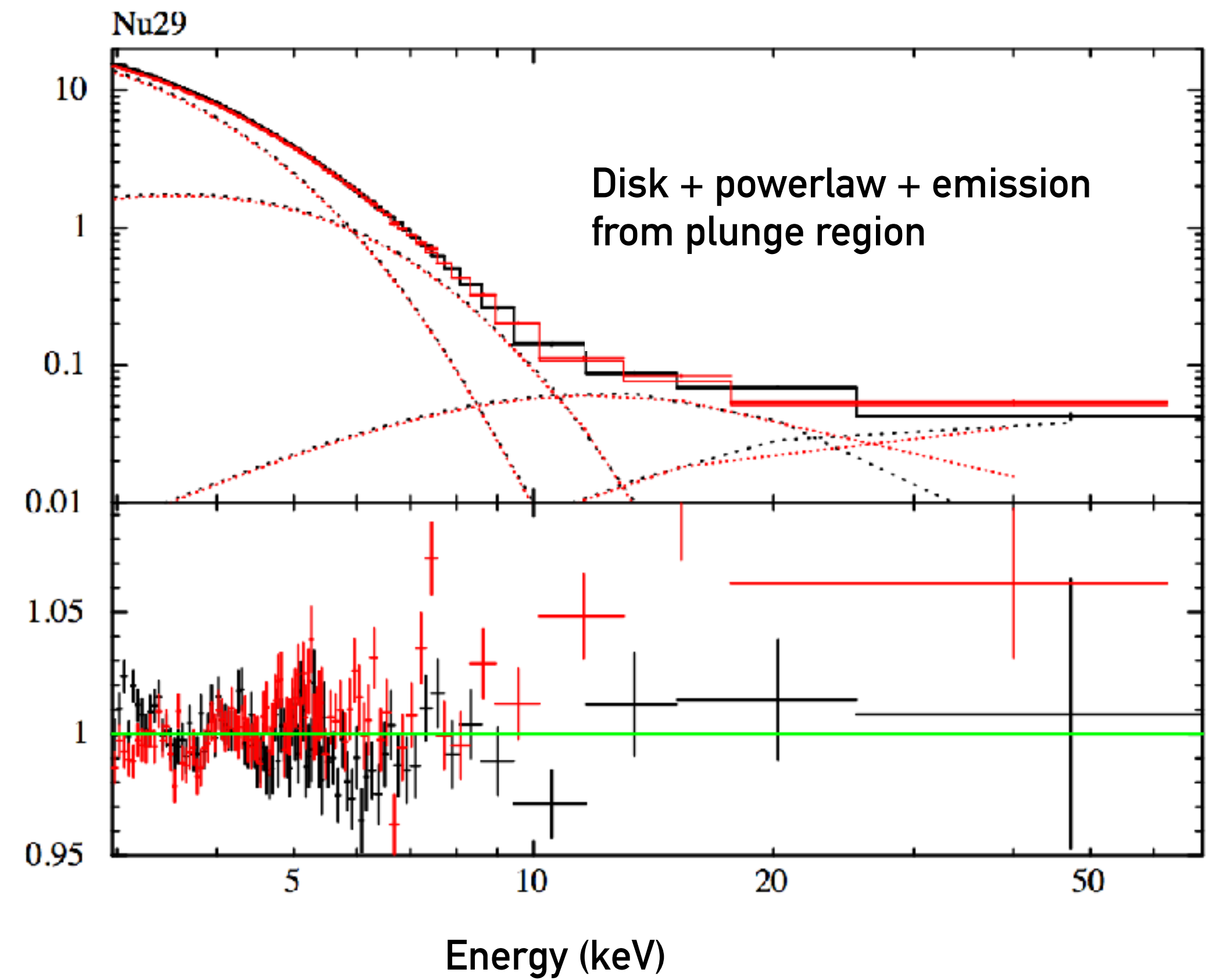
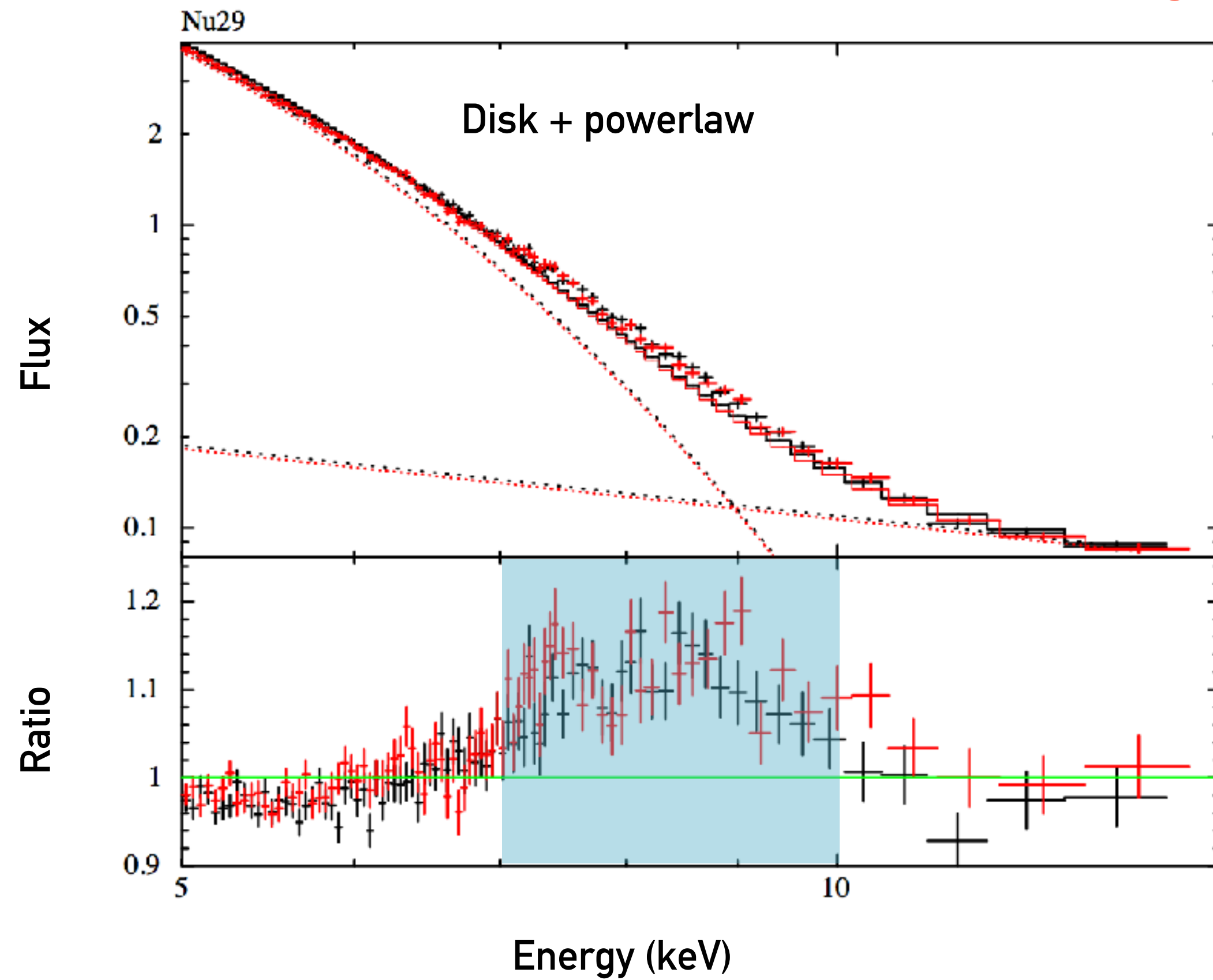
( Simulation for a 20 ks observation of a 100 mCrab source )

JG, Dauser, Ludlam+22



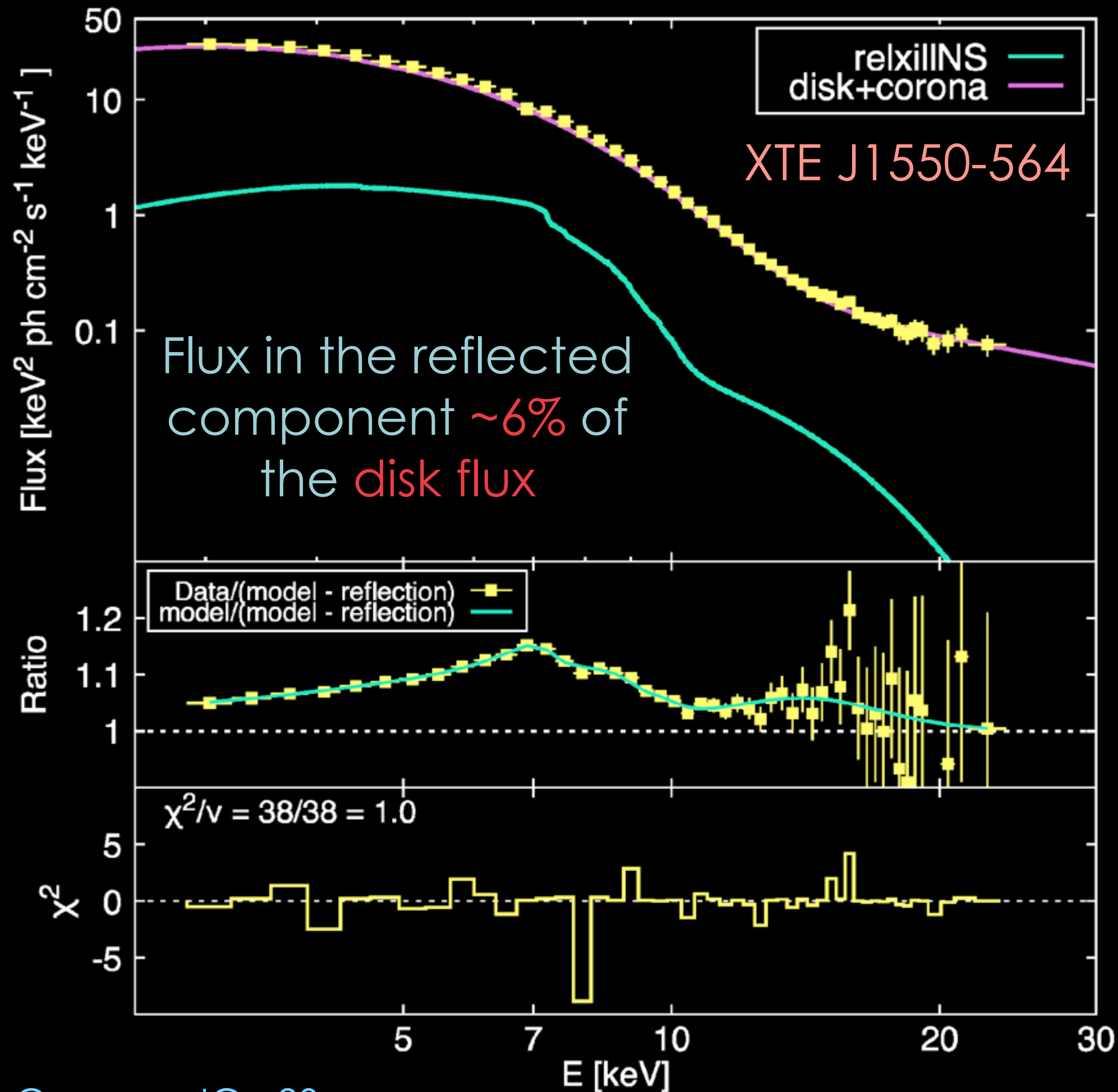
# Emission from the Plunging Region?

## MAXI J1820+070

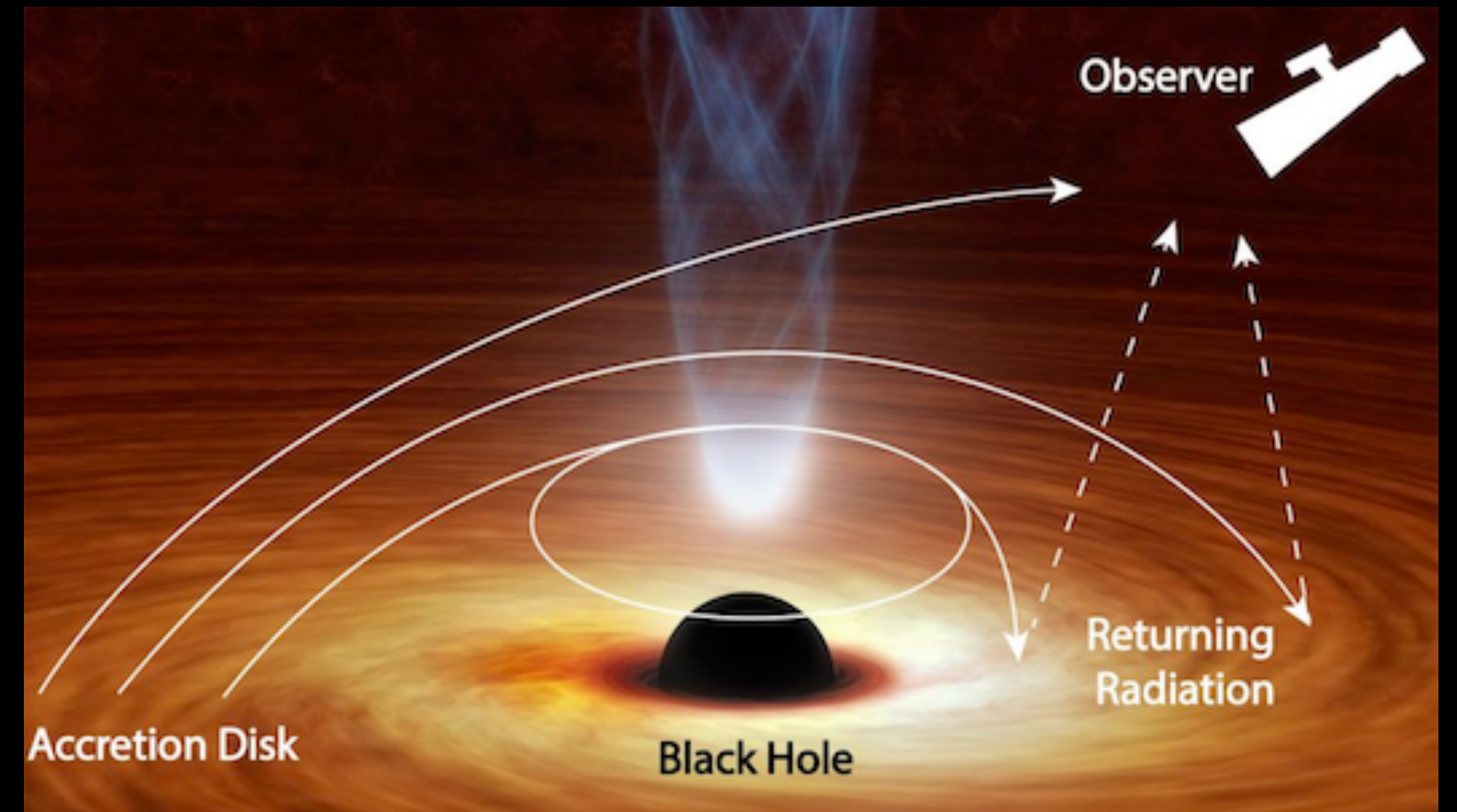




# Disk Self Irradiation (Returning Radiation)



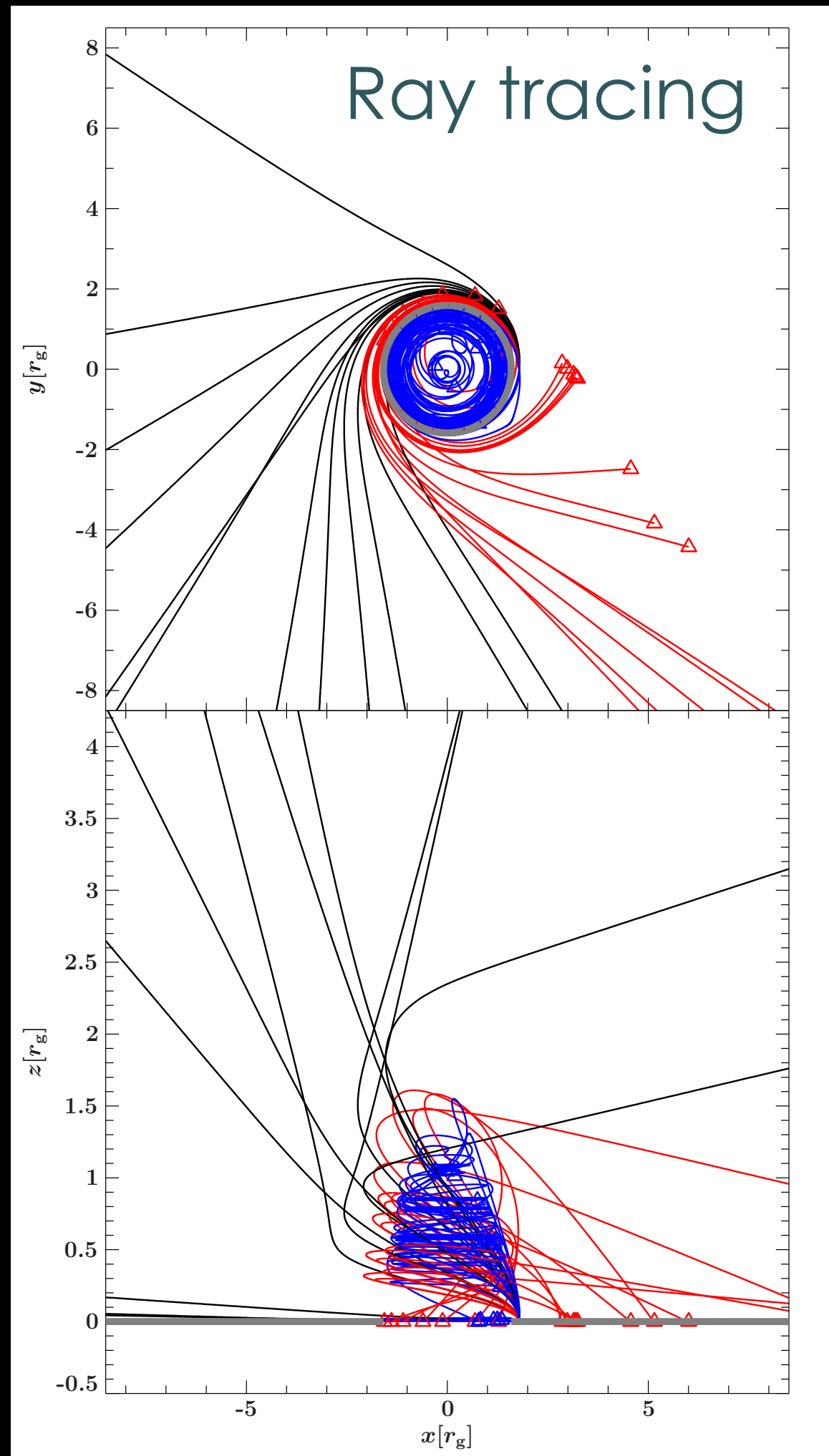
Radiation Returning to the Disk due to GR light bending



First observational evidence!  
 —> Predicted by Cunningham (1975),  
 and later by Agol & Krolik (2000)

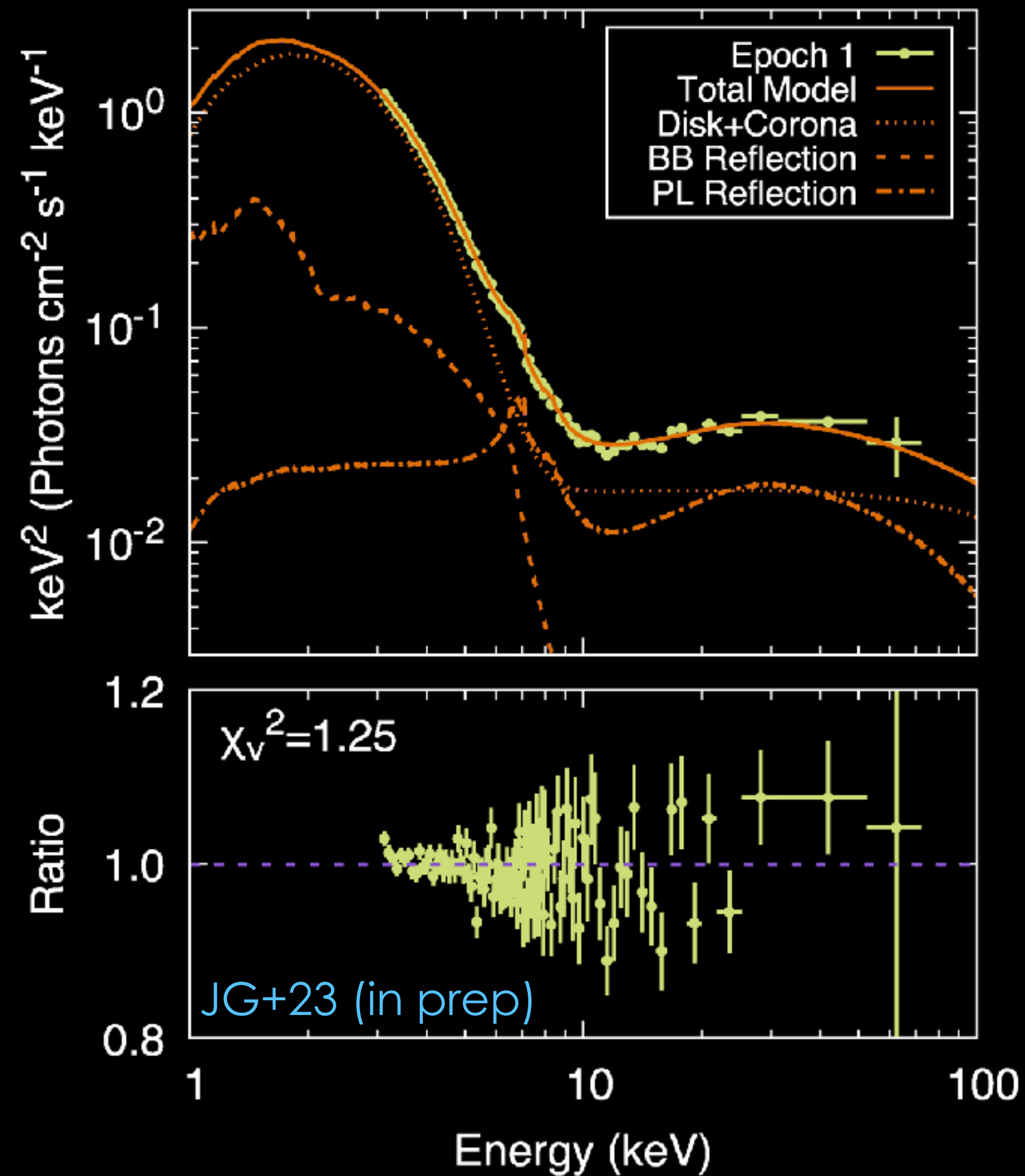


# Thermal Disk Emission



Dauser, JG+22

## Soft-State of GX 339-4



Returning radiation detected in several other sources:

- 4U 1630-47 (Connors, JG+21)
- EXO 1846-031 (Wang, ..., JG+21)
- MAXI J0637-430 (Lazar, ..., JG+21)
- GX 339-4 (JG+23)

New theoretical work:

- Effects on timing properties (Wilkins, JG+21)
- Effects on emissivity profiles (Dauser, JG+22)

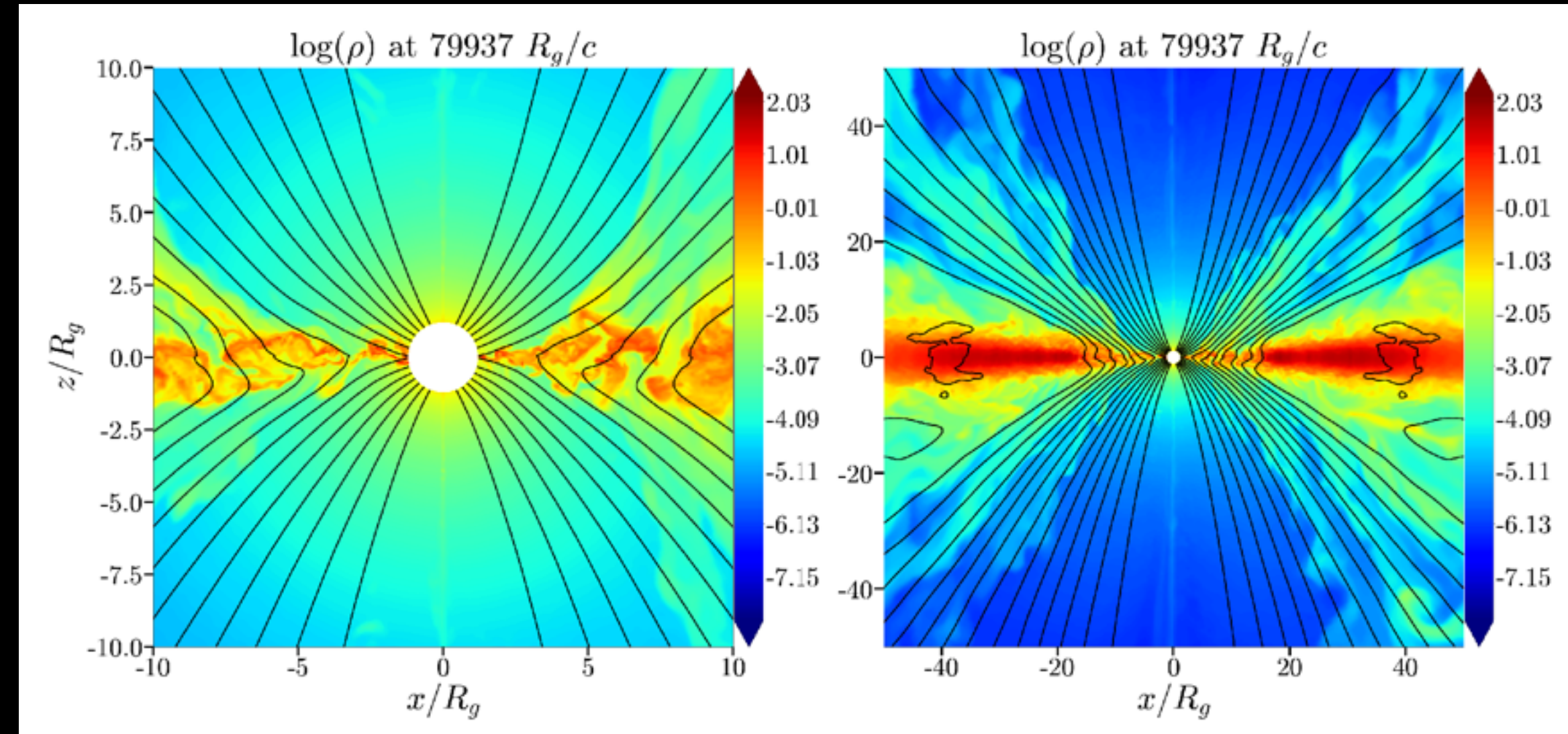


# GRMHD Density Profiles

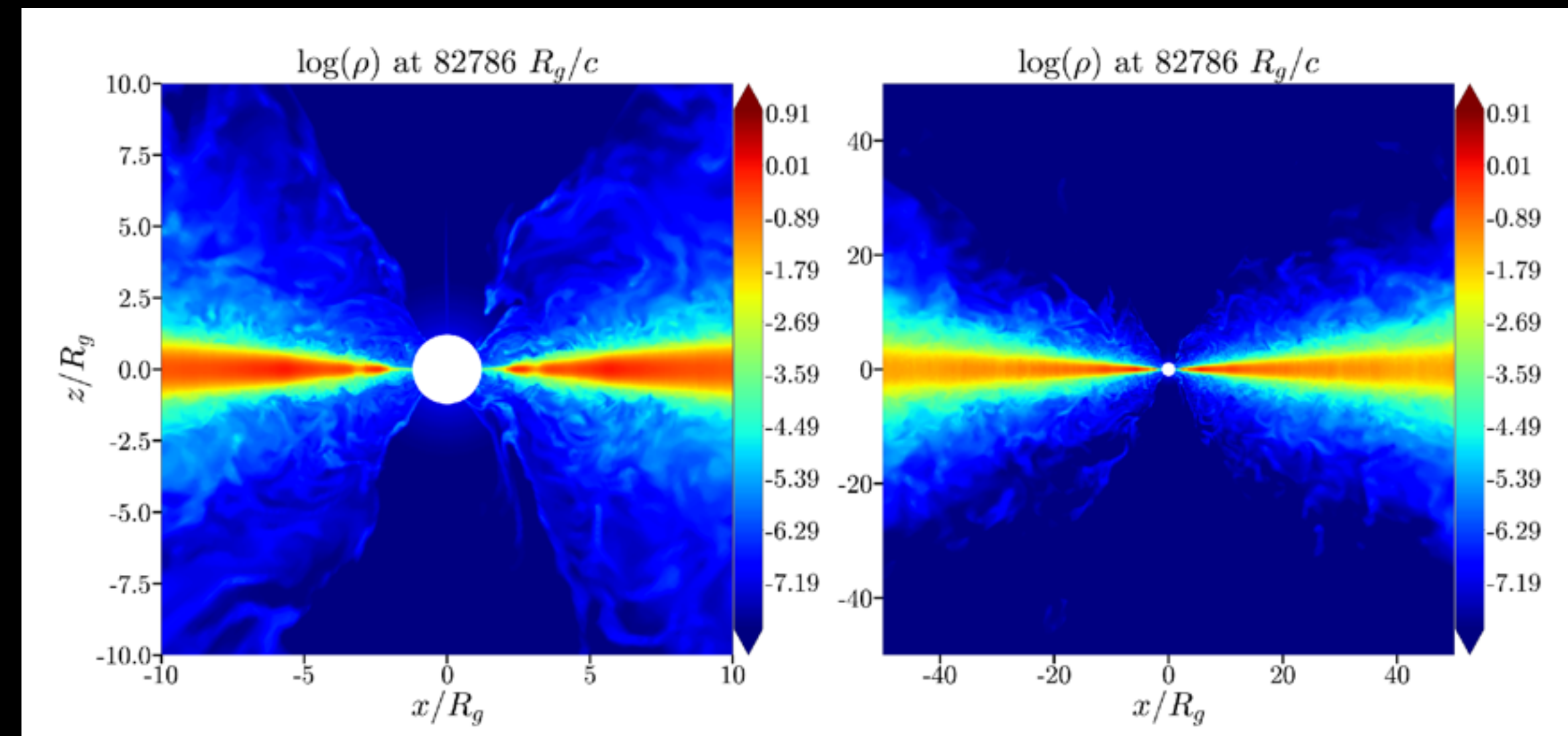
High resolution simulations without radiation.

There is no density drop inside the ISCO for the MAD case

→ Accretion does not proceed via viscous stress



**MAD**

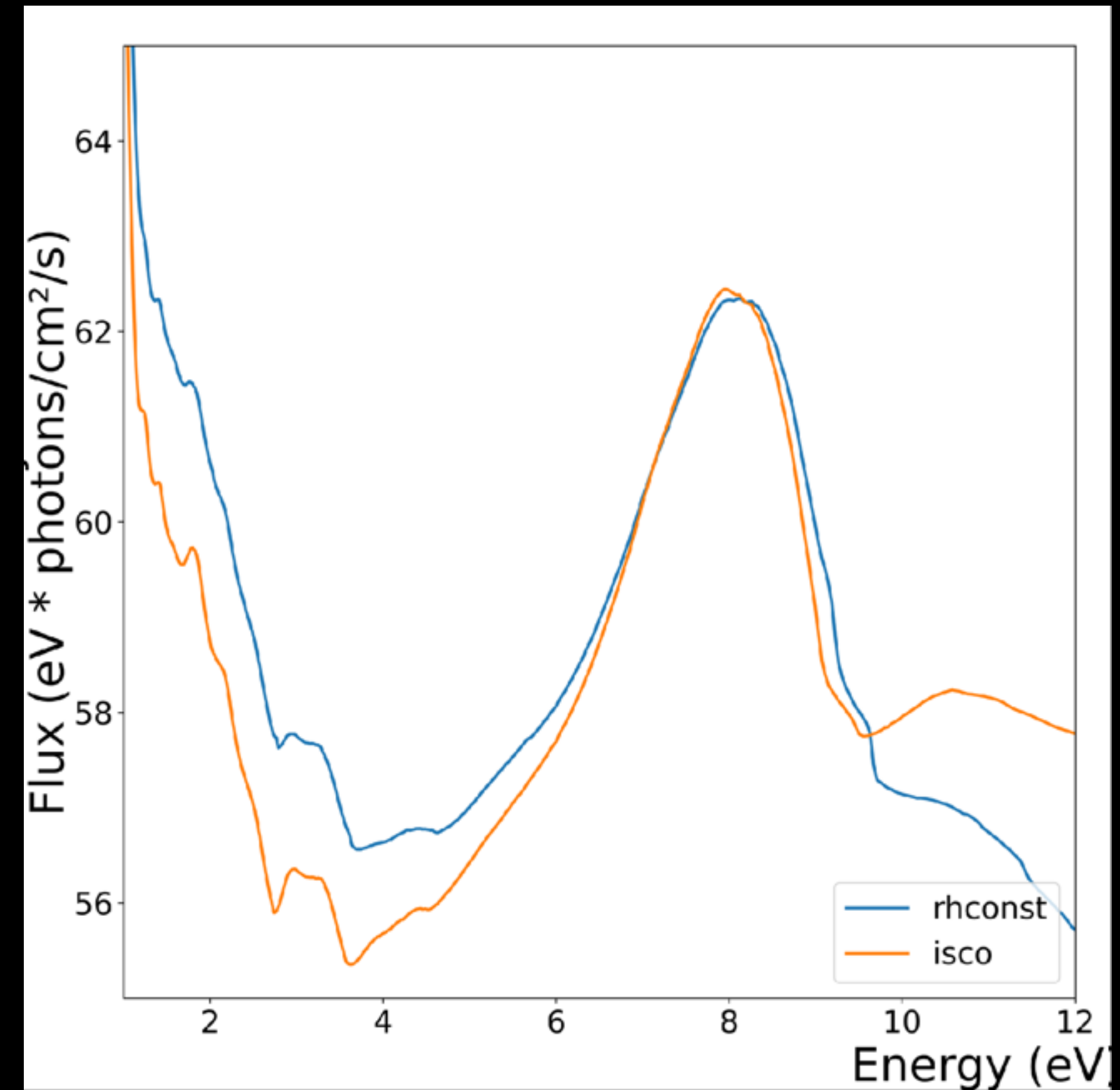
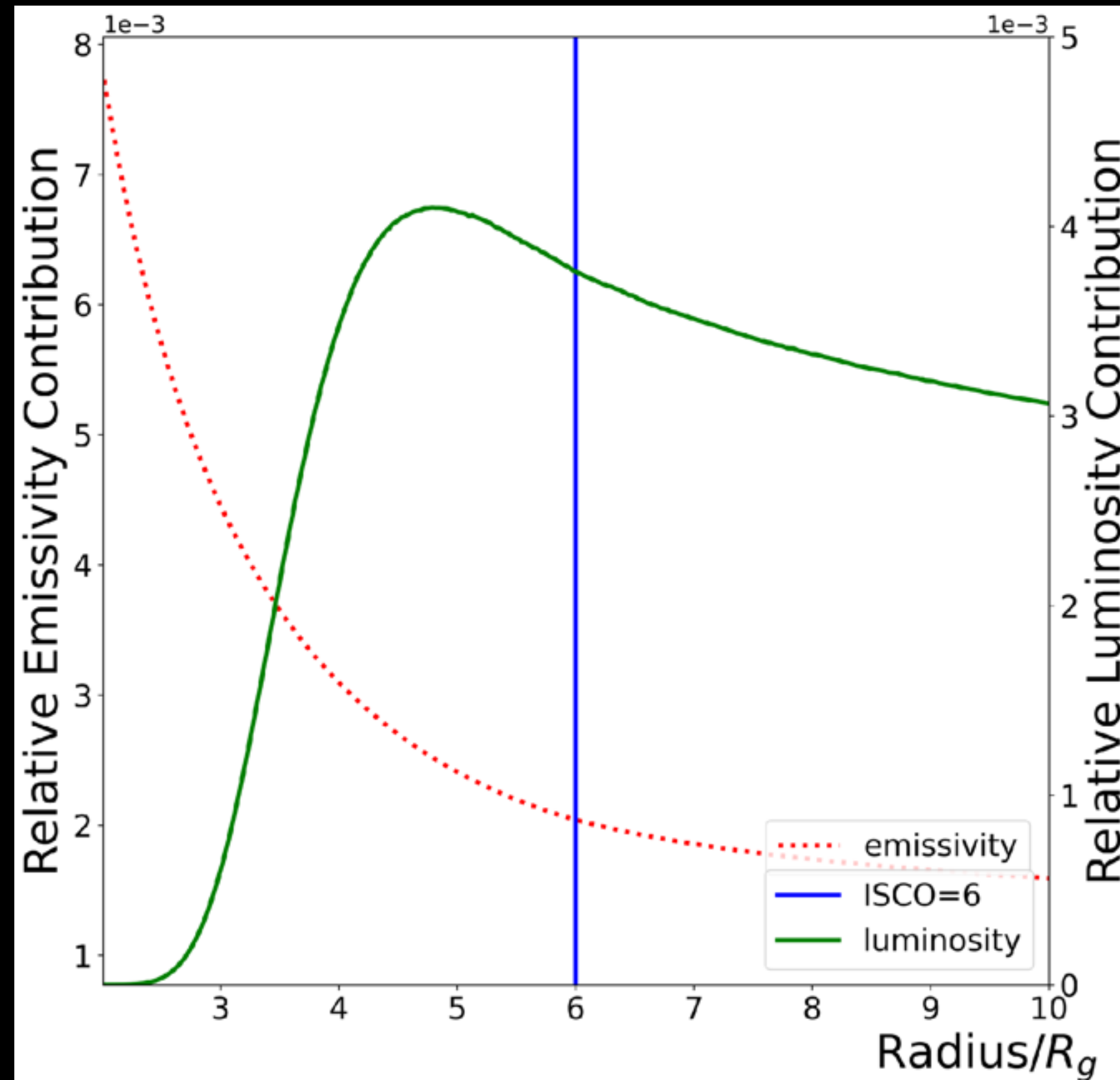


**no-MAD**



# Venturing inside the ISCO

Reflection from inside the ISCO assuming a flat density profile





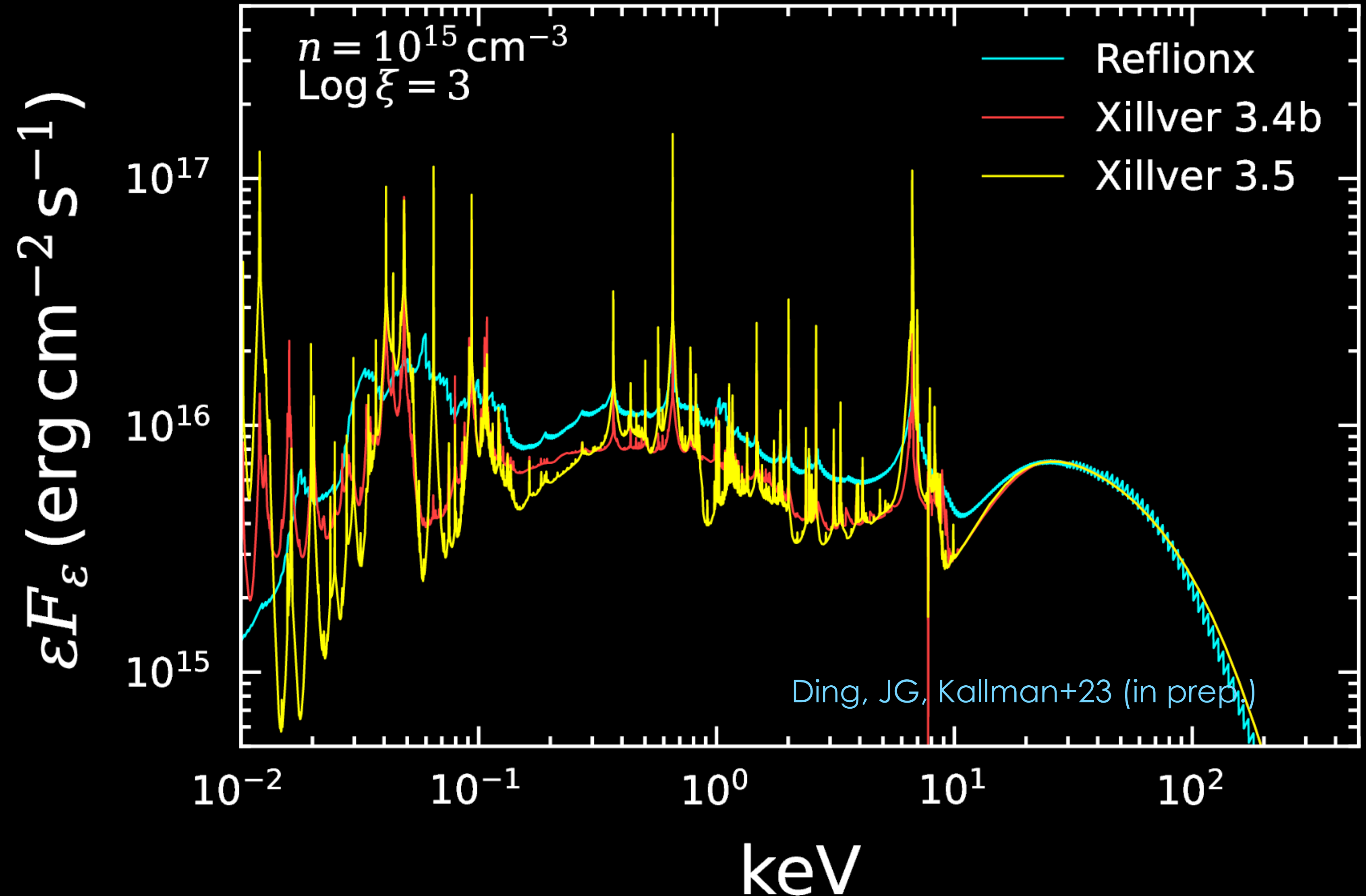
# High-Density Plasma Effects

New XSTAR routines and Atomic Data including:

- Screening of the atomic potential (Debey—Hückel approximation)
- Continuum lowering (truncation of the high- $n$  states)
- Suppression of Dielectronic Recombination (Nikolik+20 formulae)

Kallman,...,JG+21

Mendoza,...,JG+21





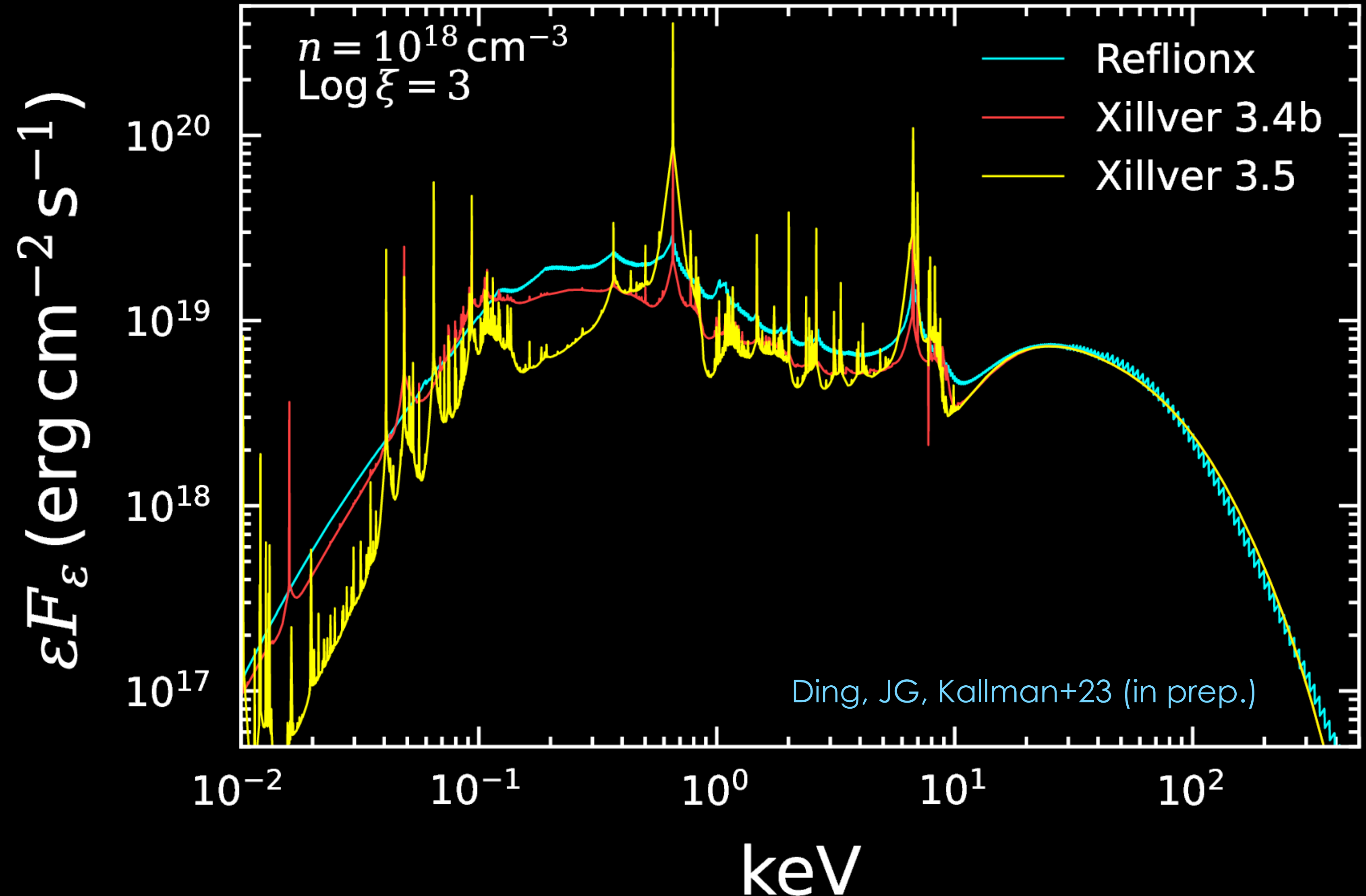
# High-Density Plasma Effects

New XSTAR routines and Atomic Data including:

- Screening of the atomic potential (Debye—Hückel approximation)
- Continuum lowering (truncation of the high- $n$  states)
- Suppression of Dielectronic Recombination (Nikolik+20 formulae)

Kallman,...,JG+21

Mendoza,...,JG+21



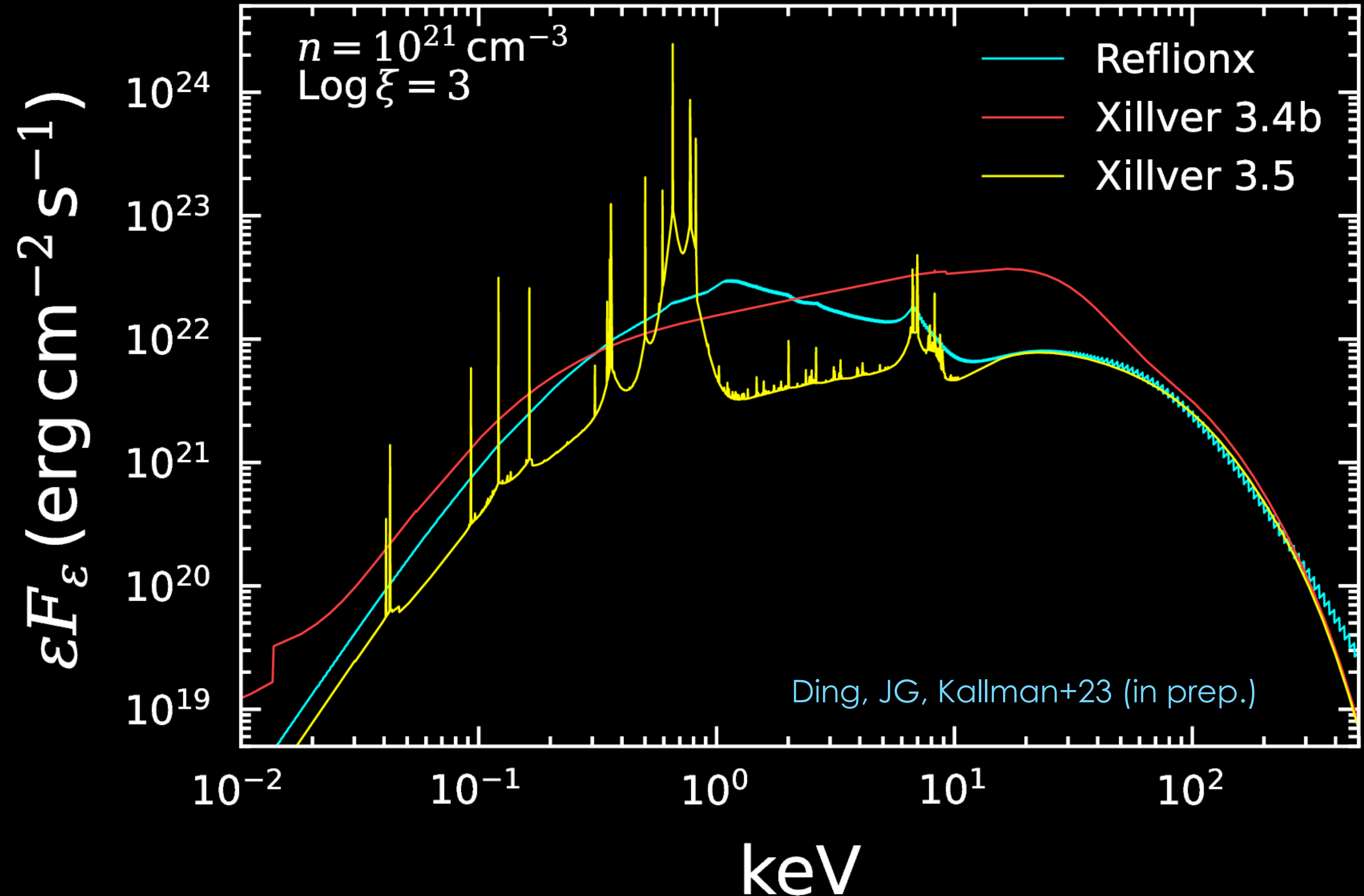


# High-Density Plasma Effects

New XSTAR routines and Atomic Data including:

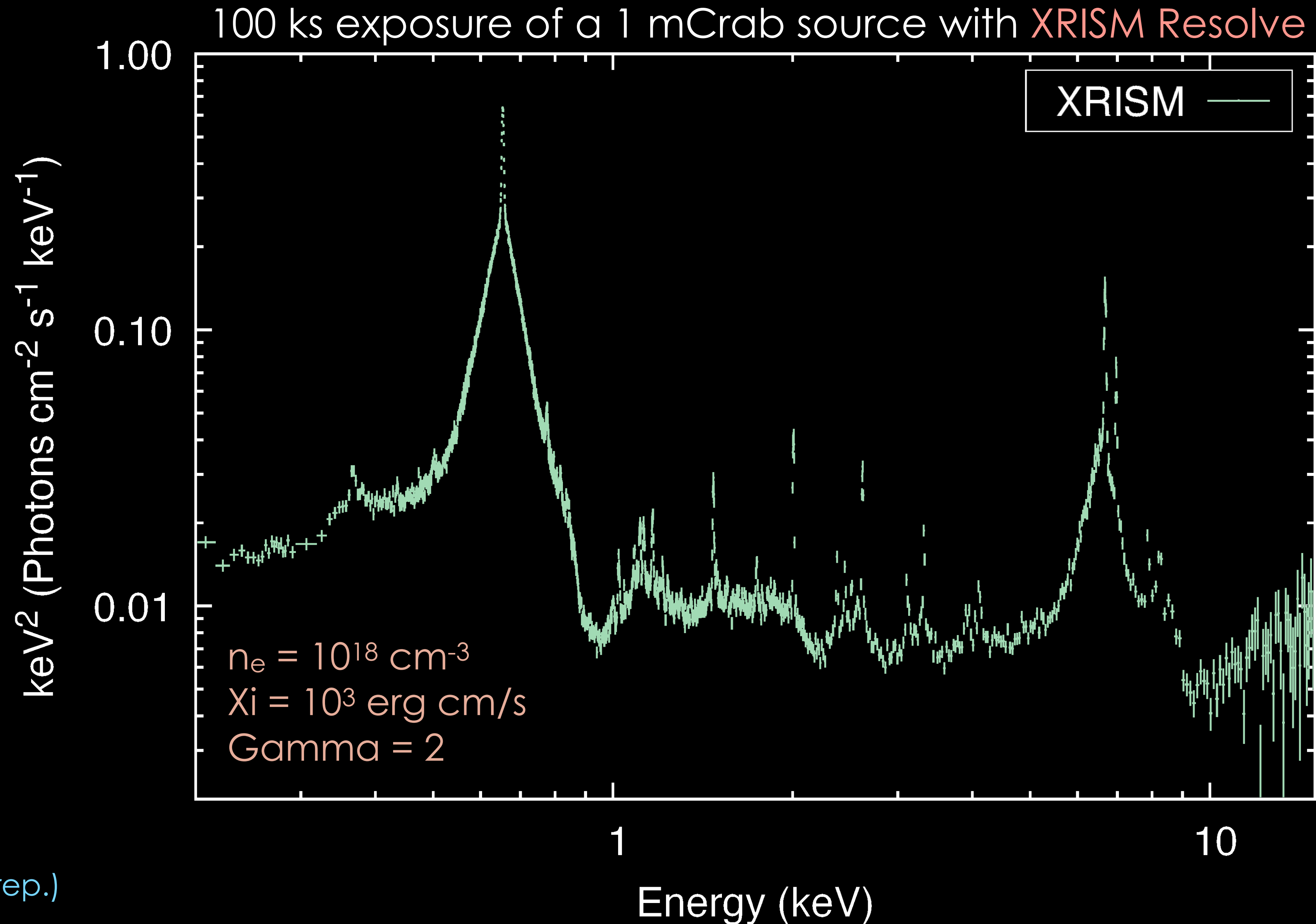
- Screening of the atomic potential (Debey—Hückel approximation)
- Continuum lowering (truncation of the high- $n$  states)
- Suppression of Dielectronic Recombination (Nikolik+20 formulae)

Kallman,...,JG+21  
Mendoza,...,JG+21





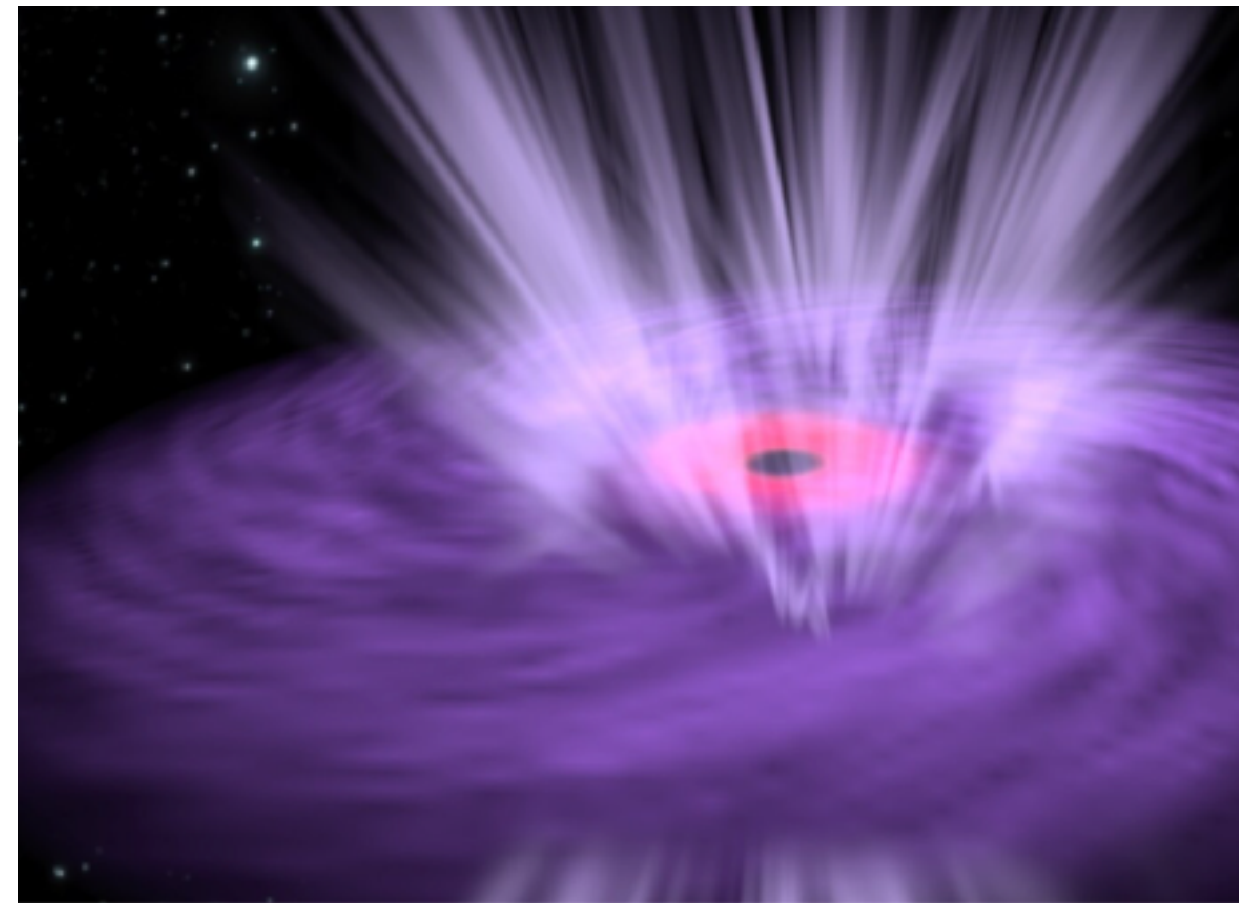
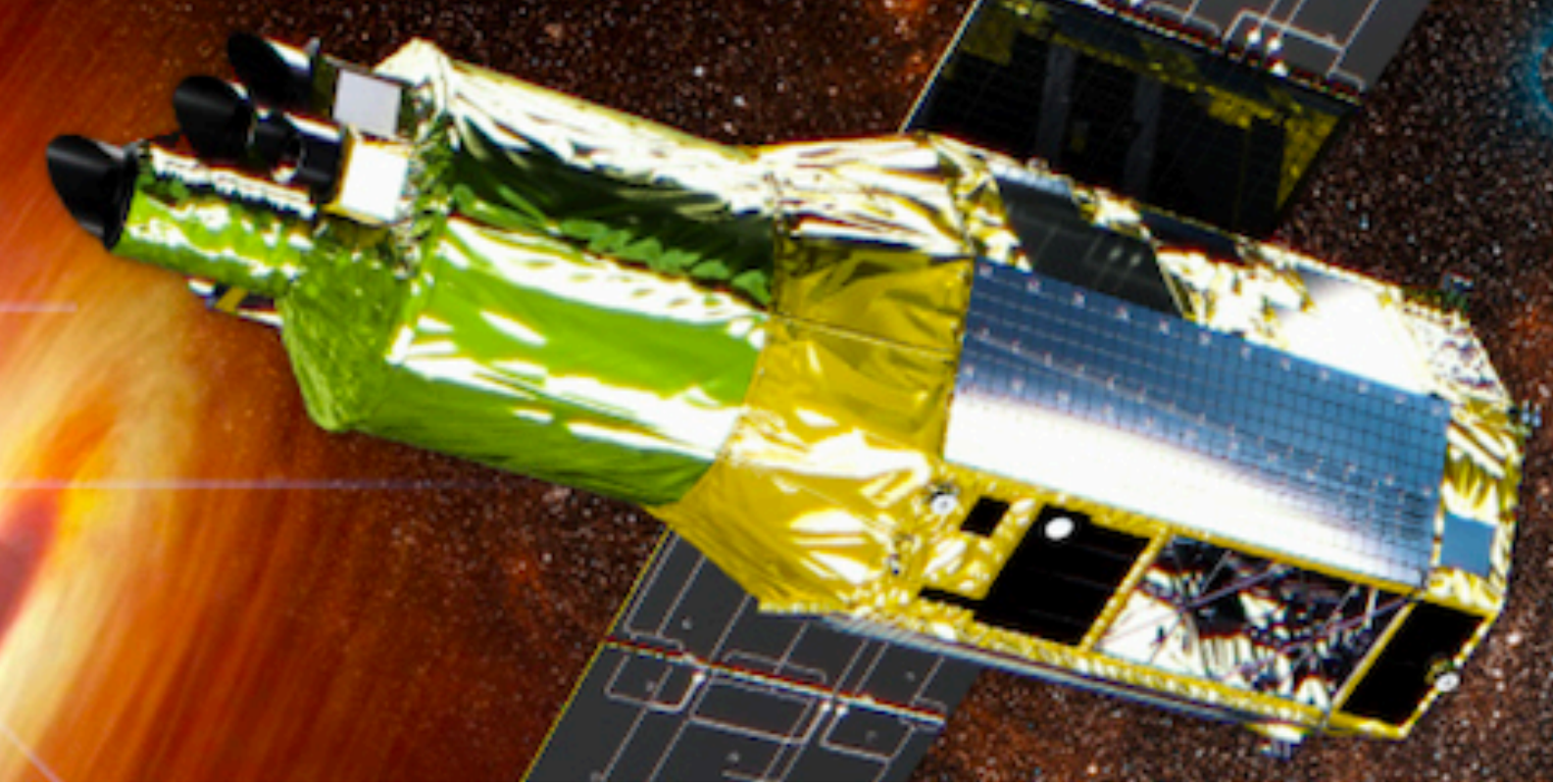
# High-Density Plasma Effects



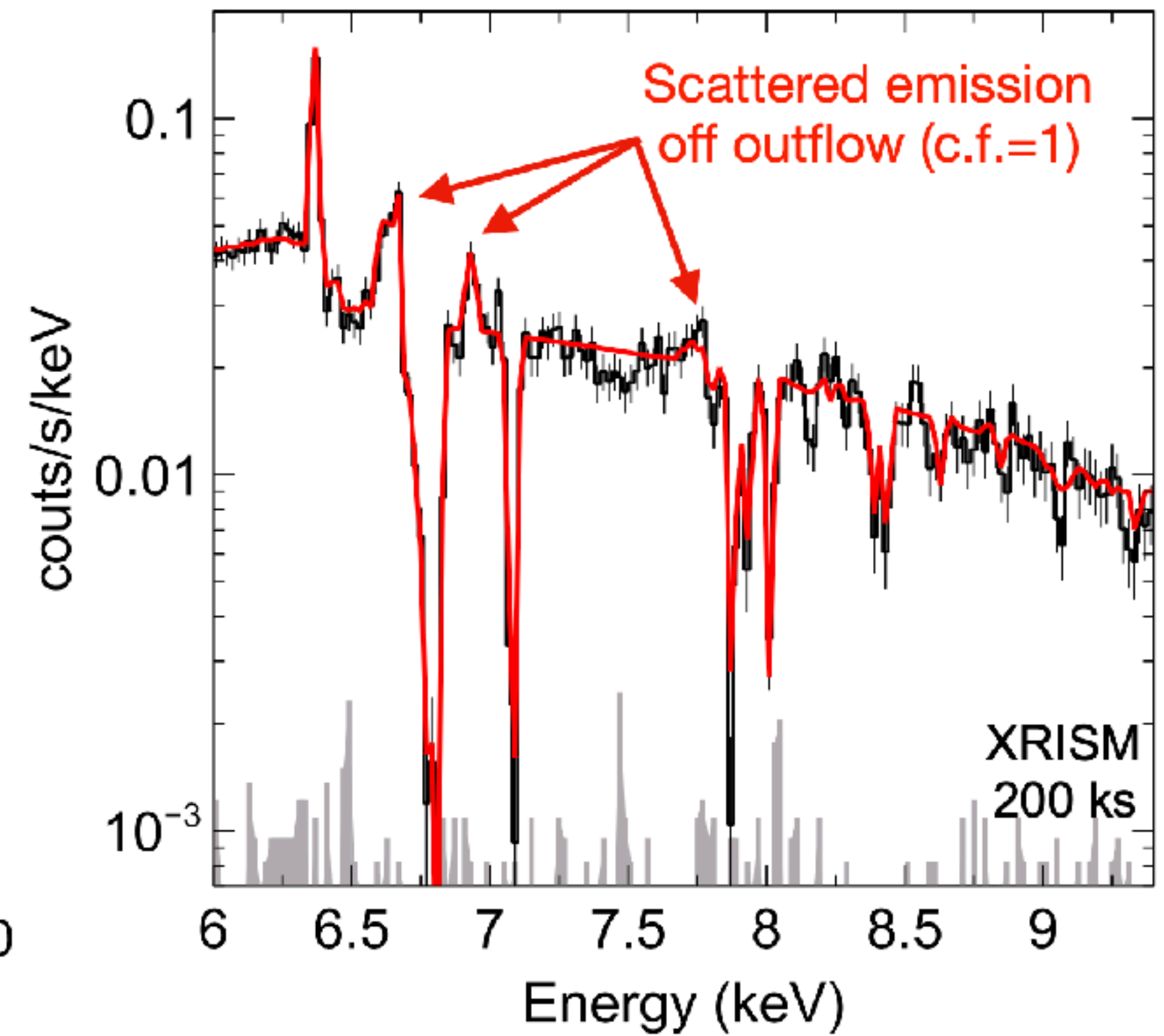
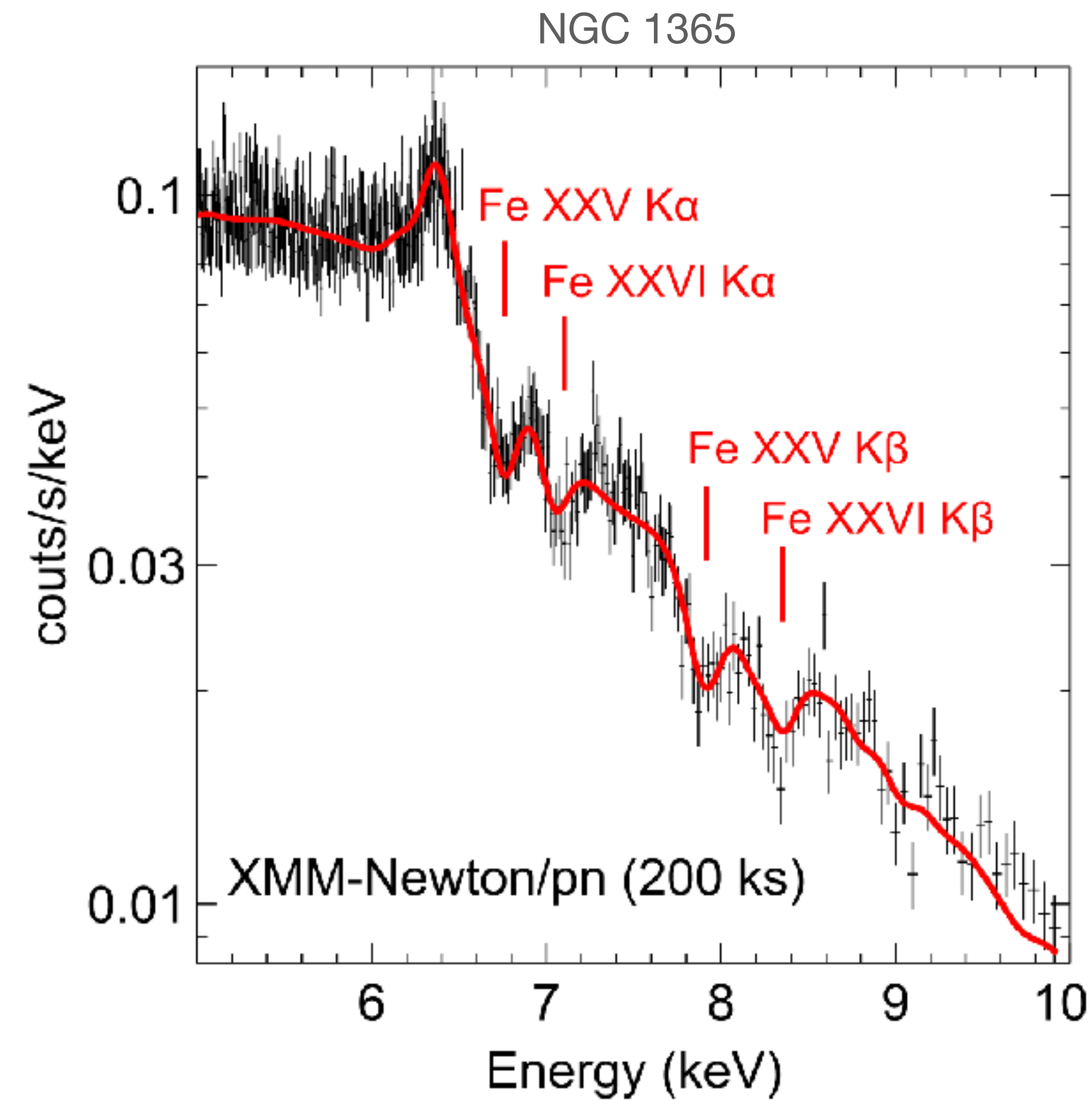


# The Present

**XRISM** X-Ray Imaging and Spectroscopy Mission



***Launching in 2023!***



Adapted from Risaliti+05



# The Future



**HEX-P**  
HIGH ENERGY X-RAY PROBE  
<https://hexp.org/>

Coronal Physics

Radius of the Neutron Star

X-ray Pulsations

Black Hole Spin

High-Density Plasma Effects

Accretion Disk Truncation

